

**PROCEEDINGS OF THE SEMINAR ON**  
**'EMERGING AREAS OF CHEMICAL**  
**SCIENCES'**

**Editor**

**Mrs. Suhada K M; M. Sc.**

Assistant Professor, PG Department of Chemistry, KAHM Unity Women's College,  
Manjeri, Narukara (PO), Malappuram (DT), PIN 676122 Kerala, India.

**Published by**

**Mrs. Suhada K M; M. Sc.**

Assistant Professor, PG Department of Chemistry, KAHM Unity Women's College,  
Manjeri, Narukara (PO), Malappuram (DT), PIN 676122, Kerala, India.

**ISBN: 978-93-5913-421-5**

© All rights reserved to the Editor.

**First Edition**

Printed at Apex Prints, Manjeri, PIN 676121, Malappuram (DT), Kerala, India.

**DEPARTMENT OF CHEMISTRY**  
**KAHM UNITY WOMEN'S COLLEGE, MANJERI**  
Narukara (PO), Malappuram (DT), Kerala-676122, India

[www.unitywomenscollege.in](http://www.unitywomenscollege.in)

*E-mail: chemistry@unitywomenscollege.in*

KAHM Unity Women's College was established in 1991 and is run by Muslim Educational and Cultural Association (MECA), a registered society. Started as a First Grade Aided College and affiliated to University of Calicut it is the only aided multi faculty (Arts, Science and Commerce) Women's College in Malappuram District. The institution aims at the upliftment of women in general and the educationally backward Muslim women in particular, through modern good quality education. The college has creditable academic as well as co-curricular accomplishments. The college has been accredited by NAAC at B\* level (2.77) in 2019. The college offers 10 UG and 6 Pg courses.

Department of Chemistry was started in 1991 with Chemistry as subsidiary subject. Chemistry as main subject was started in 1993. 28 batches have successfully completed B.Sc. Chemistry Programme. The department conducted B.Sc. Industrial chemistry course in the vocational stream with the assistance of UGC during 1999-2004, Three batches completed the course. The Department became a Post Graduate Department in 2013 and became a Research Department in 2023. 8 batches have successfully completed the M. Sc. Chemistry Programme.

Our Vision:

- To develop a sense of intellectual curiosity concerning chemical theory and an appreciation of the practical role of chemistry in life.

Our Mission:

- To give a thorough grounding in the principle of chemistry, both in theory and in practical experience.
- To produce scientifically literate graduates and post graduates with a broad and deep knowledge of fundamental chemical principles.

© All rights reserved. No part of this publication may be reproduced, stored in or introduced into retrieval system or transmitted, in any form, or by any means, electronic, mechanical, photocopying recording or otherwise without the prior written permission of the publisher. Authors are solely responsible for the contents of the chapters in this volume. The editor has taken his best effort in the preparation of this book. Errors, if any, are purely unintentional and readers are requested to intimate the errors to the editor to avoid discrepancies in the future.

₹ 500

June 2023

**ISBN: 978-93-5913-421-5**

**ISBN: 978-93-5913-421-5**

Science for  
Humanity  
and Technology  
for Society

# Kerala State Council for Science, Technology and Environment



Sasthra Bhavan, Pattom P. O., Thiruvananthapuram-695004, Kerala State, India  
Tel: 0471-258200-09, Fax: 0471-2540085

email : mail.kscste@kerala.gov.in, Website : www.kscste.kerala.gov.in  
www.facebook.com/kscsteofficial, www.twitter.com/kscsteofficial



Fostering Science,  
Technology and Innovation  
KSCSTE strives for a  
new Paradigm to link  
science with development



## Programmes and Schemes of KSCSTE

### FELLOWSHIPS AND SCHOLARSHIPS

KSCSTE – Emeritus Scientist Scheme  
Post Doctoral Fellowships  
KSCSTE Fellowships  
Fellowship for Science Writing and  
Communication  
Prathibha Scholarship for Students Opting  
Science Learning

### FINANCIAL SUPPORT

Grant For Research Projects In  
Emerging Areas of Science  
Activity in Specific Areas  
Student Projects  
Industry Linked Biotechnology Programme

### SCIENCE POPULARISATION

An Annual Mega Science Fest -  
Kerala Science Congress  
Annual Children's Science Congress  
Assistance For Seminars, Symposia  
and Workshops  
Digital Content Development on  
Science Innovation  
Technology Development and  
Patent Information  
Collaborative Projects in Technical  
and Environmental Areas  
Techfest, RIM, Greencorps & Ecoclubs

### PROMOTIONAL PROGRAMMES

Back to Lab Programme  
Sastraposhini and Sasthrabodhini  
Programmes  
Scheme for Promoting Young Talents in  
Science – SPYTIS  
Students Programme in Excellence in  
Experimental Design (SPEED)  
Nurturing Excellence in Science Teaching  
(NEST)

### AWARDS

Kerala Sasthra Puraskaram –A Prestigious  
Life Time Achievement Award For Eminent  
Scientists  
Science Literature Awards  
Dr. S. Vasudev Award For Best Research Project  
Kerala State Young Scientist Award Scheme

### RESEARCH & DEVELOPMENT CENTRES OF KSCSTE

Centre for Water Resources Development  
and Management (CWRDM), Kozhikode  
Jawaharlal Nehru Tropical Botanic Garden  
and Research Institute (JNTBGRI) Palode,  
Trivandrum  
Kerala Forest Research Institute (KFRI),  
Thrissur  
Kerala School of Mathematics (KSOM),  
Kozhikode  
National Transportation Planning  
and Research Centre (NATPAC),  
Thiruvananthapuram  
Srinivasa Ramanujan Institute for Basic  
Sciences (SRIBS), Kottayam  
Institute for Climate Change Studies (ICCS)  
Kottayam  
Malabar Botanical Garden and Institute for  
Plant Sciences (MBGIPS), Kozhikode

### GRANT-IN-AID INSTITUTIONS OF KSCSTE

Integrated Rural Technology Centre (IRTC),  
Palakkad  
Sophisticated Test and Instrumentation  
Centre (STIC), Kochi  
M S Swaminathan Research Foundation  
(MSSRF), Wayanad



**GOLDEN JUBILEE CELEBRATIONS OF  
SCIENCE AND TECHNOLOGY IN KERALA**





**TWO DAY SEMINAR ON**  
**EMERGING AREAS OF**  
**CHEMICAL SCIENCES**

*Jointly Organized By*  
RESEARCH DEPARTMENT OF  
CHEMISTRY  
*And*  
THE KERALA STATE COUNCIL FOR  
SCIENCE, TECHNOLOGY AND  
ENVIRONMENT (KSCSTE)

**05 - 06** Venue: Seminar Hall  
**June 2023**

**Register Here :**  
<https://forms.gle/tfuV5skyS4v4t32C8>

 **RESEARCH DEPARTMENT OF CHEMISTRY**  
**KAHM UNITY WOMEN'S COLLEGE, MANJERI**  
A Govt. Aided College Affiliated to University of Calicut  
Re-accredited by NAAC with B++ Grade (CPGA 2.77)



PROCEEDINGS OF THE SEMINAR ON  
'EMERGING AREAS OF CHEMICAL SCIENCES'



The Research Department of Chemistry, KAHM Unity Women's College, Manjeri has immense pleasure to invite you to the two day seminar on 'Emerging Areas of Chemical Sciences' scheduled on 5<sup>th</sup> and 6<sup>th</sup> June 2023.

### ABOUT THE COLLEGE

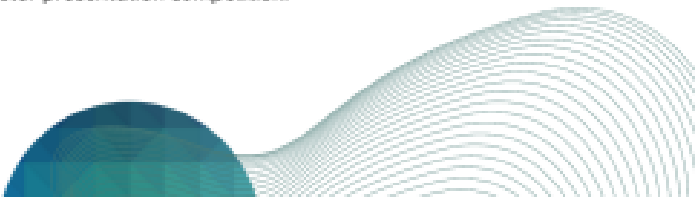
K.A.H.M. Unity Women's College, Manjeri was established in 1991 and is run by Muslim Educational and Cultural Association (MECA), a registered society and as the first women's educational institution in the field of higher education in Malappuram district in Kerala. The college was founded by the visionary, Janab Korambayil Ahamed Haji. He envisaged the institution as a center based on the values of integrity and social commitment, promoting learning and culture. The college strives to produce intellectually competent, morally upright and spiritually inspired citizens in the service of the nation. A sprawling green campus spread over 17 acres; the college is located in Pulpatta village, about 1.6 kilometers away from Manjeri-Calicut Road. Affiliated to Calicut University, Thennipalam, the institution is known for its academic excellence and research potential. The college has 10 academic departments, with around 1600 students and 72 faculty members. The college has been rated as a 'B++' Grade institution by the National Assessment and Accreditation Council (NAAC) in the third cycle with 2.77 points.

### ABOUT THE DEPARTMENT

The Department of Chemistry was established in 1991 as a subsidiary department for B.Sc. Home Science programme. It became a full fledged main department in 1993 with B.Sc. Chemistry programme. Department of Chemistry started offering subsidiary course for B.Sc. Botany programme in 1996 when Department of Botany was established in the college. During the period 1999-2004, the department offered B.Sc. Industrial Chemistry as an Vocational programme with special financial aid from UGC. M.Sc. Chemistry was started as a regular government aided programme in the year 2013. The Department started certificate courses in the year 2017. Currently the Department of Chemistry offers B.Sc. Chemistry and M.Sc. Chemistry programmes and Complementary courses for B.Sc. Botany and B. Sc. Home Science programmes. At present there are 146 students doing their B.Sc. and 40 students doing their M.Sc. in Chemistry. There are eight extremely capable, well qualified faculty members engaged in teaching with a strong motivation and commitment. The Department is upgraded as research department in the year 2023.

### ABOUT THE SEMINAR

The Research Department of Chemistry of KAHM Unity Women's College, Manjeri and The Kerala State Council for Science, Technology and Environment (KSCSTE) are jointly organizing a two day seminar on 'EMERGING AREAS OF CHEMICAL SCIENCES' on 5<sup>th</sup> and 6<sup>th</sup> June 2023 to encourage Chemistry students of this institution and nearby institutions into the advanced research areas of Chemistry. The seminar will feature thematically arranged invited lectures by eminent faculty from top institutions working in various emerging fields of Chemistry. We have also planned to arrange an oral and poster presentation competition.



## PROGRAMME SCHEDULE


**DAY 1 , 05/06/2023**

**Registration: 09.30 AM**

- Inaugural Session** : 10.00 AM-10.30 AM
- Prayer**
- Welcome Address** : Dr. Jyothi P  
(Associate Professor & Head, Dept. of Chemistry,  
KAHM Unity Women's College, Manjeri)
- Presidential Address** : Dr. Muhammed Basheer Ummathur  
(Principal, KAHM Unity Women's College, Manjeri)
- Inauguration** : Dr. Krishnakumar M  
(Scientific officer F, Chemistry Group. Atomic Minerals  
Directorate for Exploration and Research, Department of  
Atomic Energy, Bangalore)
- Felicitation** : Prof. P N Abdurahiman  
(Former Principal, KAHM Unity Women's College, Manjeri,  
Former Chairman of Chemistry UG Board of Studies,  
University of Calicut)
- : Jb. O Abdul Ali  
(Manager, KAHM Unity Women's College, Manjeri)
- : Dr. AK Shahina Mol  
(IQAC Coordinator, Assistant Professor and Head, Research  
Dept. of English, KAHM Unity Women's College, Manjeri)
- : Ms. Anitha Beegam  
(Staff Club President, Associate Professor and Head, PG  
Dept. of Family and Community Science, KAHM Unity  
Women's College, Manjeri)
- : Mr. Adham Thanari  
(NTS Representative, KAHM Unity Women's College, Manjeri)
- Votes of Thanks** : Mrs. Suhada KM  
(Coordinator, Assistant Professor, Dept of  
Chemistry, KAHM Unity Women's College, Manjeri)

**Tea Break**  
**10.30 AM - 10.45 AM**





### Technical Session 1

10.45 AM - 12.00 PM

**TOPIC** : Emerging Trends in Analytical Chemistry

**Speaker** : **Dr. KRISHNAKUMAR M**

Scientific officer F, Chemistry Group. Atomic Minerals Directorate for Exploration and Research, Department of Atomic Energy, Bangalore



**Chair** : Dr. Yamuna KM

(Assistant Professor, Dept. of Chemistry, NSS College, Manjeri)

**Vote of Thanks** : Dr. Deepa K

(Assistant Professor, Dept. of Chemistry, KAHM Unity Women's College, Manjeri)

### Technical Session 2

12.00 PM - 01.15 PM

**TOPIC** : Preserving Paradise: Tackling Plastic Pollution in Wetlands

**Speaker** : **Dr. DEVI KORAVANGATT**

Assistant Professor,  
Department of Geology,  
Farook College, Farook




**Chair** : Dr. Jyothi P

(Associate Professor & Head, Dept. of Chemistry, KAHM Unity Women's College, Manjeri)

**Vote of Thanks** : Dr. Thasnim P

(Assistant Professor, Dept of Chemistry, KAHM Unity Women's College, Manjeri)

*Lunch Break*  
**01.15 PM - 02.15 PM**



**Technical Session 3**

**02.15 PM - 03.30 PM**

**TOPIC** : Supramolecular Materials for Biological Applications

**Speaker** : **Dr. ROYMON JOSEPH**  
Assistant Professor,  
Department of Chemistry,  
University of Calicut



**Chair** : Dr. Jasna V C  
(Assistant Professor, Dept of Chemistry,  
KAHM Unity Women's College, Manjeri)

**Vote of Thanks** : Mrs. Suhada KM  
(Coordinator, Assistant Professor, Dept of Chemistry,  
KAHM Unity Women's College, Manjeri)

*Refreshment  
Poster Presentation and Evaluation*

**DAY 2 , 06/06/2023**

**Technical Session 4**

**10.00 AM - 11.15 AM**

**TOPIC** : NIR Fluorophores for Biomedical Imaging

**Speaker** : **Dr. Shimi M**  
Postdoctoral Fellow(SERB-DST)  
Department of Chemistry  
IIT Palakkad





**Chair** : Dr. Jamsheena V  
(Assistant Professor, Dept of Chemistry,  
KAHM Unity Women's College, Manjeri)

**Vote of Thanks** : Dr. Jyothi P  
(Associate Professor & Head, Dept. of Chemistry,  
KAHM Unity Women's College, Manjeri)

*Tea Break  
11.15 AM - 11.30 AM*





**Technical Session 5**

**11.30 AM - 01:00 PM**

**TOPIC** : A Green Graphene Laboratory Movement Log:  
Finale to Hazardous and Toxic Chemistry

**Speaker** : **Dr. BINITHA**  
Professor,  
Department of Chemistry,  
University of Calicut



**Chair** : Dr. Mehar Al Minnath  
(Assistant professor, Dept of chemistry,  
DGM MES Mampad College)

**Vote of Thanks** : Dr. Jasna V C  
(Assistant Professor, Dept of Chemistry,  
KAHM Unity Women's College, Manjeri)

**Lunch Break**  
**01.00 PM - 02.00 PM**

**Oral Presentations** : 02.00 PM - 03.00 PM

**Valedictory Function** : 03.00 PM - 03.30 PM

**Refreshment**

<i>Sl No.</i>	<i>CONTENTS</i>	<i>Page No.</i>
	<b>INVITED LECTURES</b>	
IL1.	<b>Emerging Trends in Analytical Chemistry</b> <i>M. Krishnakumar</i>	<b>12</b>
IL2.	<b>A Green Graphene Laboratory Movement Log: Finale to Hazardous and Toxic Chemistry</b> Binitha N Narayahan	<b>14</b>
IL3.	<b>Supramolecular Materials for Biological Applications</b> <u>Roymon Joseph</u>	<b>16</b>
IL4.	<b>Plastic pollution in wetlands</b> Devi K	<b>18</b>
IL5.	<b>Glyco-conjugated fluorophores for biomedical imaging</b> Shimi Manchery	<b>19</b>
	<b>ORAL PRESENTATIONS</b>	
OP1.	<b>Preparation, Characterization and Application of Styrene Butadiene Rubber (SBR)/ Zinc Sulfide (ZnS) Nanocomposite</b> <u>V.C Jasna</u>	<b>21</b>
OP2.	<b>Synthesis and evaluation of novel activators in vanadium catalyzed EPDM synthesis</b> <u>Sani E.P. Mohamed</u>	<b>48</b>
	<b>POSTER PRESENTATIONS</b>	
PP1.	<b>Metal-free diaryl etherification of tertiary amines by <i>ortho</i>-C(sp<sup>2</sup>)-H functionalization for synthesis of dibenzoxazepines and dibenzoxazepinones</b> <u>Vellekkatt Jamsheena, C. K. Mahesha, Nibin M. Joy, Ravi S. Lankalapalli</u>	<b>59</b>

<b>PP2.</b>	<b>Plant fibre cellulose polymer composites as a green alternative to conventional materials</b> <u>Ramlath K T</u> and Rajesh C	<b>75</b>
<b>PP3.</b>	<b>Salinity Stress Alters the Secondary Metabolites Production in <i>Abrus precatorius</i> L.</b> K.P. Lafna Farshana, P. Deepa, Shibla Banu	<b>85</b>
<b>PP4.</b>	<b>Studies on Structure and DNA interaction of Nickel(II) complexes of NO donor Schiff base</b> <u>Dr. Deepa K</u>	<b>101</b>
<b>PP5.</b>	<b>Assessment of water quality parameters of waterbodies in and near the paddy field</b> <u>Dr. Jyothi P</u>	<b>115</b>
<b>PP6.</b>	<b>Geopolymer materials: an eco-friendly next-generation alternative for construction industry</b> <u>Thasleena Panakkal</u> , Resha Kasim Vellattu Chola and Farsana Ozhukka Parambil	<b>131</b>
<b>PP7.</b>	<b>Chitosan-Cu Catalyzed Novel Ferrocenated Spiropyrrolidines: Green Synthesis, Single Crystal X-ray Diffraction, Hirshfeld Surface and antibacterial Studies.</b> Mohammad Asad, Muhammad Nadeem Arshad, Abdullah M. Asiri, <u>Snigdha. K</u> , Mohammed Musthafa T.N.	<b>133</b>
<b>PP8.</b>	<b>Adsorption characteristics of multivalent cations onto microplastic polymers from aqueous solutions</b> <u>Suhada Kottakuth Matayil</u> and Yamuna Kunhi Mouvenchery	<b>136</b>

## IL1.

### EMERGING TRENDS IN ANALYTICAL CHEMISTRY

*M. Krishnakumar*

*Chemistry Group, Atomic Minerals Directorate for Exploration and Research (AMD),*

*Department of Atomic Energy, Begumpet, Nagarbhavi, Bengaluru*

*Email: [krishnakumar.amd@gov.in](mailto:krishnakumar.amd@gov.in); Mobile: +91-8099003118*

Analytical Chemistry, an integral part of Chemical Sciences deals with obtaining, processing and communicating qualitative or quantitative information about the composition and structure of matter. It has played a major role in the discovery and separation of all the 118 known elements in the modern periodic table. The development and growth of nanotechnology to space-technology; environmental sciences to geochemistry and biochemistry to forensics are remarkably influenced by analytical methods.

The actual (true) value of an analyte in a sample can only be estimated to a reasonably good accuracy using the principles of chemistry, spectroscopy and statistics. Analytical sciences have evolved from classical methods to most modern instrumental methods. Modern trends include miniaturization of instruments (lab-on-a-chip concept) to big data analysis, machine learning and artificial intelligence based on IOT platforms. However, large thrust is given to developing Green analytical chemistry techniques considering the need for safeguarding the environment. The quality of analytical data generated is largely dependent on the validation of the method being developed and used. Use of matrix matched reference materials during the analysis is also being considered as a good laboratory practice (GLP). Reporting the measurement uncertainty (MU) of analysis results is another statutory requirement for accreditation of the laboratory by an international agency.

The quality of life on earth for humans is directly dependent on the availability of natural resources and technologies for its effective and optimal utilization. To transition from fast depleting fossil fuels to renewable energy sources require many minerals and materials. The exploration and exploitation and manufacturing of finished products are essentially supported by analytical chemistry. Accurate analysis of these complex



geomaterials is a very challenging task. The complete chemical characterization involves many steps from sampling to data analysis.

Analytical chemistry of Rare metals (RM) is an integral part of developing technologies based on U, Th, Li etc which are used directly as nuclear fuel or as their alloys for construction of nuclear reactor components. Lanthanides are important for nuclear and allied industries. Both of these materials have strategic importance in ensuring the safety and energy security of our country.



**Dr M. Krishnakumar**, joined Chemistry Group of Atomic Minerals Directorate for Exploration and Research (AMD), Department of Atomic Energy (DAE), Government of India after completing M. Sc Chemistry from University of Calicut and working as GATE-JRF at IIT Madras and CSIR-JRF at IIT Bombay. He has more than 22 years of research experience in geo-analytical chemistry and has broad research interests from Geomaterials to Green chemistry and Nanomaterials. He is a recognized PG Teacher of Homi Bhabha National Institute (HBNI), Mumbai, a Deemed to be University under DAE. He has published over 35 research articles in peer reviewed journals/seminars/symposia and has also co-authored two books. He is the recipient of DAE-Group Achievement Award-2016. He is also a life member of Indian Society of Analytical Scientists, Indian Nuclear Society and Association of Environmental Analytical Chemists of India.

## IL2.

### A GREEN GRAPHENE LABORATORY MOVEMENT LOG: FINALE TO HAZARDOUS AND TOXIC CHEMISTRY

Binitha N Narayanan<sup>1,\*</sup>

<sup>1</sup>Department of Chemistry, University of Calicut, Thenhipalam, Kerala, India

Ph: +91 4942407413, [\\*binithann@yahoo.co.in](mailto:*binithann@yahoo.co.in)

#### Abstract

Graphene is ideal for various applications because of its outstanding chemical and thermal resistance and excellent electron mobility. By virtue of the large surface area of graphene, various organic and inorganic materials can be dispersed over it effectively, resulting in the development of a range of nanocomposites with complementary features. Graphite oxide exfoliation is primarily used to aid in the commercial and economic manufacture of graphene (graphene oxide (GO)), but this GO is having organic functional groups in the matrix that disrupts its  $\pi$ -conjugation and thus the conductivity and stability. The use of graphene for biological and environmental applications is questionable by the hazardous chemicals and highly oxidising conditions utilised in GO production. So as to overcome the hurdles in graphene production, new movements are there towards the green and cost-effective means of graphene production via graphite exfoliation. Here, exploration of the new and eco-friendly modes of graphite peeling via chemical and physical means that are cost-effective and facile are targeted aiming for easy commercialization. A few significant applications are further explored with the goal of showcasing the significance of graphene to humankind.

#### References

1. Geim, A.K.; Novoselov, K.S. The rise of *graphene*. *Nat. Mat.* 2007, 6, 183-191.
2. Hummers, W.S.; Offeman, R.E. Preparation of Graphitic Oxide. *J. Am. Chem. Soc.* 1958, 80, 1339.

3. Zhu, Y.; Murali, S.; Cai, W.; Li, X.; Suk, J.W.; Potts, J.R.; Ruoff, R.S. Graphene and graphene oxide: Synthesis, properties, and applications. *Adv. Mater.* **2010**, *22*, 3906-3924.
4. S. Balasubramanyan, S. Sasidharan, R. Poovathinthodiyil, R. M. Ramakrishnan, and B. N. Narayanan, "Sucrose-mediated mechanical exfoliation of graphite: a green method for the large scale production of graphene and its application in catalytic reduction of 4-nitrophenol," *New J. Chem.*, **2017**, *41*, 11969.

IL3.

## SUPRAMOLECULAR MATERIALS FOR BIOLOGICAL APPLICATIONS

Roymon Joseph

*Department of Chemistry, University of Calicut, Thenhippalam, Kerala – 673635, INDIA*

*roy@uoc.ac.in*

Supramolecular systems functionalized with appropriate binding moieties are well-known receptors for ion/molecule sensing and excellent candidates for various biological applications.<sup>1</sup> Among various supramolecular systems, pillar[n]arenes and its derivatives have received much attention among the researchers, and these molecular systems are excellent host systems for the formation of inclusion complexes with various guest molecules which have relevance both in chemistry and biology.<sup>2</sup> Synthesis of water-soluble cationic pillararenes and its inhibition towards the formation of bacterial biofilms by clinically important Gram-positive pathogens will be discussed in the talk.



**Figure 1.** Structure of functionalized pillar[5]arene.



## References

- 1) (a) Wu, D.; Sedgwick, A. C.; Gunnlaugsson, T.; Akkaya, E. U.; Yoon, J.; James, T. D. *Chem. Soc. Rev.* **2017**, *46*, 7105–7123. (b) Joseph, R.; Rao, C. P. *Chem. Rev.* **2011**, *111*, 4658–4702.
- 2) (a) Uhlenheuer, D. A.; Petkau, K.; Brunsveld, L. *Chem. Soc. Rev.* **2010**, *39*, 2817–2826. (b) Joseph, R.; Naugolny A.; Feldman, M.; Herzog, I. M.; Fridman, M.; Cohen, Y. *J. Am. Chem. Soc.* **2016**, *138*, 754–757. (c) Joseph, R.; Kaizerman, D.; Herzog, I. M.; Hadar, M.; Feldman, M.; Fridman, M.; Cohen, Y. *Chem. Commun.* **2016**, *52*, 10656–10659.

**IL4.**

**PLASTIC POLLUTION IN WETLANDS**

Dr. Devi K.

Assistant Professor (C)

Department of Geology

Farook College (Autonomous) Kozhikode

Wetlands, one of the third major ecosystem on the earth, contribute nearly 40% of the ecosystem functions i.e., groundwater recharge, nutrient cycling and biogenic habitats. Wetlands are dangerously affected by plastic pollution with more than 800 marine and coastal species affected by this pollution through ingestion, entanglement and other dangers. World Environment Day 2023 focuses on #beatplasticpollution, globally the production is around 430 million tonnes of plastic a year, two-thirds of which are short-lived products which soon become waste. Plastic pollution can have devastating impacts on our ecosystems and wildlife, our health and well-being and the global economy. At least 5.25 trillion plastic particles are afloat in the world's oceans. Wetlands are often equated with waste grounds and used for litter and waste, and this ecosystem are being lost at alarming rate and it led to 4875 wetland dependent species being identified as threatened with extinction. An immediate action is needed to stop this loss. The talk will cover the basic idea of wetlands, their importance, how plastic pollution affects this ecosystem and our environment, the effect and remedies of plastic pollution.

## IL5.

# GLYCO-CONJUGATED FLUOROPHORES FOR BIOMEDICAL IMAGING

Shimi Manchery

Postdoctoral Fellow (SERB-NPDF) at IIT Palakkad, Kerala

### Abstract

Fluorescence imaging is an excellent tool for use in both fundamental scientific research and clinical practice. Most of the medical-imaging modalities used in clinical practice today fall under the category of tomographic imaging, which relies on deep-penetrating radiation to probe both structural and functional information of the imaged subject. Major limitations of the aforementioned tomographic imaging modalities include adverse effects to hazardous ionizing radiation (CT, PET and SPECT), intrinsically limited spatial resolutions (MRI and PET), reconstruction-dependent poor temporal resolution (CT, MRI, PET and SPECT) and lack of both exogenous and endogenous probes for molecular or functional imaging. In contrast, *in vivo* fluorescence-imaging doesn't suffer from the same drawbacks as tomographic imaging modalities, and instead provides the benefits of real-time wide-field image acquisition and diffraction-limited, spatial resolution in living organisms through the interaction of non-hazardous optical radiation with the many available fluorescent labels.

Fluorescent imaging technique is performed with the aid of a fluorophore tagged with a targeting ligand chemically or biologically to it. Most commonly used targeting ligands are biomolecules such as antibodies, proteins, amino acids and peptides which are amenable to structural modification. Carbohydrates are naturally abundant, eco-friendly, economical scaffolds which play a critical role in many biological events like cell-cell recognition, cell growth regulation, immune response, cancer cell metastasis, and also as energy source. But the structural modification of carbohydrates is a tiresome process mostly functionalization led to alteration in the structure and their binding properties. Therefore, fluorescently labeled glycans/ carbohydrates are less exploited and a challenging topic in the clinical diagnostics and chemical biology.

Almost a century ago, the German scientist Otto Warburg observed that cancerous tissues consume large amounts of glucose compared to non-transformed tissue and have

high rates of aerobic glycolysis. Today this phenomenon is known as the Warburg effect and is recognized as one of the hallmarks of cancer. Glycolytic enzymes, as well as the insulin-independent glucose transporter GLUT-1 are widely overexpressed in human cancers, and high expression levels of these proteins in tumor biopsy samples correlate with poor cancer prognosis, making them attractive therapeutic targets. Afterwards, large number of glyco-conjugated fluorophores have been developed for the tumour diagnosis and therapy.

### **Biodata**

Shimi Manchery received her BSc degree in Chemistry from Calicut University and MSc degree from Mahatma Gandhi University, Kerala. She completed PhD (Under the combined guidance of Dr. K. V. Radhakrishnan and Dr. Suresh Das) from CSIR-NIIST, Thiruvananthapuram, Kerala. Then, she worked as a Senior Research Fellow with Prof I. N. N. Namboothiri, IIT Bombay and as Research associate with Dr. Ravishankar L., CSIR-NIIST, Thiruvananthapuram. Currently she is a Postdoctoral Fellow (SERB-NPDF) at IIT Palakkad, Kerala.



## OP-1

### **Preparation, Characterization and Application of Styrene Butadiene Rubber (SBR)/ Zinc Sulfide (ZnS) Nanocomposite**

V.C Jasna\*

Assistant professor, PG Department of Chemistry,  
KAHM Unity Women's College, Manjeri, Kerala, India, 676122

Email: jasnavc@gmail.com

#### **Introduction**

Over the last few years, nanoparticles have fascinated the academic and industrial community. Nanocomposites, especially polymers as matrix-like elastomers lead to improved mechanical properties, flame retardancy, air, and liquid barrier properties coupled with dimensional and thermal stability. Since they have the potential to replace engineering materials, find use as excellent substitute in construction and automotive sectors. Among the broad variety of nanoparticles available for the development of elastomeric nanocomposites, nanoparticles having specific functional group are desirable due to their novel properties, which further widen their applications [1–4].

Even though, elastomers are good insulators, flexible dielectric composite materials with a high dielectric constant and low dielectric loss tangent are of immense interest at present. Their uses include application as charge storage capacitors, electrostriction artificial muscles and as a materials for controlled drug delivery. Metal oxides or metal sulfide nanoparticles are unique dielectric materials, having excellent thermal stability and therefore number of studies have been carried out to make the polymers thermally stable and conductive, by introducing metal nanoparticles [5,6]. Flame retardancy, thermal stability and electrical properties such as the AC conductivity, dielectric constant and dielectric loss tangent of a polymeric system depend on the nature and amount of metal nanoparticles [7,8]. The increase in AC conductivity of such nanocomposites stems from the formation of a continuous network of nanoparticles in the polymer matrix. These conductive nanocomposite materials are being widely applied in the area of electrostatic discharge dissipation, electro-magnetic interference shielding and other electronic applications [9–11].

Among the widely used synthetic elastomers, styrene-butadiene rubber (SBR) deserves a prominent place due to excellent abrasion resistance; thermal and aging stability. SBR is a major and unavoidable component of tyres, cables and insulating materials [12–14]. However, unfilled SBR has poor tensile strength, flame retardancy and oil resistance. The poor tensile strength is due to the absence of strain induced crystallisation and the highly amorphous nature of SBR. The mechanical properties can be improved by the reinforcement of SBR with filler particles, and the novel is by the incorporation of nanoparticles [15–17].

Polymer composites are widely used in the construction and automobile industries. In the automobile industry they serve as oil seals and gaskets. In order to have satisfactory performance, the oil seals should be thermally very stable [18]. During service if they subjected to excess temperature, the material may undergo thermal degradation and may become soft. Also the contact of these materials with industrial solvents/fuels results in leakage problems and failure in sealing. The study of sorption, diffusion, and permeation in elastomeric nanocomposite provides valuable information about the interaction of the components, the mobility of the chain, and the distribution of organic solvent molecules in polymeric compounds. This study is essential to the successful use of the elastomeric composites in a wide range of applications. The transport properties of nanocomposites strongly depends on the nature of the polymer, the nature of the penetrant, crosslink density and nature of crosslinks, temperature, and the polarity of the matrix [19]. Several works were carried out on the effect of nano-clay on the diffusion and sorption processes [20–22]. However, the studies on the transport of inorganic nanofillers with elastomers are few.

The main purpose of the work is to explore on the insertion of ZnS nanoparticles in SBR to study the interaction between ZnS and SBR and the diffusion and transport properties of SBR/ZnS. The effect of ZnS nanoparticles on the structural properties of SBR was investigated by FTIR and UV spectroscopy. Moreover, the structure and morphology of the composites were examined by XRD and SEM whereas the glass transition temperature and thermogravimetric analysis were examined by DSC and TGA. The diffusion and sorption behavior of both aromatic and industrial solvents through the cross-linked SBR nanocomposite were studied. The dielectric and mechanical properties of the nanocomposites were investigated with respect to various frequencies and volume fractions of nanoparticles.

## Results and Discussion

### FT-IR spectroscopy

**Figure 3.1** shows the FT-IR spectra of SBR, ZnS nanoparticles and SBR/ZnS nanocomposites. The characteristic absorption band of SBR is observed at  $2910\text{ cm}^{-1}$ , which arise from the CH stretching of phenyl ring. The band centered around  $1470\text{ cm}^{-1}$  from the C=C modes in the phenyl ring. The absorption at  $703\text{ cm}^{-1}$  is due to the out-of-plane aromatic ring. The *trans* -CH= mode of butadiene part appeared at  $989\text{ cm}^{-1}$  [23]. FT-IR spectrum of ZnS shows an absorption band centered at  $3483\text{ cm}^{-1}$ , which is attributed to the O-H stretching vibrations and the HO-H bending vibration (from atmospheric absorbed water) at  $1622\text{ cm}^{-1}$ . The main characteristic band of metal sulphide is observed as a broad and strong peak at  $615\text{ cm}^{-1}$ , which is the typical absorption of ZnS. The SBR/ZnS composite shows the characteristic absorption band of SBR with the typical stretching of metal sulphide. The typical ZnS vibration of composite appears at  $609\text{ cm}^{-1}$ , indicating the interaction of nanoparticles with the SBR matrix. Moreover, the stretching vibration of *trans* -CH= group ( $989\text{ cm}^{-1}$ ) in the composite shifts to a lower wave number region ( $976\text{ cm}^{-1}$ ). Hence, it can be inferred that the absorption frequencies of nanocomposite are strongly influenced by the insertion of nanoparticles into the elastomeric matrix [24].

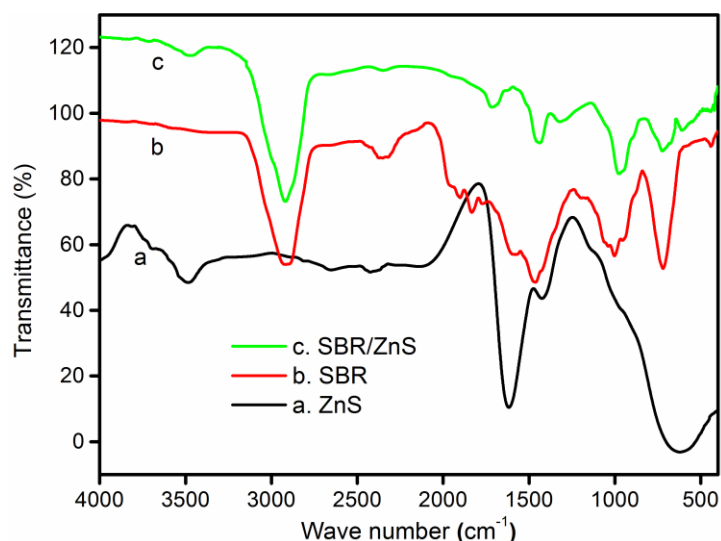


**Figure 3.1** FTIR spectra of SBR and ZnS filled SBR

## UV-Vis Spectra

**Figure 3.2** shows the optical properties of SBR and SBR with different contents of ZnS nanoparticles. SBR shows a sharp and prominent peak at 297 nm due to the  $\pi$ - $\pi^*$  transition of the polymer.

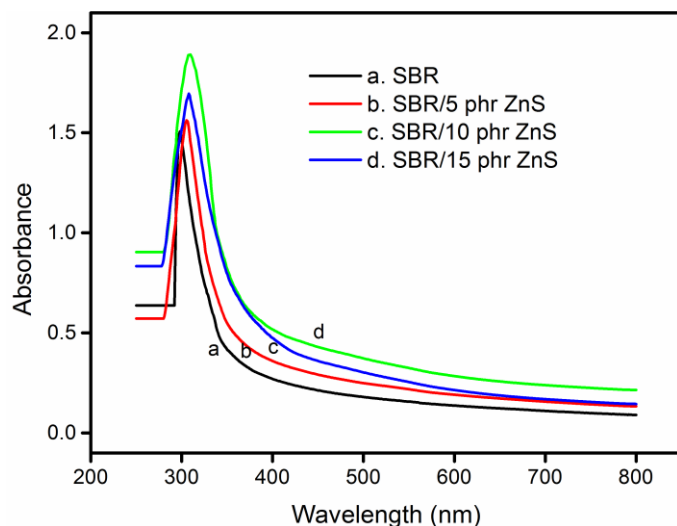


**Figure 3.2** UV spectra of SBR with different contents of ZnS nanoparticles

From the UV spectrum of nanocomposite, it can be seen that the characteristic peak of SBR is slightly shifted into a higher wavelength region and the intensity of the absorption peaks of all the composites are higher than that of pure SBR. For example, the sample with 10 phr loading shows a higher UV absorption peak at 309 nm. This suggests that the nanoparticles are uniformly dispersed into the elastomeric matrix which, in turn, increases the interfacial adhesion between the nanoparticles and the SBR chain. It can also be seen from the figure that the absorption edge of nanocomposite is higher than SBR in the entire range of UV absorbance from 200 to 800 nm. The intensity and broadness of the nanocomposite is found to be increasing with the addition of nanoparticles up to 10 phr loading. This means that the interfacial adhesion is the maximum at this loading. The lower absorption edge of the composite beyond 10 phr loading is due to the clustering of nanoparticles in the elastomer and this leads to the poor interaction in the polymer matrix.

## X-ray diffraction analysis (XRD)

XRD was used to probe the structure of SBR/ZnS nanocomposites and is displayed in **figure 3.3**. The XRD of ZnS (**Figure 3.3 (e)**) shows that the  $2\theta$  values at  $28.79^\circ$ ,  $48.23^\circ$  and  $56.97^\circ$  are the corresponding crystal plane of (111), (220), and (311) respectively

of the cubic phase of ZnS matching with JCPDF 80-0020. The XRD peaks are broadened due to nanocrystalline nature of the synthesised ZnS. No additional peaks are detected for impurities in the sample confirming the phase purity of the synthesised ZnS nanoparticles. The average crystallite size of the powder has been estimated automatically from corresponding XRD data using Scherrer formula,  $D=0.94\lambda/\beta\cos\theta$  and the average crystallite size is 2.9 nm. SBR shows a broad peak at  $2\theta = 20.17^\circ$  indicating its amorphous nature. It is evident from the figure that the amorphous peak is slightly shifted along with a decrease in the broadness of the peak than that of the corresponding position in pure SBR. For example, the diffraction of 15 phr composite is slightly shifted to a lower diffraction angle from  $2\theta = 20.17^\circ$  to  $18.76^\circ$ . The decrease in amorphous nature of SBR with the shift in diffraction angle is assigned to the strong interfacial interaction between the nanoparticles and the elastomeric chain. In order to obtain more structural information, the average crystallite size of ZnS nanoparticles in the composite is calculated from corresponding XRD data and the average size is 16.4 nm [25].

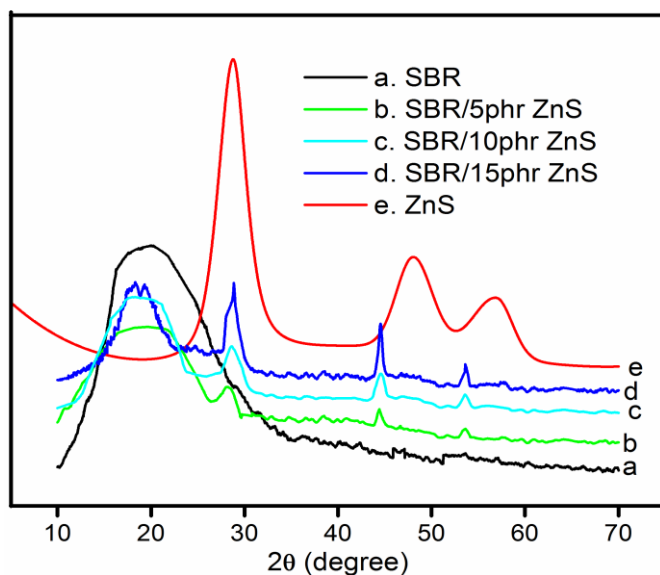


**Figure 3.3** XRD pattern of ZnS, SBR and different contents of ZnS filled SBR

### Scanning Electron Microscopy (SEM)

The morphological studies of SBR nanocomposite with different contents of ZnS nanoparticles are analysed by SEM and given in **figure 3.4**. The SEM image of SBR (**Figure 3.4 (a)**) presents a smooth and homogeneous structure. However, the inclusion of nanoparticles into the SBR matrix changes the surface morphology of the elastomer

composite [26,27]. From **figure 3.4 (b)**, it is clear that the sample with 10 phr of the ZnS particles containing SBR shows a uniform structure with several nanoparticles which are uniformly distributed. The change in the structural morphology of the composite is attributed to the strong interfacial interaction of the SBR phase with the nanoparticles. At 15 phr loading of the nanoparticles (**figure 3.4 (c)**), the surface morphology of the elastomeric composite changes drastically and shows some agglomeration of nanoparticles in the matrix.

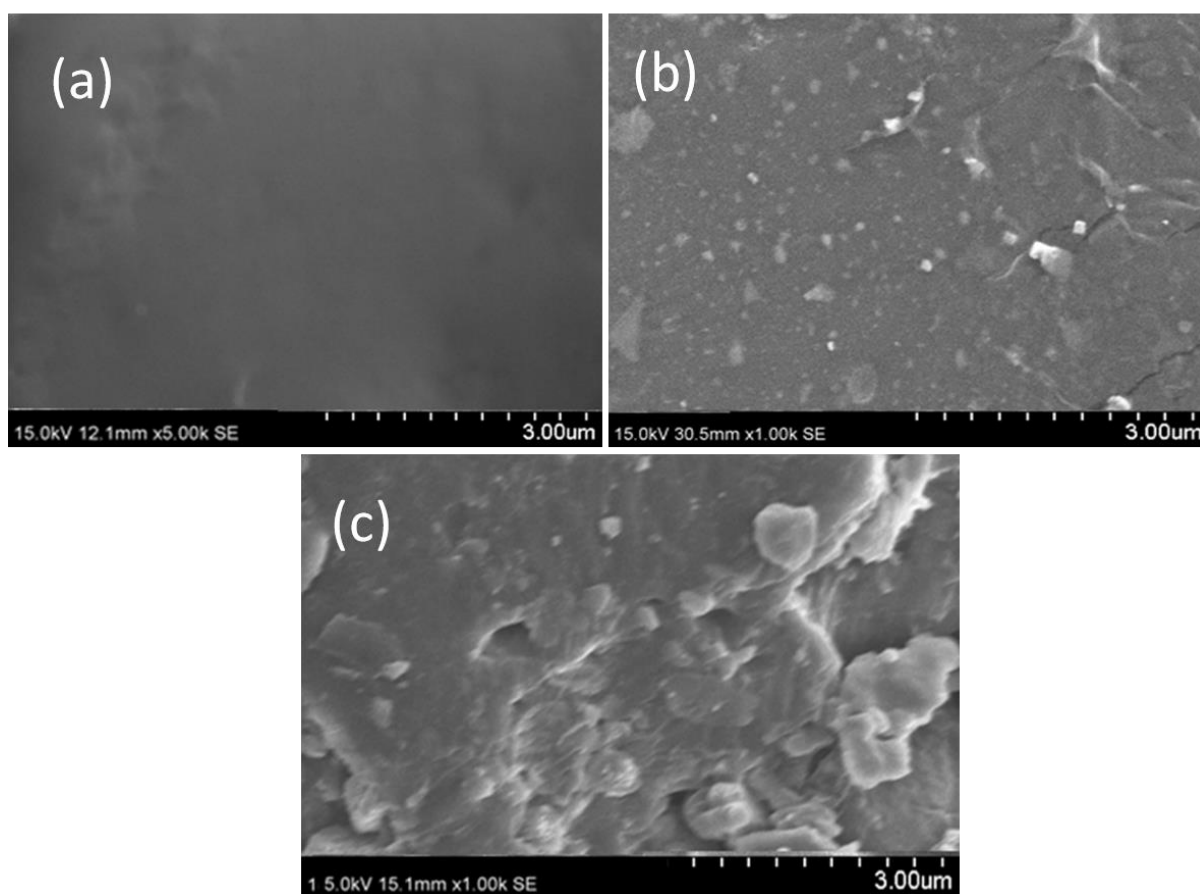


**Figure 3.4** SEM pictures of (a) SBR (b) SBR with 10 phr and (c) SBR with 15 phr ZnS nanoparticles

### Thermal properties

#### Differential scanning calorimetry (DSC)

The DSC profile of SBR and SBR/ZnS nanocomposite with 5, 10 and 15 phr of ZnS nanoparticles is given in **figure 3.5**. It can be seen that the glass transition temperature ( $T_g$ ) of SBR appears at  $-56\text{ }^\circ\text{C}$ . However, the  $T_g$  values of nanocomposite with 5, 10 and 15 phr loading of ZnS nanoparticles are observed at  $-54.2\text{ }^\circ\text{C}$ ,  $-51.3\text{ }^\circ\text{C}$ , and  $-49.1\text{ }^\circ\text{C}$ ,

respectively. Generally, the  $T_g$  of elastomeric composite depends on the mobility of the chain, polarity of polymer and filler particles, free volume, and the interaction between filler particles and the macromolecular chain. The high  $T_g$  values of nanocomposites, while increasing the loading of nanoparticles, are due to the interfacial interaction between nanoparticles and the macromolecular chain of SBR. In addition to this, the inter-particle distance is short at higher loading, which increases the immobile polymer chain and thereby leads to higher  $T_g$  values [28].

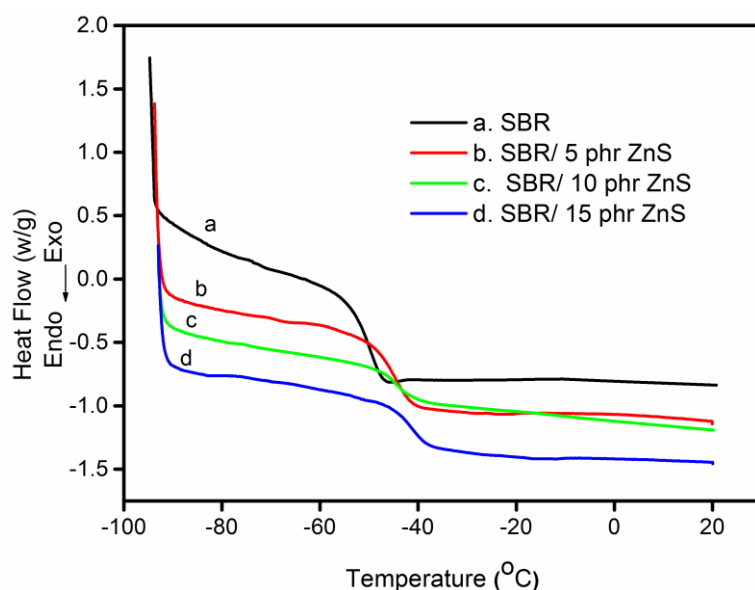


**Figure 3.5** DSC thermograms of SBR and SBR with different contents of ZnS nanoparticles

### Thermogravimetric analysis (TGA)

The thermal stability of neat SBR and the different contents of ZnS nanoparticles filled SBR at a heating rate of  $10\text{ }^{\circ}\text{C min}^{-1}$  is shown in **figure 3.6**. From the figure it can be seen that all samples shows a single step degradation. The onset degradation of SBR is at  $401^{\circ}\text{C}$  which ends around  $491^{\circ}\text{C}$ . The improved thermal stability of SBR/ ZnS nanocomposites is clear from the initial and final temperature of the thermograms. The higher thermal stability of nanocomposites with the increase in concentration of nanoparticle is due to the increased interfacial adhesion between the ZnS nanoparticles and the elastomeric chain. The nanoparticles with a large surface area can strongly reinforce the SBR matrix, producing a protective layer on the surface of SBR and thereby acquire excellent thermal stability. The char residue remaining at  $600\text{ }^{\circ}\text{C}$  is 9.61 % for the neat SBR. However, the composites with 5, 10 and 15 phr of nano-ZnS filled SBR show the residue of 14.62, 18.68 and 22.94% respectively at  $600\text{ }^{\circ}\text{C}$ . The char



layers act as a protective coating on the surface of nanocomposite, which prevents further burning. The higher char residue is an indication of the better thermal and flame resistance of the polymer matrix [29,30]. This broadens the utility of these materials in various applications.

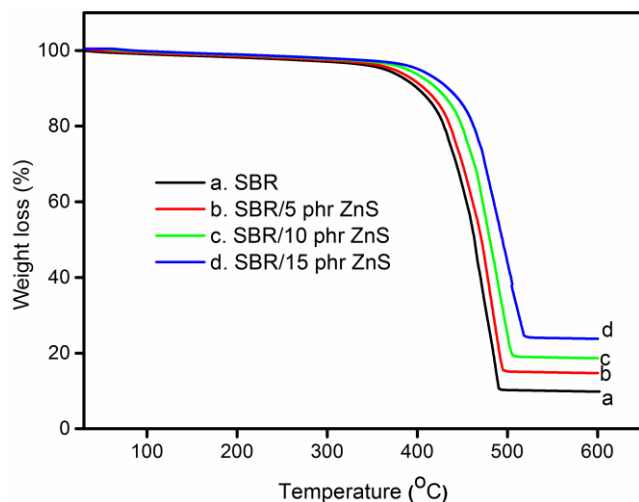


**Figure 3.6** TGA curves of SBR and SBR with different contents of ZnS nanoparticles  
**Cure characteristics**

The effect of loadings of ZnS nanoparticles on the rheometer processing characteristics such as cure time and torque values of SBR is presented in **table 3.1**. The scorch time and optimum cure time values decrease with the loading of ZnS nanoparticles in SBR. This shows that the rate of SBR curing increases with the addition of nanoparticles. This is advantages because it can enhance the production rate of elastomer products developed using these materials. As shown in **table 3.1**, the addition of nanoparticles significantly increases the minimum and maximum torque values. The increase in rheometric torque indicates a better polymer-filler interaction. Here the metal sulphide act as co-activators during the chemical vulcanization process, creating better linkages between the molecular chains of rubber by sulfur, which ultimately led to the increase in crosslinking. The composite with 10 phr sample shows the maximum torque value and beyond 10 phr loading, the torque value is found to decrease. At higher loading, greater stress develops in the elastomeric matrix which leads to poor crosslinks between the polymer and ZnS nanoparticles [23].

**Table 3.1** Processing characteristics of SBR and SBR with different loading of ZnS nanoparticles

Sample code	Cure time, $t_{90}$ (min)	Scorch time, $t_2$ (min)	Maximum torque (dNm)	Minimum torque (dNm)
SZ <sub>0</sub>	15.7	4.8	29	6.9
SZ <sub>3</sub>	15.3	4.6	32	7.5
SZ <sub>5</sub>	14.6	4.32	35	7.9
SZ <sub>7</sub>	14.1	4.05	37	8.0
SZ <sub>10</sub>	12.8	3.83	40	8.2
SZ <sub>15</sub>	12.3	3.55	38	8.1

### Mechanical properties

The mechanical properties of SBR nanocomposites namely tensile strength, modulus, elongation at break, tear resistance, hardness, abrasion loss, heat build-up and compression set were determined for all nano-filler loadings. The tensile strength, modulus (at 200% elongation) and tear resistance values are greater than pure SBR (**Table 3.2**). The variation in composite tensile properties is more pronounced at 10 phr loading. This means primarily that the nano- ZnS filler acts as a reinforcing filler in SBR and secondarily there is homogeneous dispersion of nanoparticles in the polymer matrix [31]. The slight decrease in tensile strength, modulus and tear strength observed at higher loadings (15 phr), may be due to the agglomeration of ZnS nanoparticles. This fact is supported by the SEM analyses discussed earlier in this work. The elongation at break (EB) given in **table 3.2** shows that the EB decreases with the loading of nanoparticles in all cases and it is well known that a decrease in EB is indicative of higher reinforcement by nanoparticles [19].

**Table 3.2** Mechanical properties of SBR and SBR with various contents of ZnS nanoparticles

Properties	Loading of ZnSnanoparticles (phr)					
	0	3	5	7	10	15
Tensile strength (MPa)	2.13	3.87	4.65	5.94	7.19	6.63
Elongation at break (%)	425	419	407	390	381	363
Modulus (300%)	1.94	2.94	4.21	5.19	6.99	5.88
Tear strength (kN/m)	18	23	26	29	32	30
Hardness (Shore A)	33	34	35	36	38	40
Heat build-up (°C)	10	10.5	11.9	12.8	14.3	15.8
Compression set (%)	19.8	19.2	18.32	17.44	16.9	16.3
Abrasion loss (mm <sup>3</sup> )	66.8	66.6	66.3	66.0	65.5	65.2

Durometer hardness is one of the most commonly used hardness tests for elastomeric materials; it assesses the material resistance to indentation and is widely employed in the elastomer industry. The hardness of the nanocomposite vulcanizates at different filler loadings is shown in **table 3.2**. A progressive increase in the hardness of composite can be seen with the increase in ZnS nanoparticle content, which is again due to the better interaction between SBR matrix and the nano-filler. Abrasion resistance is the material ability to resist the rubbing, scraping or erosion that tends to progressively remove material from its surface. The abrasion resistances of SBR vulcanizates with various loadings of nanoparticles are also given in the same table. The abrasion resistance of the composite increased with an increase in the nanoparticles

up to 10 phr loading. The voids or cracks at the growing tip of flaw are arrested by the nano-sized and crystalline ZnS particles which increases the abrasion resistance. The decrease in abrasion resistance beyond 10 phr loading of ZnS can be attributed to the poor interfacial interaction between SBR and the nanoparticles resulting from agglomeration of ZnS. The compression set measurement is used to measure the ability of elastomeric materials to maintain elastic properties even after prolonged compressive stress. Table 2 shows the compression set values of the SBR vulcanizates with different loadings of ZnS nanoparticles. Pure SBR has higher compression set values than nanocomposites and on increasing filler loading the compression set values decreases. A lower compression set is the key property for the rubber industry in sealing applications. Heat build-up is another important property of elastomers, arising from the internal friction in the compounds. From **table 3.2**, it is clear that the heat build-up of the elastomeric composite enhances with the amount of ZnS nanoparticles and this is mainly due to the higher internal friction resulting from more extensive crosslinking and improved thermal conductivity of the nanocomposites. The magnitude of the increase in heat build-up is higher at 15 phr ZnS loading. The reinforcing effect and higher thermal conductivity of metal sulphide filled compounds is responsible for the high heat build-up value.

### **Conductivity studies**

#### **AC conductivity**

The AC conductivity of various concentrations of nano-ZnS filled SBR and unfilled SBR at different frequencies at room temperature is given in **figure 3.7**. The SBR shows minimum electrical conductivity than that of the metal sulphide nanoparticles filled SBR. Owing to the highly amorphous nature of SBR (confirmed from XRD analysis), the macromolecular chains are randomly oriented in the SBR matrix. Therefore, the linkages through grain boundaries are poor, leading to the lower electrical conductivity of the elastomer. The AC conductivity increases continuously with an increase in frequencies for all the samples. This is due to the rapid transport of hopping charge carriers within the polymer matrix and its composites. From the figure, it can be seen that the AC conductivity of the composite greatly increases with the addition of nanoparticles; the composite with 10 phr filler shows the maximum AC conductivity. This indicates the strong interfacial interactions between the ZnS nano-filler particles and the SBR matrix. The interfacial interaction changes the molecular orientation of

SBR from a randomly oriented conformation to a well-defined compact structure. It may also be noted that the bulk conductivity of nanocomposites depends on the loading of fillers, filler-rubber adhesion and uniform dispersion of nanoparticles within the polymer matrix [32]. However at a higher concentration of nanoparticles (15 phr) the interfacial adhesion between the polymer and filler decreases due to the high aggregating tendency of nanoparticles. This breaks the formation of effective conducting chains of ZnS nanoparticles and therefore the conductivity is lower at a higher concentration of nanoparticles.

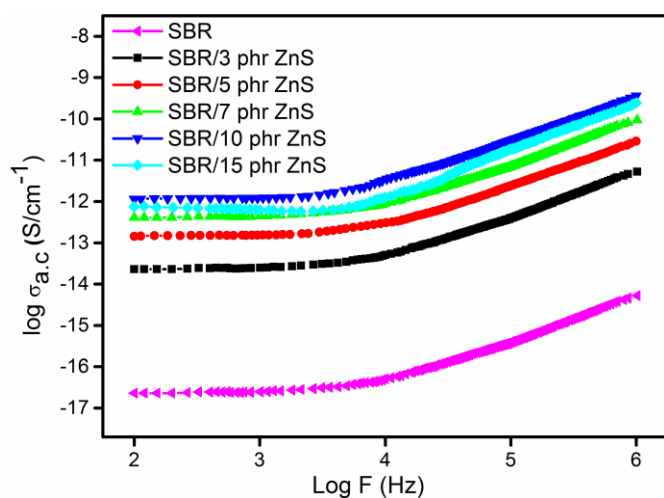


**Figure 3.7** AC conductivity of SBR and SBR with different contents of ZnS nanoparticles

### Dielectric constant

**Figure 3.8** shows the variation of dielectric constant with the frequency of SBR and different loading of ZnS nanoparticles containing SBR. The dielectric constant of polymeric material is directly related to the polarizability of the materials and the interfacial interactions. Also, the presence of aromatic ring, zinc, nitrogen, and sulphur is considered as highly polarisable by the application of an electric field. The dielectric constant of all the composites continuously decreases with an increase in frequency. This is attributed to the tendency of dipoles to orient themselves in the direction of the applied field. The dielectric constant of all the nanocomposites is higher than that of SBR in the entire range of frequencies. In the present study, the higher dielectric constant of the composite is due to the enhanced interfacial interaction between the nanoparticles and the presence of aromatic ring in SBR [33]. The dielectric property of the composite is found to be increasing with the loading of nanoparticles up to 10 phr.

When the concentration of nanoparticles reaches to 15 phr, the dielectric constant is found to be decreasing. The poor dielectric constant of nanocomposite at higher loading is due to the generation of more and more clusters in the elastomeric matrix (as evident from the UV study).

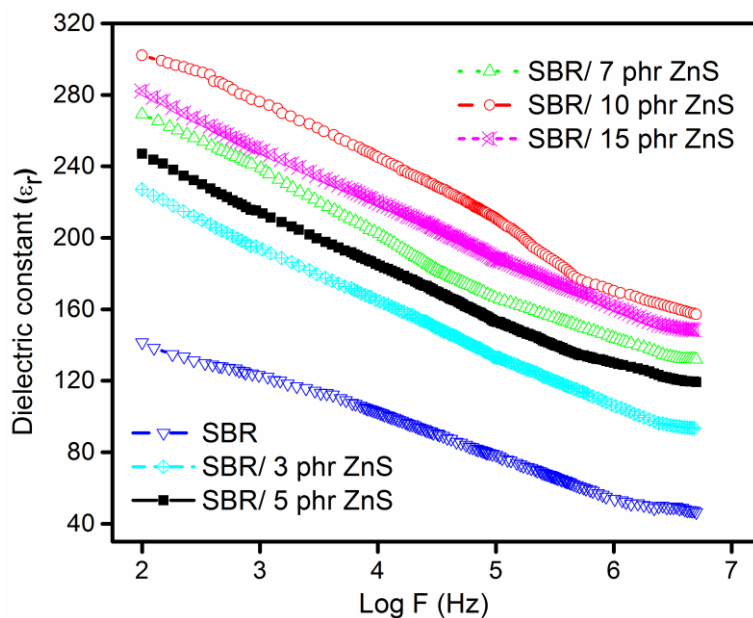


Figure 6

**Figure 3.8** Dielectric constant of SBR and different contents of nano-ZnS filled SBR

### Dielectric loss ( $\tan \delta$ )

Dielectric loss tangent ( $\tan \delta$ ) is the ratio of the electrical energy dissipated in a material to the total power in a circuit. **Figure 3.9** shows the variation of the dielectric loss tangent ( $\tan \delta$ ) as a function of frequency ranging from 100-10<sup>6</sup> Hz of SBR and SBR-ZnS nanocomposites at room temperature. It is observed that the  $\tan \delta$  of composite with different contents of **nano-filler** is higher than that of pure SBR. It is evident that dielectric loss of all the samples decreases steadily with the frequency and reaches a constant  $\tan \delta$  value at 10<sup>4</sup> Hz. This is due to the time lag associated with the orientation of dipoles within the polymer matrix. The  $\tan \delta$  values of SBR/ ZnS nanocomposite is greater than that of the pure SBR. The nanoparticles present in the macromolecular chain of SBR increases the interactions between the components, leading to field distortions and thus an increase in dielectric loss. It is interesting to note that a higher dielectric loss is observed for 10 phr of ZnS, which might be due to the large surface area, surface domain polarisation and the effective electrical network formation [11]. The dielectric loss of the 15 phr loading is lower than that of 10 phr

loaded composite. This is due to the formation of clusters or discrete aggregates in the SBR matrix, which prevents charge carriers from migrating through the elastomeric system.

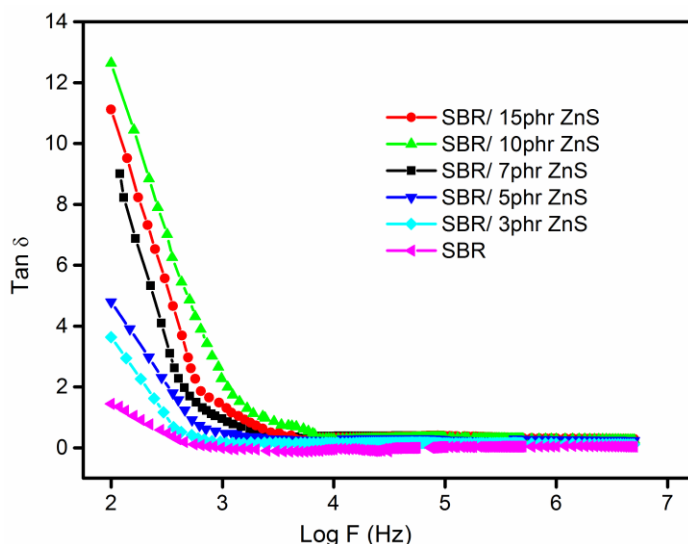


**Figure 3.9** Dielectric loss tangent of SBR and different contents of nano-ZnS filled SBR

### Analysis of swelling data of aromatic and industrial solvents

#### Mol % uptake

The mole % uptake of aromatic solvents through SBR/ZnS nanocomposite is studied at room temperature and the mole% uptake of solvent ( $Q_t$ ) was calculated from the **equation 3.1**.

$$Q_t(\text{mol}\%) = \frac{\text{mass of solvent sorbed/molecular weight of penetrant}}{\text{initial weight of polymer sample}} \times 100 \quad (\text{Eq: 3.1})$$

The mol % uptake ( $Q_t$  %) was plotted against square root of time ( $\sqrt{t}$ ) in order to get diffusion curves with special reference to the effect of filler loading, effect of solvent and effect of temperature.

#### Effect of filler loading

The mole % uptakes of benzene and petrol through the SBR with different loading of ZnS nanoparticles are given in **figures 3.10** and **3.11** respectively. It is clear from the figures that the mole uptake progresses first; then it reaches equilibrium and finally becomes constant. It can be seen that, on increasing the ZnS concentrations, the equilibrium sorption decreases and the minimum solvent uptake is observed for the nanocomposite with 10phr of ZnS. This indicates a better polymer-filler interaction,



which in turn leads to the decreased flexibility of the polymer chain and the nanocomposite becomes less permeable [34]. On adding filler to the matrix, the free volume inside the matrix decreased, which restricts the free movement of solvent inside the matrix. Thus, upon reinforcement with the filler, the solvent resistance also increases. A better distribution of nanoparticles in the matrix causes an increased surface area of the reinforcing phase, which is the reason for the higher solvent resistance of 10 phr of the composite. However, it is found that, upon further addition of ZnS nanoparticles (above 10 phr), the mole uptake again increases due to the decreased filler-matrix interaction, which leads to the agglomeration of nanoparticles in the SBR matrix. Sorption experiments are found in a similar trend in other two aromatic (toluene and xylene) and industrial (kerosene and diesel) solvents.

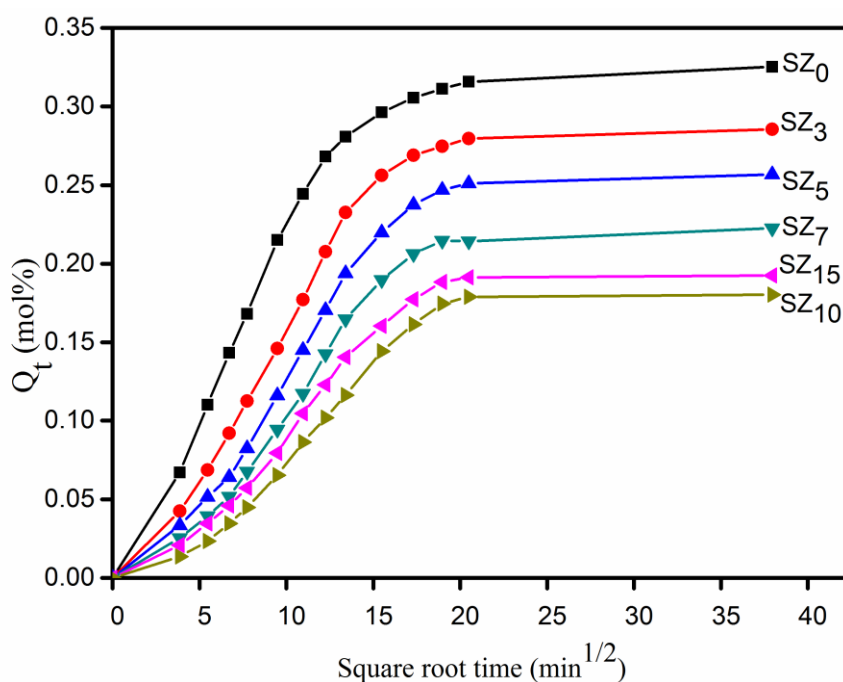


**Figure 3.10** mol % uptake of SBR and different contents of nano-ZnS filled SBR in benzene

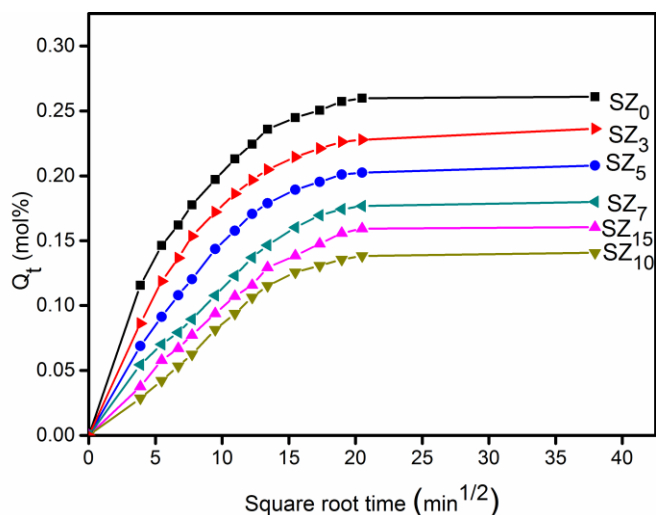


**Figure 3.11** mol % uptake of SBR and different contents of nano-ZnS filled SBR in petrol

### *Effect of penetrant size*

The nature of the solvent also affects the mole uptake of the nanocomposite. The transport properties of SBR/ ZnS nanocomposites with 10 phr of ZnS nanoparticles in homologous series of both aromatic and industrial solvents are shown in **figure 3.12** and **3.13** respectively. From the figure it is evident that on increasing solvent density/penetrant size benzene showed highest mol uptake and xylene showed the lowest and the decreasing order is benzene > toluene > xylene. In the case of industrial solvents the order is petrol > kerosene > diesel.

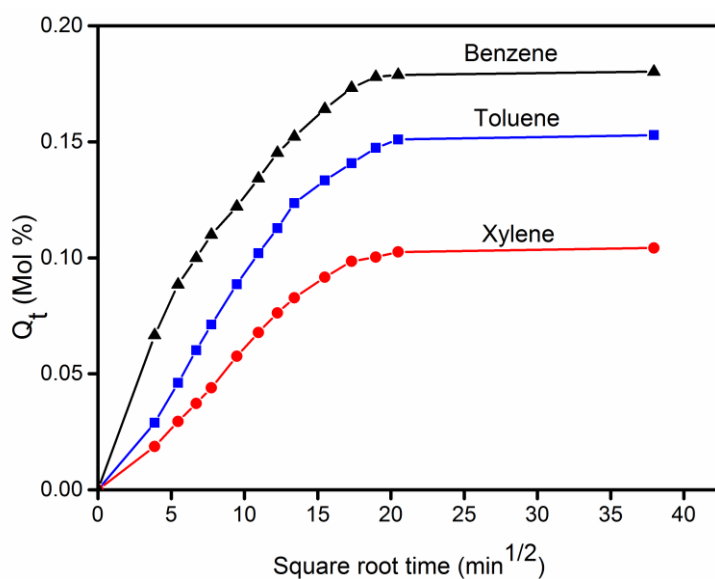


**Figure 3.12** Solvent uptake of SBR with 10 phr of ZnS in different aromatic solvents

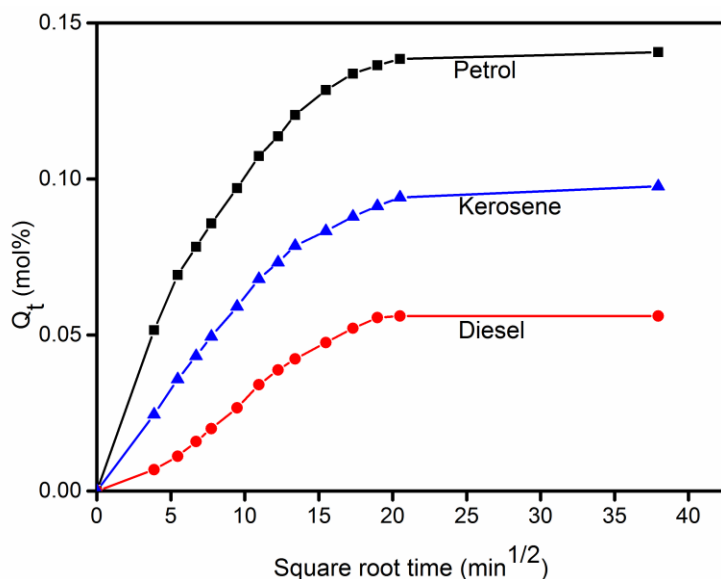


**Figure 3.13** Solvent uptake of SBR with 10 phr of ZnS in different industrial solvents. The decrease in solvent uptake on increasing molar volume is reported by many researches. On increasing the molar volume, it needs more space and the exchange become very difficult. It is well established from free volume theory that the increased molar volume will impart restriction on the solvent to enter into the polymer matrix and high activation energy is needed for large molecules to penetrate [35].

***Temperature dependence on sorption and diffusion of solvents***

The effect of temperature on transport properties of composite is analyzed at different temperatures such as 50 and 70 °C for aromatic solvents and 40 and 50 °C for industrial solvents. **Figure 3.14** depicts the effect of temperature on solvent uptake for SBR/ZnS nanocomposite in benzene and **figure 3.15** in petrol at different temperatures. It can be seen that the solvent uptake of 10 phr nanocomposite is found to be increasing with the temperature. This is mainly due to the increased segmental mobility; as a result, the free volume inside the matrix increases. This again causes the kinetic energy inside the polymer chain to rise [36]. Similar trend is observed for all the samples in all solvents.

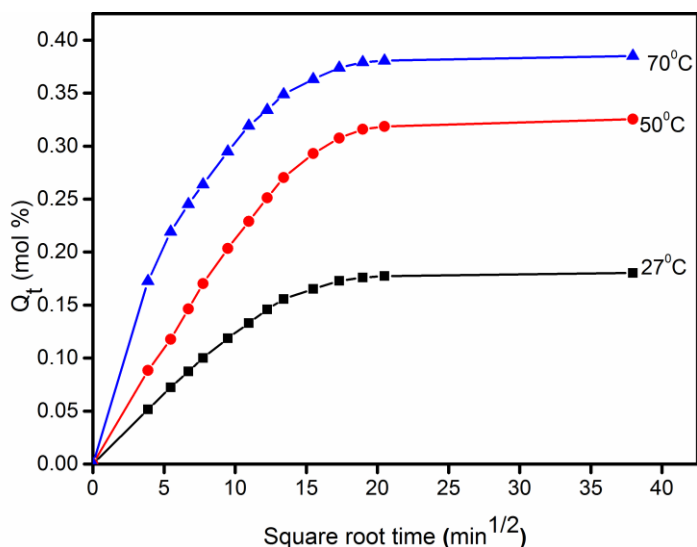


**Figure 3.14** The  $Q_t$  (mol %) of SBR /10 phr of ZnS in benzene at 27, 50 and 70 °C

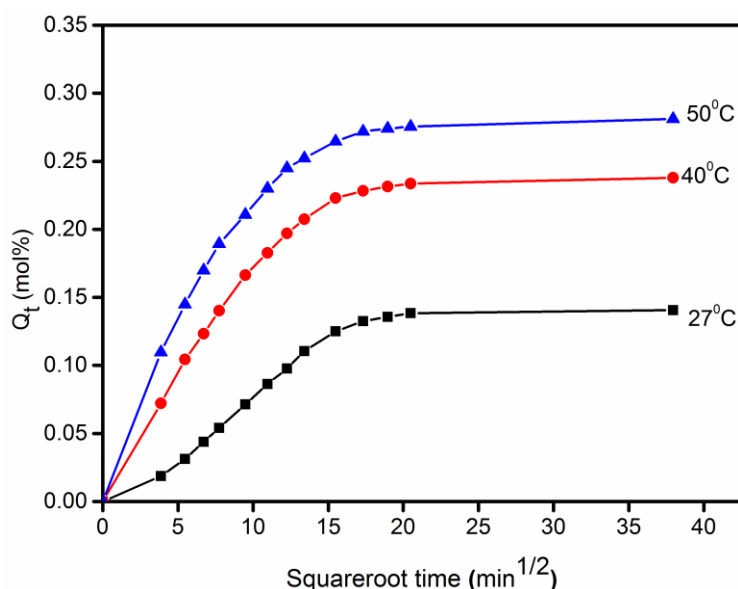


**Figure 3.15** The  $Q_t$  (mol %) of SBR and SBR /10 phr of ZnS in petrol at 27, 40 and 50 °C

### Diffusion (D), sorption (S) and permeation (P) coefficients

The diffusion coefficient (D) is a kinetic parameter, on the basis of segmental mobility which controls diffusion rate. It is calculated using the **equation 3.2**

$$D = \pi \left( \frac{h\theta}{4Q_\infty} \right)^2 \quad \text{(Eq: 3.2)}$$

Where h is the thickness of the sample,  $\theta$  is the slope of the initial linear region of plot of  $Q_t$  versus the square root time and  $Q_\infty$  is the equilibrium mol uptake. **Table 3.3** and

**3.4** clearly demonstrate that the investigations are done for all samples in all three aromatic and industrial solvents. The D values decrease with an increase in concentration of the ZnS nanoparticles up to 10 phr loading. The lowest value of the diffusion coefficient is observed for 10 phr of ZnS containing composite. This is due to the strong interfacial adhesion between the elastomer and nanoparticles. The D value increases upon further addition of filler to the matrix beyond 10 phr. This is because of the agglomeration of nanoparticles cause a decreased interfacial interaction and non-uniform distribution of ZnS filler particles in polymer matrix. Upon increase of penetrant size, diffusivity decreases, petrol shows a higher D value and diesel shows the lowest D value. This is explained on the basis of the free volume theory in terms of the effect of solvent on the mole % uptake of solvent [37,38].

**Table 3.3.** D, S and P values of SBR/ ZnS nanocomposites in aromatic solvents

Sampl es	Diffusion coefficient			Sorption coefficient			Permeation coefficient		
	D x 10 <sup>5</sup> (cm <sup>2</sup> /s)			S (mol %)			P x 10 <sup>5</sup> (cm <sup>2</sup> /s)		
	Benzen e	Toluen e	Xylen e	Benzen e	Toluen e	Xylen e	Benzen e	Toluen e	Xylen e
S <sub>0</sub>	1.81	1.67	1.42	1.20	1.16	1.13	2.17	1.93	1.60
SZ <sub>3</sub>	1.79	1.61	1.39	1.18	1.14	1.11	2.11	1.83	1.54
SZ <sub>5</sub>	1.77	1.55	1.31	1.17	1.12	1.09	2.07	1.74	1.43
SZ <sub>7</sub>	1.73	1.52	1.22	1.15	1.09	1.06	1.98	1.65	1.29
SZ <sub>10</sub>	1.54	1.37	1.09	1.11	1.05	1.01	1.71	1.43	1.10
SZ <sub>15</sub>	1.67	1.44	1.13	1.13	1.07	1.03	1.88	1.54	1.16

**Table 3.4** D, S and P values of SBR/ ZnS nanocomposites in Industrial solvents

Sample s	Diffusion coefficient			Sorption coefficient			Permeation coefficient		
	D x 10 <sup>5</sup> (cm <sup>2</sup> /s)			S (mol %)			P x 10 <sup>5</sup> (cm <sup>2</sup> /s)		
	Petro l	Kerosen e	Diese l	Petro l	Kerosen e	Diese l	Petro l	Kerosen e	Diese l
SZ <sub>0</sub>	1.51	1.36	1.25	1.21	1.17	1.14	1.81	1.59	1.42
SZ <sub>3</sub>	1.38	1.24	1.18	1.19	1.13	1.11	1.64	1.40	1.31

S Z <sub>5</sub>	1.34	1.18	1.13	1.11	1.07	1.06	1.48	1.26	1.19
SZ <sub>7</sub>	1.19	1.13	1.11	1.09	1.03	1.01	1.29	1.16	1.12
SZ <sub>10</sub>	1.11	0.94	0.88	1.01	0.92	0.88	1.21	0.86	0.77
SZ <sub>15</sub>	1.14	1.06	1.03	1.07	0.98	0.95	1.22	1.03	0.97

This study observed that the sorption, diffusion and permeation coefficients are highest for petrol and lowest for diesel and intermediate for kerosene. It is explained that smaller molecules will diffuse and get accommodated more easily into the polymer matrix, due to steric reasons. The decreased sorption values upon increased nano-filler loading can be explained by the fact that the reinforcing materials create obstacles for the penetrating molecules. The bigger the penetrant molecule, the stronger the resistance and hence less will be the penetrant uptake. The Permeation coefficient is the combined effect of the diffusion and sorption coefficients. i.e.,  $P=D.S$ , the measure of the amount of solvent that permeated per unit area of the sample in one second. Hence it shows a trend similar to that of D and S.

### The transport mechanism

The mechanism of transport can be explained from the **equation 3.3**

$$\log \frac{Q_t}{Q_\infty} = \log k + n \log t \quad \text{(Eq: 3.3)}$$

Where  $Q_t$  and  $Q_\infty$  are the mol % sorption at time  $t$  and at equilibrium respectively,  $k$  indicates the interaction between the penetrant and the polymer and  $n$  represents the mode of transport. On regression analysis of  $\log \frac{Q_t}{Q_\infty}$  and  $\log t$  the values of  $n$  and  $k$  are obtained for aromatic and industrial solvents and these values are given **table 3.5** and **3.6** respectively. From the table it is clear that the value of  $n$  is found to be no Fickian first and then on increasing filler loading and solvent size it comes above 0.6 and is nearest to 1. This indicates an anomalous mode of transport and is mainly due to the comparable diffusivity and chain relaxation [39]. The increased swelling stress due to reinforcement is also another reason for the anomalous mode of transport. The value of  $k$  proves the structural properties and the increased polymer filler interaction. Generally, the value of  $k$  decreases when the distribution of the nanoparticles in the matrix increases. Here, the lowest value for  $k$  is noted for 10 phr composite. Upon

increasing the penetrant's size, the interaction becomes less and therefore the value of k increases.

**Table 3.5** n and k values of SBR/ZnS with different filler loading in aromatic solvents at room temperature

Samples	Benzene		Toluene		Xylene	
	n	Kx10 <sup>2</sup> (min <sup>-1</sup> )	n	kx10 <sup>2</sup> (min <sup>-1</sup> )	n	Kx10 <sup>2</sup> (min <sup>-1</sup> )
S <sub>0</sub>	0.51	0.24	0.59	0.15	0.69	0.13
SZ <sub>3</sub>	0.53	0.19	0.66	0.13	0.77	0.11
SZ <sub>5</sub>	0.59	0.17	0.73	0.11	0.81	0.11
SZ <sub>7</sub>	0.67	0.14	0.77	0.10	0.84	0.12
SZ <sub>10</sub>	0.73	0.11	0.83	0.08	0.88	0.07
SZ <sub>15</sub>	0.69	0.13	0.79	0.09	0.85	0.11

**Table 3.6** n and k values of SBR/ZnS with different filler loading in industrial solvents at room temperature

Samples	Petrol		Kerosene		Diesel	
	n	Kx10 <sup>2</sup> (min <sup>-1</sup> )	n	kx10 <sup>2</sup> (min <sup>-1</sup> )	n	Kx10 <sup>2</sup> (min <sup>-1</sup> )
SZ <sub>0</sub>	0.37	0.28	0.49	0.26	0.52	0.22
SZ <sub>3</sub>	0.45	0.29	0.56	0.24	0.66	0.21
SZ <sub>5</sub>	0.67	0.21	0.62	0.19	0.68	0.17
SZ <sub>7</sub>	0.69	0.19	0.66	0.16	0.71	0.14
SZ <sub>10</sub>	0.77	0.13	0.79	0.12	0.83	0.11
SZ <sub>15</sub>	0.75	0.15	0.66	0.17	0.72	0.12

### Activation energy of diffusion (E<sub>D</sub>) and permeation (E<sub>P</sub>)

The activation energy of sorption can be calculated from the Arrhenius **equation 3.4**

$$X = X_0 \exp\left(\frac{-E_X}{RT}\right) \quad (\text{Eq: 3.4})$$

Where X is D or P, and X<sub>0</sub> is D<sub>0</sub> or P<sub>0</sub>. E<sub>x</sub> is the activation energy from the plots of log D or logP against 1/T. From the slopes of the curves, the Arrhenius parameters for the samples in aromatic and industrial solvents are obtained and are given in **table 3.7** and **3.8**.

**Table 3.7** E<sub>D</sub>, and E<sub>P</sub> values of SBR-ZnS nanocomposites in aromatic solvents



Samples	Benzene		Toluene		Xylene	
	E <sub>P</sub>	E <sub>D</sub>	E <sub>P</sub>	E <sub>D</sub>	E <sub>P</sub>	E <sub>D</sub>
S <sub>0</sub>	6.16	4.97	6.39	5.22	6.62	5.43
SZ <sub>3</sub>	6.29	5.21	6.51	5.32	6.77	5.51
SZ <sub>5</sub>	6.43	5.29	6.62	5.44	6.86	5.57
SZ <sub>7</sub>	6.47	5.38	6.64	5.51	6.89	5.62
SZ <sub>10</sub>	6.54	5.51	6.75	5.67	6.95	5.69
SZ <sub>15</sub>	6.51	5.44	6.68	5.58	6.90	5.64

The activation energy of diffusion and permeation is found to be increasing with the loading of nanoparticles (**Table 3.7** and **3.8**). The free space in the matrix decreases with increasing filler loading and therefore more energy is needed to obtain free space. Also, on increasing the penetrant's size, the difficulty to enter into the matrix increases and E<sub>P</sub> and E<sub>D</sub> values increase [40]. Also, the maximum value is for 10 phr composite. A further addition of nanoparticles lowers the activation energy. This is due to the agglomeration of nanoparticles on the surface of polymer or to the decreased interfacial interaction between the rubber and nanoparticles.

**Table 3.8** E<sub>D</sub> and E<sub>P</sub> (kJ mol<sup>-1</sup>) values of SBR/ZnS nanocomposites in different industrial solvents

Samples	Petrol			Kerosene			Diesel		
	E <sub>D</sub>	E <sub>P</sub>	ΔH	E <sub>D</sub>	E <sub>P</sub>	ΔH	E <sub>D</sub>	E <sub>P</sub>	ΔH
SZ <sub>0</sub>	3.59	4.22	0.63	3.97	4.72	0.75	4.62	5.46	0.84
SZ <sub>3</sub>	4.49	5.41	0.92	4.54	5.65	1.11	4.63	6.15	1.52
SZ <sub>5</sub>	5.92	7.07	1.15	6.18	7.44	1.26	7.08	8.89	1.81
SZ <sub>7</sub>	6.08	7.29	1.21	6.32	7.69	1.37	7.19	9.09	1.9
SZ <sub>10</sub>	6.29	7.54	1.25	6.49	8.36	1.87	7.59	9.64	2.05
SZ <sub>15</sub>	6.16	7.39	1.23	6.39	7.88	1.49	7.29	9.23	1.94

### Thermodynamic parameters

Thermodynamic parameters such as ΔH<sub>s</sub> and ΔS<sub>s</sub> can be obtained from Van't Hoff's **equation 3.5**

$$\log K_s = \frac{\Delta S_s}{2.303R} - \frac{\Delta H_s}{2.303RT} \quad (\text{Eq: 3.5})$$

Where  $K_s$  is the equilibrium sorption constant, which is the ratio of the number of moles of solvent sorbed at equilibrium to the mass of the polymer sample. On regression analysis of  $\log K_s$  against  $1/T$ , the values of  $\Delta H$  and  $\Delta S$  are obtained. The thermodynamic properties of SBR and SBR/ZnS composites in aromatic (benzene, toluene and xylene) solvents are given in **table 3.9** while **table 3.10** depicts the thermodynamic parameters of SBR/ZnS in industrial solvents.

**Table 3.9**  $\Delta H$ ,  $\Delta S$  and  $\Delta G$  of SBR- ZnS nanocomposites in aromatic solvents

Samples	$\Delta H(\text{J/mol})$			$\Delta S(\text{J/mol/K})$			$-\Delta G(\text{J/mol})$		
	Benzene	Toluene	Xylene	Benzene	Toluene	Xylene	Benzene	Toluene	Xylene
S <sub>0</sub>	0.871	0.884	0.896	0.071	0.058	0.052	20.43	16.51	14.70
SZ <sub>3</sub>	0.877	0.889	0.902	0.068	0.054	0.044	19.52	15.31	12.29
SZ <sub>5</sub>	0.882	0.894	0.907	0.065	0.051	0.042	18.61	14.41	11.69
SZ <sub>7</sub>	0.889	0.899	0.914	0.061	0.048	0.038	17.41	13.50	10.48
SZ <sub>10</sub>	0.899	0.912	0.921	0.055	0.041	0.031	15.60	11.39	8.37
SZ <sub>15</sub>	0.891	0.903	0.917	0.059	0.044	0.034	16.81	12.29	9.28

The positive  $\Delta H$  value proves the sorption is endothermic. Sorption will occur only by the creation of free space inside the matrix [41]. The reduced entropy on adding filler is due to the decreased interfacial interaction, and is lower in benzene at 10 phr. The value of  $\Delta G$  also increases upon reinforcement. Among the nanocomposites, 10 phr composite shows the minimum spontaneous sorption which indicates a better interaction between the nanoparticles and the SBR matrix.

**Table 3.10**  $\Delta H$ ,  $\Delta S$  and  $\Delta G$  ( $\text{kJ mol}^{-1}$ ) values of SBR/ZnS nanocomposites in industrial solvents

Samples	$\Delta H$			$\Delta S$			$-\Delta G$		
	Petrol	Kerosene	Diesel	Petrol	Kerosene	Diesel	Petrol	Kerosene	Diesel
SZ <sub>0</sub>	0.635	0.758	0.848	0.068	0.048	0.042	19.77	13.64	11.752
SZ <sub>3</sub>	0.927	1.117	1.527	0.058	0.044	0.039	16.47	12.08	10.173

SZ <sub>5</sub>	1.158	1.268	1.81 7	0.047	0.032	0.029	12.94	8.332	6.883
SZ <sub>7</sub>	1.217	1.378	1.97 9	0.043	0.029	0.022	11.68	7.322	4.621
SZ <sub>10</sub>	1.258	1.879	2.05 9	0.029	0.024	0.014	7.44	5.321	2.141
SZ <sub>15</sub>	1.239	1.497	1.94 6	0.037	0.026	0.017	9.86	6.303	3.154

## Conclusions

The SBR/ZnS nanocomposites were prepared using a simple and environmentally-friendly two-roll mill mixing technique. The composites were characterized by FT-IR, UV, XRD, SEM, DSC, conductivity, and solvent penetration studies. The interaction of nanoparticles with SBR was confirmed from the spectroscopic studies through the shift in absorption peaks of the nanocomposite. The XRD showed the ordered arrangement of filler particles in SBR and the amorphous nature of composite decreased with an increase in content of nanoparticles. The SEM images showed a uniform dispersion of the fillers in SBR. The glass transition temperature of the composites increased with the loading of metal sulphide nanoparticles. TGA results showed increase in thermal stability of nanocomposites upon increasing filler content. The dielectric constant continuously decreased with an increase in frequency for all the systems. The processability, mechanical properties, thermal stability, electrical conductivity and transport behaviour of SBR/ZnS nanocomposites were investigated. Despite the reduction in scorch safety, the compounded SBR/ZnS samples indicated higher production rate resulting from lowering of optimum cure time. Presence of ZnS nanoparticles reduced the amorphous nature of SBR, which is complementary to the enhancement in overall mechanical performance of the composites. A general trend noted was the regular improvement in mechanical properties up to 10 phr loading of ZnS, which dropped with further additions. Mechanical properties such as tensile, tear strength, modulus, hardness, abrasion resistance, heat build-up and compression set were in agreement with the reinforcement by ZnS particles. This is advantages because elastomer nanocomposite with improved mechanical properties tends to be highly performing and durable in service life. Mechanical properties were also supported by the filler distribution analysed by SEM and diffusion studies by using petroleum fuels.

The AC conductivity of SBR was significantly enhanced by the addition of ZnS nanoparticles. Dielectric constants of composites were greater than pure SBR and the maximum dielectric value was obtained for 10 phr composite. Diffusion and sorption of aromatic and industrial solvents through SBR/ZnS nanocomposites was studied at different temperatures. The diffusion results were explained in terms of the size of liquid molecules and the diffusion mechanism was found to follow the anomalous trend. The diffusion and permeation coefficient values decreased with an increase in the molar volume of the solvent. The enhanced dielectric property, solvent resistance, and glass transition temperature of the elastomeric nanocomposites can be used in various applications such as electromagnetic shielding, flexible energy storage and other nanoelectronic devices. To sum up, nano-ZnS acts as a good reinforcement for SBR, especially at 10 phr loading.

1. H. J. Maria, N. Lyczko, A. Nzihou, C. Mathew, S. C. George, K. Joseph, and S. Thomas, *J. Mater. Sci.* **48**, 5373 (2013).
2. Q. Liu, Y. Zhang, and H. Xu, *Appl. Clay Sci.* **42**, 232 (2008).
3. V. C. Jasna and M. T. Ramesan, *J. Inorg. Organomet. Polym. Mater.* **27**, 968 (2017).
4. M. Jacob, K. T. Varughese, and S. Thomas, *J. Mater. Sci.* **41**, 5538 (2006).
5. K. Suhailath and M. T. Ramesan, *J. Mater. Sci. Mater. Electron.* **28**, 13797 (2017).
6. H. N. Pazhooh, R. Bagheri, and A. Adloo, *Polym. (United Kingdom)* **108**, 135 (2017).
7. P. Jayakrishnan and M. T. Ramesan, *Polym. Bull.* **74**, 3179 (2017).
8. E. Jayamani, S. Hamdan, M. R. Rahman, and M. K. Bin Bakri, *Mater. Today Proc.* **2**, 2757 (2015).
9. B. Seentrakoon, B. Junhasavasdikul, and W. Chavasiri, *Polym. Degrad. Stab.* **98**, 566 (2013).
10. M. J. Jiang, Z. M. Dang, and H. P. Xu, *Eur. Polym. J.* **43**, 4924 (2007).
11. M. T. Ramesan, V. Nidhisha, and P. Jayakrishnan, *Mater. Sci. Semicond. Process.* **63**, 253 (2017).
12. Y. Zhang, Q. Zhang, Q. Liu, H. Cheng, and R. L. Frost, *J. Therm. Anal. Calorim.* **115**, 1013 (2014).

13. A. Zanchet, L. N. Carli, M. Giovanela, R. N. Brandalise, and J. S. Crespo, *Mater. Des.* **39**, 437 (2012).
14. L. Guo, G. Huang, J. Zheng, and G. Li, *J. Therm. Anal. Calorim.* **116**, 359 (2014).
15. H. H. Hassan, E. Ateia, N. A. Darwish, S. F. Halim, and A. K. Abd El-Aziz, *Mater. Des.* **34**, 533 (2012).
16. S. Mishra and N. G. Shimpi, *J. Appl. Polym. Sci.* **98**, 2563 (2005).
17. D. Yin, Y. Zhang, R. Fan, and Y. Zhang, *Hecheng Xiangjiao Gongye/China Synth. Rubber Ind.* **25**, 161 (2002).
18. M. Liu, Z. Jia, D. Jia, and C. Zhou, *Prog. Polym. Sci.* **39**, 1498 (2014).
19. M. T. Ramesan, *Int. J. Plast. Technol.* **19**, 368 (2015).
20. Q. T. Nguyen and D. G. Baird, *Adv. Polym. Technol.* **25**, 270 (2006).
21. B. Xu, Q. Zheng, Y. Song, and Y. Shangguan, *Polymer (Guildf)*. **47**, 2904 (2006).
22. A. Sorrentino, M. Tortora, and V. Vittoria, *J. Polym. Sci. Part B Polym. Phys.* **44**, 265 (2006).
23. V. C. Jasna and M. T. Ramesan, *AIP Conf. Proc.* **1849**, (2017).
24. S. Kango, S. Kalia, A. Celli, J. Njuguna, Y. Habibi, and R. Kumar, *Prog. Polym. Sci.* **38**, 1232 (2013).
25. A. Stroyuk, A. Raevskaya, A. Korzhak, and S. Kuchmii, *J. Nanoparticle Res.* **9**, 1027 (2007).
26. S. Mitra, S. Chattopadhyay, and A. K. Bhowmick, *Polym. Compos.* **32**, 103 (2011).
27. L. Flandin, A. Chang, S. Nazarenko, A. Hiltner, and E. Baer, *J. Appl. Polym. Sci.* **76**, 894 (2000).
28. M. T. Ramesan and T. Sampreeth, *J. Mater. Sci. Mater. Electron.* **1** (2017).
29. A. Dasari, Z. Z. Yu, Y. W. Mai, and S. Liu, *Nanotechnology* **18**, (2007).
30. D. W. van Krevelen, *Polymer (Guildf)*. **16**, 615 (1975).
31. T. Johnson and S. Thomas, *Polymer (Guildf)*. **41**, 7511 (2000).
32. M. T. Ramesan and K. Surya, *Polym. Compos.* (2016).

PROCEEDINGS OF THE SEMINAR ON  
'EMERGING AREAS OF CHEMICAL SCIENCES'

33. K. Suhailath, M. T. Ramesan, B. Naufal, P. Periyat, V. C. Jasna, and P. Jayakrishnan, *Polym. Bull.* **74**, 671 (2017).
34. S. George, K. T. Varughese, and S. Thomas, *Polymer (Guildf)*. **41**, 579 (2000).
35. C. Sareena, M. T. Ramesan, and E. Purushothaman, *Fibers Polym.* **14**, 1674 (2013).
36. S. K. Sen, B. Dasgupta, and S. Banerjee, *J. Memb. Sci.* **343**, 97 (2009).
37. V. C. Jasna and M. T. Ramesan, *J. Chem. Pharm. Sci.* **2016–Janua**, 45 (2016).
38. G. Unnikrishnan, S. Thomas, and S. Varghese, *Polymer (Guildf)*. **37**, 2687 (1996).
39. R. Stephen, K. Joseph, Z. Oommen, and S. Thomas, *Compos. Sci. Technol.* **67**, 1187 (2007).
40. C. Sareena, M. P. Sreejith, M. T. Ramesan, and E. Purushothaman, *Polym. Bull.* **72**, 1683 (2015).
41. S. Padhi, P. G. R. Achary, and N. C. Nayak, *Bull. Mater. Sci.* **38**, 925 (2015).

**OP2.**

**SYNTHESIS AND EVALUATION OF NOVEL ACTIVATORS IN  
VANADIUM CATALYZED EPDM SYNTHESIS.**

**SANI E.P. MOHAMED**

email id- [epshani@gmail.com](mailto:epshani@gmail.com)

**Abstract**

The elastomeric terpolymers of ethylene-propylene-dienes (EPDM) are commercially important materials and are normally synthesized using vanadium-based Ziegler-Natta catalysts, activated by alkyl aluminium compounds. The simplicity of their preparation, the inherent low cost of the monomers and the large growing potential market for these elastomers has made this copolymer popular. The objective of the work are- Standardization of Synthesis and Characterization of EPDM, Optimization of EPDM polymerization conditions using a 200 ml Buchi SS reactor, Comparative study of EPDM synthesis using some known activators, Synthesis of Butyl-2-methyl-2,4,4-trichlorobut-3-enoate and its evaluation as a potential activator and characterization of the polymers.

**Introduction**

**Ethylene Propylene Diene Monomer Terpolymers**

EPDM are amorphous random copolymers based on ethylene and propylene, prepared by Natta et al. soon after the discovery of stereospecific polymerization, are today largely used for the preparation of elastomers. Two types of products are prepared: - EPM and EPDM, resulting in the absence and in the presence of a non-conjugated diene introduced to allow sulphur vulcanization of copolymer obtained. Ethylene-propylene rubber & elastomers (EPDM & EPM) is one of the most widely used and fastest growing synthetic rubbers having both specialty and general-purpose applications. Polymerization and catalyst technologies in use today provide the ability to design polymers to meet specific and demanding application and processing needs.



**EPDM** is a copolymer of Ethylene and Propylene, with a diene as a termonomer, which introduces unsaturation into the macromolecule. The last letter "M" refers to the polymethylene  $(-\text{CH}_2-)$  type backbone according to the nomenclature. A third, non-conjugated diene monomer can be terpolymerized in a controlled manner to maintain a saturated backbone and place the reactive unsaturation in a side chain available for vulcanization or polymer modification chemistry. The ethylene-propylene copolymers are called EPM. The chemically saturated, stable polymer backbone provides excellent heat, oxidation, ozone and weathering ageing. The average molecular weight of EPDM lies between 30,000 and 1,50,000, depending on the polymerization variables and the ethylene: propylene: diene ratio.

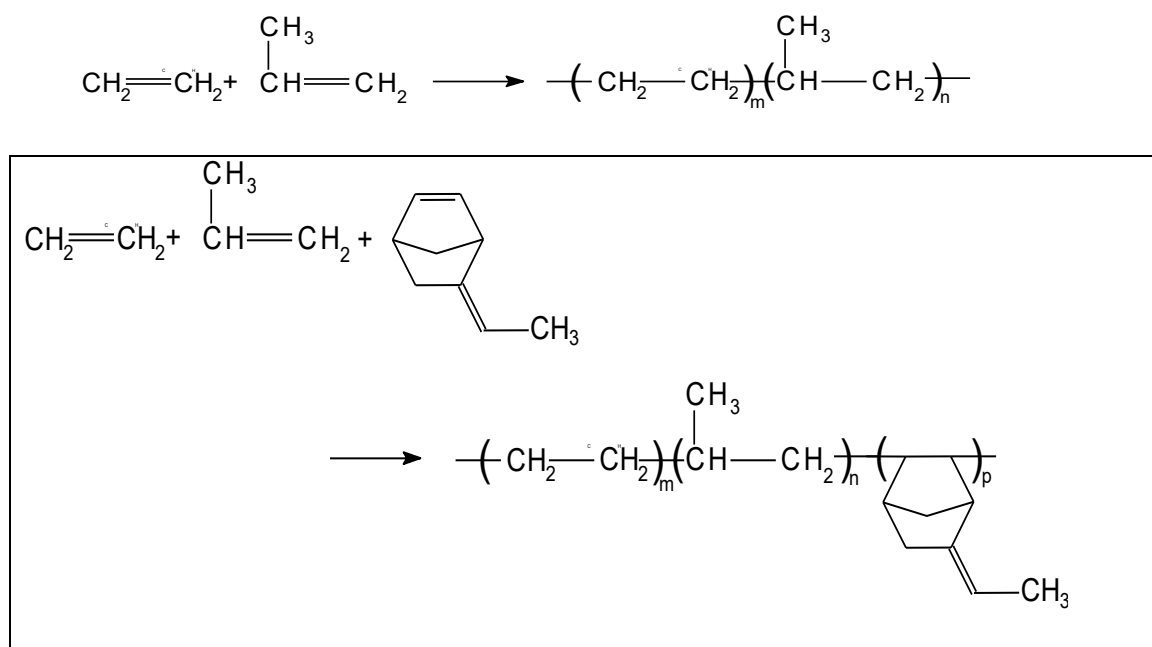


*Figure 1.2 Structural formula of EPDM containing ENB*

## Results and discussion

### Synthesis of Butyl-2-methyl-2,4,4-trichlorobut-3-enoate-

Butyl-2-methyl-2,4,4-trichlorobut-3-enoate was synthesized by chlorinating Butyl methacrylate with  $\text{CCl}_4$  in presence of  $\text{RuCl}_2 (\text{PPh}_3)_3$  as catalyst refluxed at a temperature of  $75^\circ\text{C}$  (+ or  $-5^\circ\text{C}$ ) for 96 hrs, the pale-yellow liquid which was distilled at a temperature of  $80^\circ\text{C}$  in vacuum was isolated and further treated with triethyl amine in presence of THF as solvent at a temperature of  $40^\circ\text{C}$ , for 15 hrs to yield the required

product. The reaction was monitored by TLC technique. The obtained product was characterized using  $^1\text{H}$  NMR.

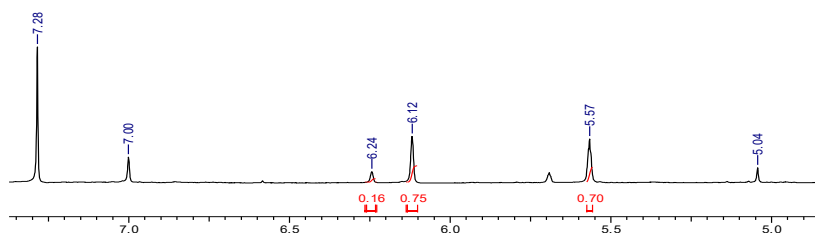


**Figure 4.3**  $^1\text{H}$  NMR in  $\text{CDCl}_3$  of *Butyl-2-methyl-2,4,4-trichlorobut-3-enoate*

### Typical properties and uses of EPDM elastomeric copolymers

- (i) Outstanding resistance to weathering
- (ii) Good heat ageing properties
- (ii) Ability to compound with large quantities of fillers and plasticizers resulting in low cost compounds which are particularly useful in automotive and industrial, mechanical, goods applications.
- (iv) Typical automotive uses include tire sidewalls, inner tubes, radiator and heater hose, vacuum tubing, weather stripping and sponge door seals and viscosity index (V.I.) improvers for lubricating oil compositions.
- (v) Typical mechanical uses include mechanical appliances, industrial and garden hoses, both molded and extruded sponge parts, gaskets and seals and conveyor belt covers
- (iv) Used as adhesive, appliances parts as in hoses and gaskets, wires and cables and plastic blend

The ultimate properties of an EPM or EPDM copolymer are determined by such factors as composition, compositional distributions, sequence distribution, molecular weight and molecular weight distribution. The properties of EPM and EPDM copolymers are a function of the catalyst system and polymerization process used.<sup>11</sup>

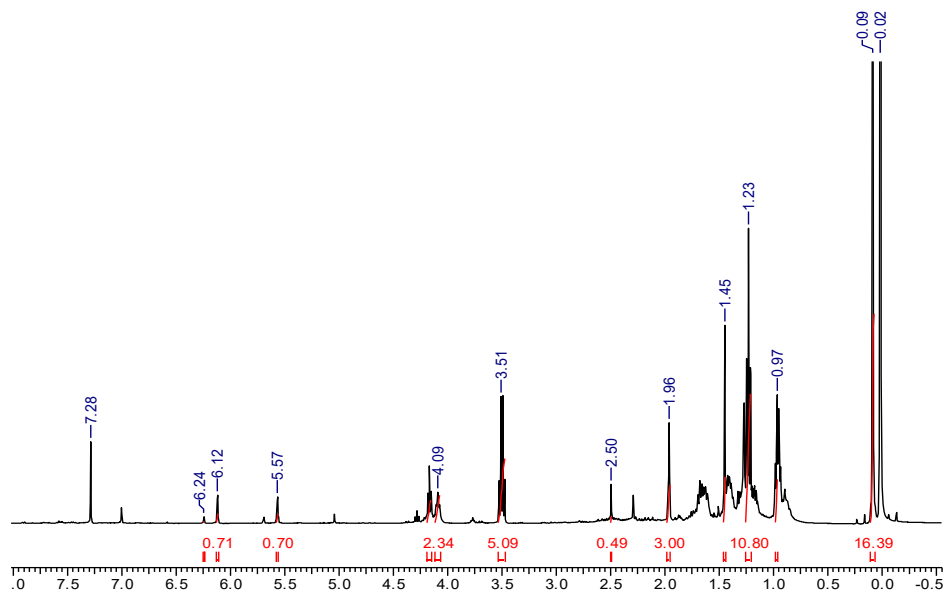


*Figure 4.4*  $^1\text{H}$  NMR in  $\text{CDCl}_3$  of Butyl-2-methyl-2,4,4-trichlorobut-3-enoate

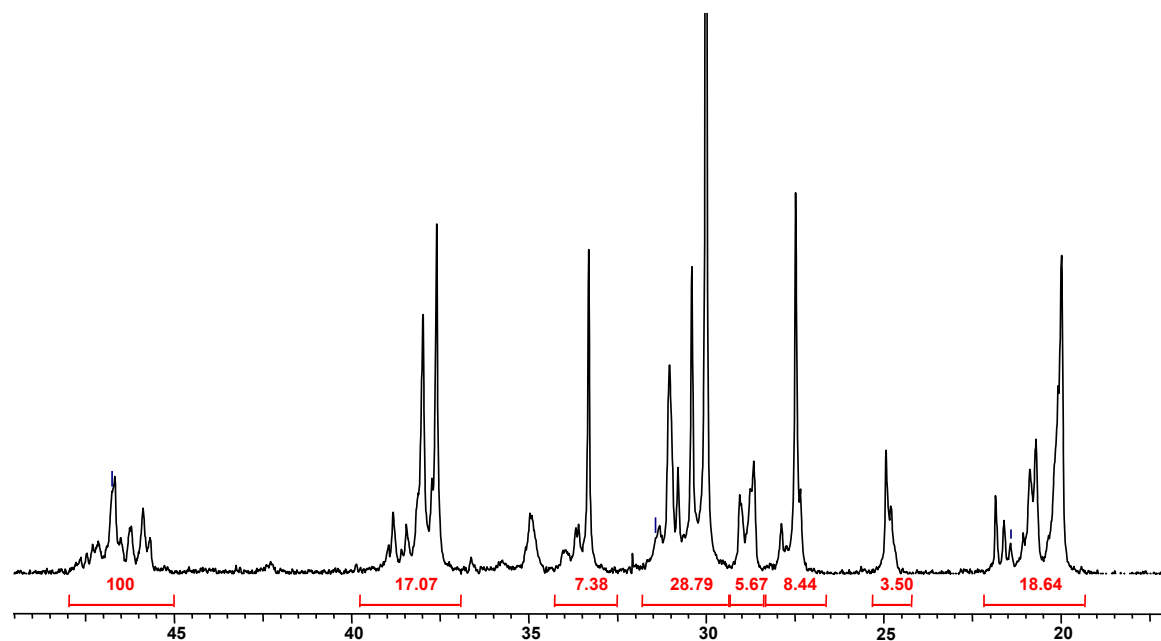


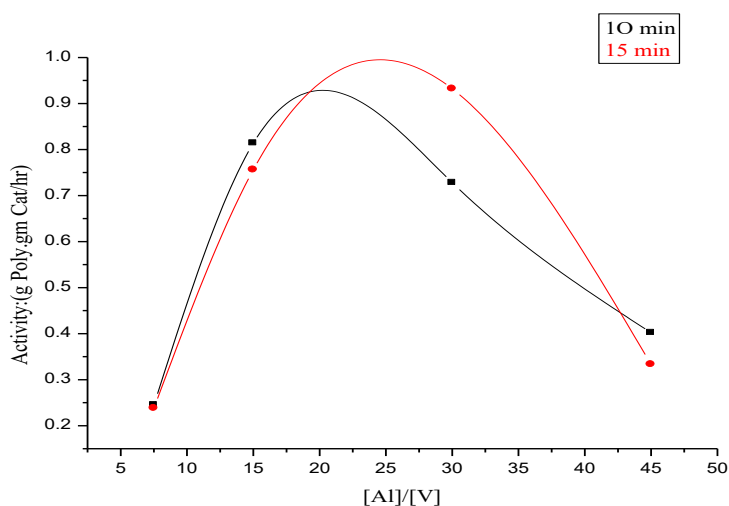
*Figure 4.9*  $^{13}\text{C}$  NMR Spectrum of sample EPDM

**Role of activators-** Butyl-2-methyl-2,4,4-trichlorobut-3-enoate and Butyl,2,4,4,4-tetrachloro-2-methylbutanoate were used as activators in this study.

**Table 4.3 Effect on activity in the absence of activators**

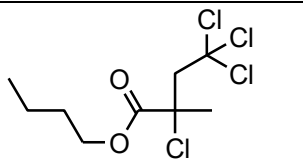
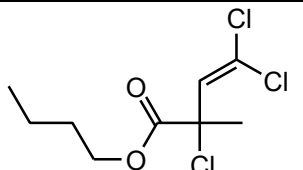
Run	[Al]/[V]	Time (min)	Yield (gm)	Activity <b>(gm) Polymer</b> <b>(gm) Catalyst/hr.</b>
12	7.5	10	0.245	21.20
14	15	10	0.814	140.88
17	30	10	0.728	252.04
19	45	10	0.402	208.83
13	7.5	15	0.238	13.73
15	15	15	0.756	87.24
16	30	15	0.932	215.11
21	45	15	0.333	115.32

$VOCl_3 = 1 \times 10^{-4} \text{ mol}$ ;  $EASC = 3 \times 10^{-3} \text{ mol}$ ;  $E: P = 90:10$ ;  $ENB = 7.42 \times 10^{-3} \text{ mol}$ ; Pressure = 3 bar; Temperature = 30°C; Stirring rate = 1500rpm



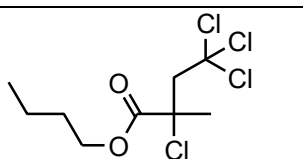
**Figure 4.5 Activity Vs [Al]/[V] with respect to time**

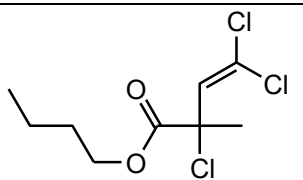
**Table 4.4 Effect on activity in presence of activators, reaction time 10 minutes.**

Activator Used	Run	[Al]/[V]	Yield (gm)	Activity (gm) Polymer (gm)Catalyst/hr.	Increase in Activity
 Butyl, 2,4,4,4- tetrachloro-2-methyl butanoate. (ACT-I)	26	7.5	0.200	17.31	---
	29	15	0.943	163.24	22.36
	33	30	1.246	431.39	179.35
	35	45	0.583	302.85	94.02
 Butyl-2-methyl-2,4,4- trichlorobut-3-enoate. (ACT-II)	28	7.5	0.187	16.18	---
	30	15	1.025	176.5	35.62
	31	30	1.423	492.67	240.63
	34	45	0.262	138.7	----

$VOCl_3 = 1 \times 10^{-4}$  mol;  $EASC = 3 \times 10^{-3}$  mol;  $E: P = 90:10$ ;  $ENB = 7.42 \times 10^{-3}$  mol; Activators:  
 $1 \times 10^{-4}$  Time; 10 min, Pressure = 3 bar; Temperature = 30°C; Stirring rate = 1500 rpm.

**Table 4.5. Effect on activity in presence of activators, reaction time- 15 min**

Activator Used	Run	[Al]/[V]	Yield (gm)	Activity (gm) Polymer (gm)Catalyst/hr.	Increase in Activity
 Butyl,2,4,4,4-tetrachloro- 2-methylbutanoate.	38	7.5	0.269	15.52	1.79
	41	15	0.984	113.56	26.32
	43	30	1.311	302.59	87.48
	47	45	0.421	145.8	30.48

 Butyl-2-methyl-2,4,4 trichlorobut-3-enoate.	39	7.5	0.198	11.42	---
	42	15	0.863	99.59	12.35
	45	30	1.502	346.68	131.57
	48	45	0.677	234.45	119.13

$VOCl_3 = 1 \times 10^{-4}$  mol;  $EASC = 3 \times 10^{-3}$  mol;  $E: P = 90:10$ ;  $ENB = 7.42 \times 10^{-3}$  mol; Activators:  
 $1 \times 10^{-4}$  Time; 15min, Pressure = 3 bar; Temperature = 30°C; Stirring rate = 1500 rpm

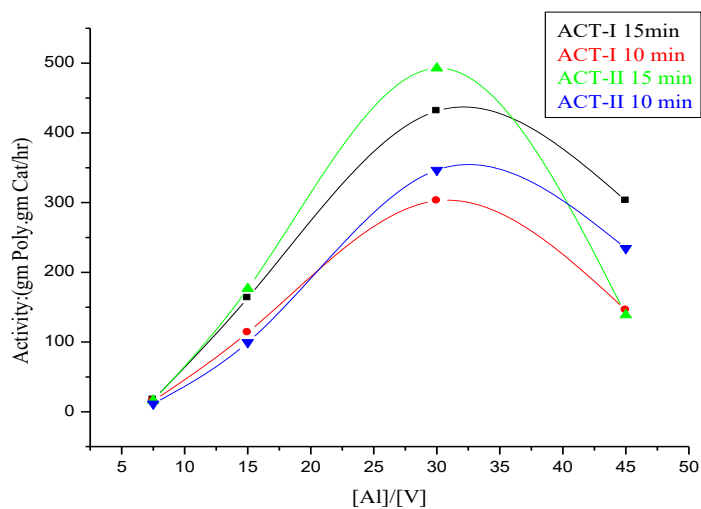


Figure 4.6 Effect of ACT-I and ACT-II with respect to time

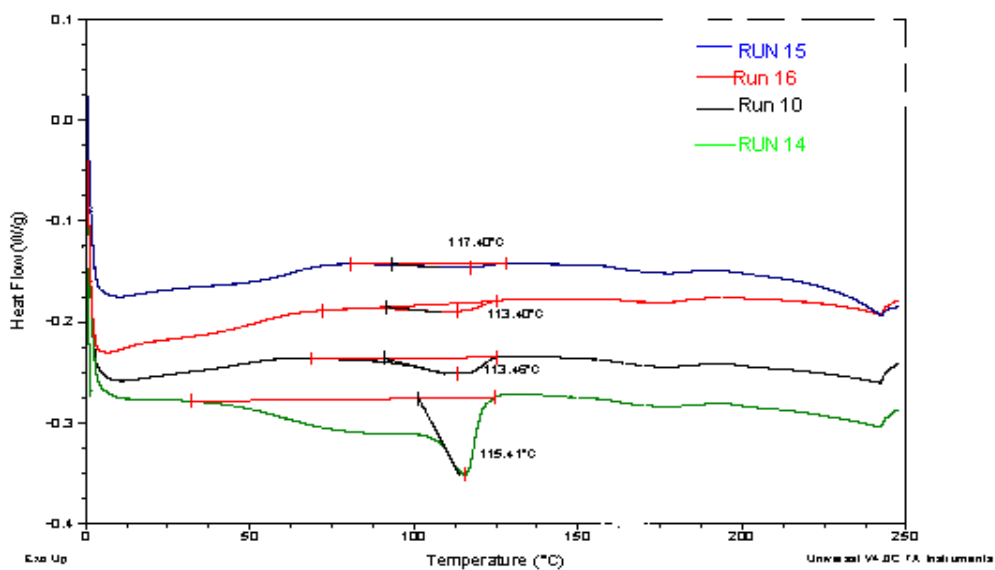


Figure 4.12. An overlay of DSC thermograms of EPDM copolymers

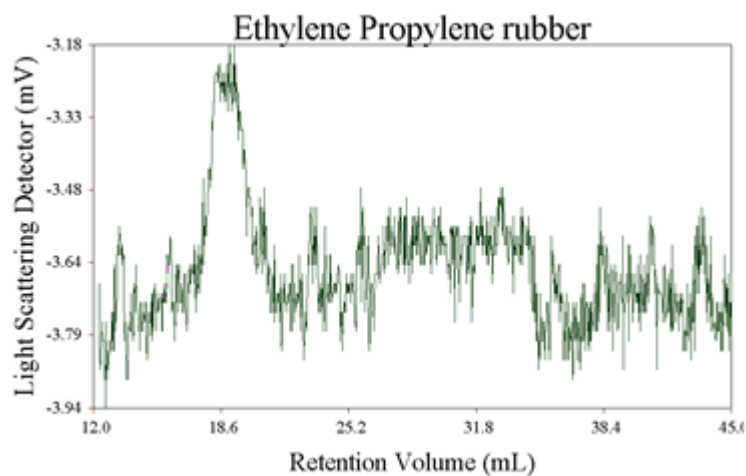


Figure 4.14 GPC PLOTS for ethylene propylene rubber

Table 4.7 Light Scattering Summary for EPDM

Molecular weight		Intrinsic viscosity(dL/gm)	
Mn	4,300	IVn	0.285
Mw	41,000	Ivw	0.472
Mz	1,08,300	IVz	0.660
Mp	44,600	Pd =9.535	

## Conclusion

The development of transition metal catalysts for olefin polymerization/ EPDM synthesis has progressed significantly in the recent past years. The catalyst developmental work has two aspects. One relates to improvement of catalyst performance, productivity and process ability for commercialization of conventional polyolefin. The other is the designing of new catalytic systems.

The results obtained in this work have allowed the clarification of some aspects of vanadium catalyzed ethylene-propylene-diene copolymerization.

- 1.) The structural and compositional study of EPDM /EPR prepared by the vanadium catalytic system has been characterized using  $^1\text{H}$  NMR,  $^{13}\text{C}$  NMR spectroscopy, GPC and DSC.
- 2.) The effect of reaction conditions on the catalyst productivity and molar composition was investigated.
- 3.) The activity of the catalyst increases with pressure. Ethylene and termonomer incorporation also increase with pressure.
- 4.) The activity of the catalyst increases with increase in  $[\text{Al}]/[\text{V}]$  ratio upto 15 then it decreases due to the over reduction of catalyst to inactive state by the cocatalyst.
- 5.) Butyl-2-methyl-2,4,4-trichlorobut-3-enoate and Butyl-2,4,4,4-tetrachloro-2-methyl butanoate were synthesized and used as activators. It was found that Butyl-2-methyl-2,4,4-trichlorobut-3-enoate was showing more activity than Butyl, 2,4,4,4-tetrachloro-2-methyl butanoate.
- 6.) Characterization of the EPR and EPDM copolymers synthesized was done using DSC and high temperature GPC technique. It was found that the polymer obtained is amorphous and has a  $T_g$  of  $-52.35^\circ\text{C}$ .

## References

1. Ziegler, K., Holzkamp, E., Breil, H., Martin, H.: *Angew. Chem.* 67, 541 (1955).
2. 2a. Boor, L: *Macromolecular Reviews*, Vol. II, p. 115. New York, N.Y.: John Wiley and Sons 1967.



- 2b. Gaylord, N.G., Mark, H.F.: Linear and Stereoregular Addition Polymers. New York-London: Interscience Publ. Inc. 1959.
3. Reich, L., Schindler, A.: Polymerization by Organometallic Compounds. New York-London: John Wiley and Sons 1966.
4. Moore, E.P. Jr., *Polypropylene*, in: Salamone, J.C. (Editor), *The polymeric materials encyclopedia* (on CD-ROM), CRC Press, **1996**.
5. Parshall, G.W.; Ittel, S.D., *Homogeneous catalysis, the applications and chemistry of catalysis by soluble transition metal complexes*, 2nd Edition, Wiley & Sons inc., New York, **1992**, Chapter 4.
6. S.Cesca, *Macromol. Rev.* **10**, 5(1975).
7. John R. Anderson and Michel Boudart, *Catalysis science and technology, Vol-6* Springer-Verlag, 1984.
8. M.C. Haag, J. H. Z. Dos Santos, F. C. Stedile, M. A. De Araujo, W. Kaminsky and M. Miri, *J. Polym. Sci.*, **23**, 2151(1985).
9. Anneli Malmberg and Barbro Lofgren, *J. Appl. Polym. Sci.*, **66**, 35-44(1997).
10. W. Kaminsky and H. Drogemuller, *Macromol. Rapid Commun.*, **11**, 89(1990).
11. Mohamad Dolatkhani, Henri Cramail, Alain Deffieux, *Macromol. Chem. Phys.* **196**, 3091-3105 (1995)
12. Donald L. Christman, Gerald I. Keim, *Macromolecules*, 1, No.4, 358-363(1968).
13. M. C. Haag, J.H.Z. Doz Santos, F.C. Stedile, M.A. De Araujo, J. Dupont, I. J. R. Baumvol *J. Appl. Poly. Sci Vol.* **68**, 535-541(1998)
14. G. Natta, P. Pino, P. Corradine, F. Danusso, E. Mantica, G. Mazzanti, G. Moraglio, *J. Am. Chem. Soc.* **77**,1708(1955).
15. W. L. Carrick, *J. Am. Chem. Soc.* **80**, 6455(1958).

16. Lee, D-H., *Olefin polymerization catalysts*, in: Salamone, J.C. (Editor), *The polymeric materials encyclopedia* (on CD-ROM), CRC Press, **1996**.
17. Adisson, E.; Deffieux, A.; Fontanille, M.; Bujadoux, K., *J. Pol. Sci. A, Pol. Chem.*, **1994**, 32, 1033.
18. Enzo Giannetti, Romano Mazzocchi, Enrico Albizzati, Tiziana Fiorani, *Makromol. Chem.* **185**, 2133-2151(1984)
19. Natta,G., Mazzanti,G., Valvassori,A., Sartori,G., Fiumani,D.,*J. Polym. Sci.* **51**, 411, (1961).
20. R. Pearce and W.R. Patterson., *Catalysis and Chemical processes*.
21. Henk Hagen, Jaap Boersma, Gerard van Koten, *Chem. Soc. Rev.*,**31**, 357-364(2002).
22. E. Adisson, A. Deffieux, M. Fontanille, K. Bujadoux, *J. Polym. Sci.:Part A Polymer Chemistry*, Vol.**32**, 1033-1041(1994).
23. French Pat., 1,451,585 (1965)
24. French Pat., 1,471,472 (1966)
25. French Pat., 1,450,407 (1964)
26. French Pat., 1,370,358 (1963)
27. U.S. Pat., 3,349,064 (1967)
28. Can. Pat., 733,585 (1965)
29. French Pat., 1,565,850 (1968)
30. French Pat.,1,569,933(1968)
31. V. Pandya and K. V. Latha, *J. Appl. Poly. Sci.*, **43**, 637(1991)
32. Paul D. Bolton, Philip Mountford, *Adv. Synth. Catal.*, **347**, 355 (2005)

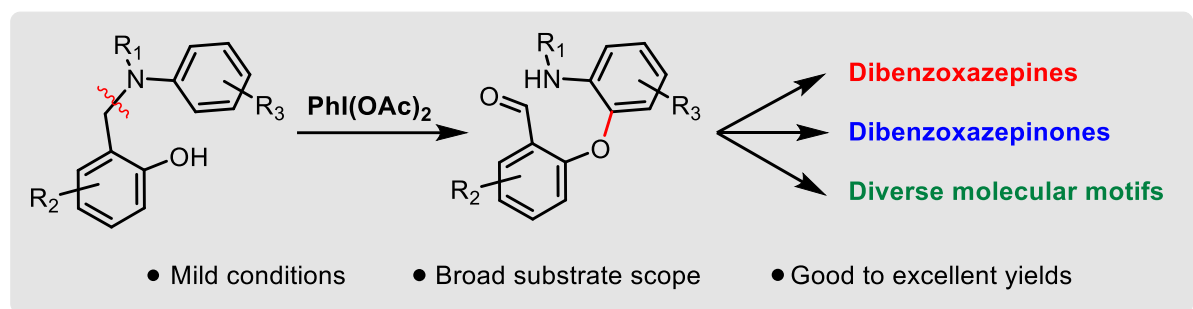
PP1.

## Metal-free diaryl etherification of tertiary amines by *ortho*-C(sp<sup>2</sup>)-H functionalization for synthesis of dibenzoxazepines and dibenzoxazepinones

Vellekkatt Jamsheena, C. K. Mahesha, Nibin M. Joy, Ravi S. Lankalapalli\*

Chemical Sciences and Technology Division and Academy of Scientific and Innovative Research (AcSIR), CSIR-National Institute for Interdisciplinary Science and Technology (CSIR-NIIST), Thiruvananthapuram 695019, India

E-mail: [ravishankar@niist.res.in](mailto:ravishankar@niist.res.in)



### Abstract:

A phenyliodine(III) diacetate (PIDA) mediated umpolung reactivity of tertiary amines with suitably substituted *ortho*-hydroxybenzyl, phenyl units is exploited to facilitate *ortho*-C(sp<sup>2</sup>)-H functionalization to afford diaryl ethers. Presence of an *ortho*-CHO and secondary amine functionalities in the resulting diaryl ether, generated *in situ*, were utilized for synthesis of dibenzoxazepines and dibenzoxazepinones. Mild conditions, broad substrate scope with good to excellent yields, and scope for further diversification of diaryl ether are highlights of this methodology.

### Introduction:

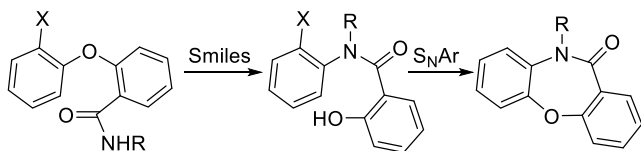
Dibenzoxazepines and dibenzoxazepinones are pharmaceutically relevant molecules present in antidepressants and antipsychotics. These privileged structural motifs possess

broad range of biological activities such as anti-HIV, antitumor, antioxidant, oral contraceptive, TRPA1 agonist, sodium channel blocker, CNS depressant, antiinflammatory, and antinociceptive property.<sup>[1]</sup> As natural products, dibenzoxazepinones were reported as antioxidant metabolites isolated from the leaves of *Carex distachya*.<sup>[1c]</sup> Many approaches have been developed for the synthesis of dibenzoxazepine core skeleton. Traditionally, base-promoted nucleophilic aromatic substitution ( $S_NAr$ ) reaction was employed to construct the seven-membered ring of dibenzoxazepinones via Smiles rearrangement of suitable electrophilic substrates by a domino C–O and C–N coupling reactions.<sup>[2]</sup> A base-promoted green protocol has been developed for synthesis of dibenz[*b,f*][1,4]oxazepin-11-amines by  $S_NAr$  with concomitant addition reaction.<sup>[3]</sup> Post-Ugi reaction, an intramolecular microwave-assisted Ullman diaryl etherification was used as an attractive strategy to synthesize highly substituted dibenz[*b,f*][1,4]oxazepine scaffold.<sup>[4]</sup> Key precursors generated from diaryl etherification methodology served as suitable substrates for various intramolecular seven-membered ring formation strategies such as reductive lactamization, Pd-catalyzed condensation, cyclocarbonylation, Smiles rearrangement, Cu-catalyzed Goldberg reaction to afford dibenzoxazepinones.<sup>[5]</sup> Alternatively, intramolecular diaryl etherification as the later annulation event under metal-catalyzed and base-promoted conditions from substrates with suitably tethered phenol and halo-substituted phenyl units was also developed.<sup>[6]</sup> Dibenzoxazepines have also been used as valuable synthetic intermediates in the development of more complex heterocyclic structures.<sup>[7]</sup>

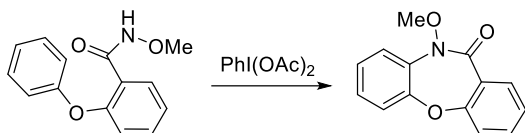
Recently, dibenzoxazepinone synthesis was reported by hypervalent iodine (III) reagent (HIR) mediated intramolecular C–N bond formation from 2-(aryloxy)benzamides synthesized by Cu-mediated diaryl etherification,<sup>[8]</sup> but failed with substrates containing strong electron withdrawing and donating groups. Another example involving usage of HIR reagent such as phenyliodine(III) diacetate (PIDA) involved intramolecular cyclization of two aryl groups from 2-hydroxy-*N*-phenylbenzamides affording dibenz[*d,f*][1,3]oxazepin-6(7*H*)-ones.<sup>[9]</sup> HIR is considered as a mild and metal-free alternative for the construction C–C and C–heteroatom bonds.<sup>[10]</sup> HIR mediated oxidative dearomatizing transformations for ortho-substituted phenols were utilized in synthesis of complex natural products.<sup>[11]</sup> Similar to phenolic substrates, tertiary amines were also

efficient substrates in HIR mediated transformations involving functionalization of C(sp<sup>3</sup>)-H bond adjacent to nitrogen.<sup>[12]</sup> Herein, we report *ortho*-C(sp<sup>2</sup>)-H bond functionalization of tertiary amines in presence of PIDA to afford diaryl ether (Figure 1). Diaryl etherification is an important synthetic strategy achieved mostly by Cu- and Pd-catalyzed cross-coupling reactions.<sup>[13]</sup> The metal-free alternative for diaryl etherification with HIR involving diaryliodonium salts is an attractive strategy,<sup>[14]</sup> applied towards synthesis of *ortho*-CHO diaryl ethers.<sup>[15]</sup> In the present study, PIDA induced umpolung reactivity of tertiary amines affords diaryl ether with an *ortho*-CHO and secondary amine substituents that upon subsequent treatment with NaBH(OAc)<sub>3</sub> and PCC provided dibenzoxazepines and dibenzoxazepinones, respectively (Figure 1). The present method serves as a metal-free alternative to the existing methods *vide supra* with a broad substrate scope. Further synthetic applications of this methodology from diaryl ether were demonstrated with an array of transformations to access other bioactive skeletons.

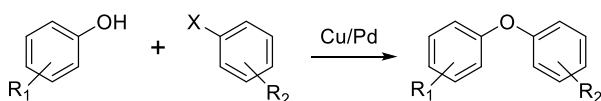
**Dibenzoxazepinones via Smiles rearrangement (Ref. 2)**



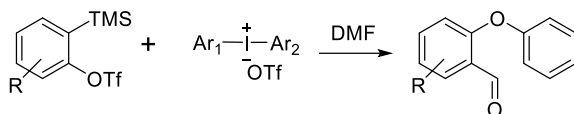
**HIR mediated dibenzoxazepinone synthesis (Ref. 8)**



**Metal mediated diaryl etherification (Ref. 13)**



**HIR mediated diaryl etherification (Ref. 14)**



**This work:**

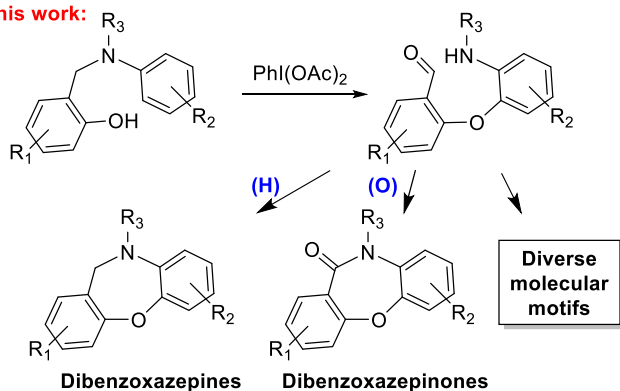


**Figure 1.** Strategies for dibenzoxazepinone, diaryl ether synthesis and present work

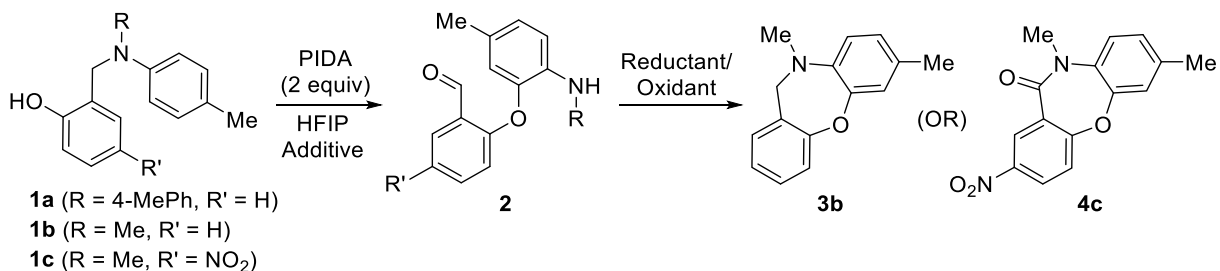
**Results and Discussion:**

A novel intramolecular diaryl etherification strategy for the key seven-membered ring formation to afford dibenzoxazepines was envisaged using tertiary amines with suitably substituted *ortho*-hydroxybenzyl, phenyl units under metal-free conditions by using HIRs. In an initial attempt (Table 1), tertiary amine **1a** treated with one equivalent of PIDA at

room temperature using conventional HFIP as the solvent did not lead to complete consumption of the starting material. However, tertiary amine **1a** underwent a complete transformation within 10 min with two equivalents of PIDA forming a new C-O bond with concomitant C-N bond cleavage affording compound **2a** in 34% yield (entry 1). The structure of compound **2a** was unambiguously confirmed by single crystal X-ray analysis (see Supporting Information). Further variation of the solvents, other HIRs, oxidants and mode of additions examined were not effective for the formation of **2a** which led to the choice of PIDA and HFIP as the optimal combination. The reaction conducted in presence of  $K_2CO_3$ , to scavenge the generated acetic acid by-product from PIDA, did not significantly improve the yield of compound **2a** (entry 2). Compound **2** with appropriately substituted aldehyde and secondary amine is prone to undergo reductive amination to afford the desired dibenzoxazepine. Accordingly, a simple tertiary amine **1b** substrate was initially subjected to PIDA mediated oxidation to afford compound **2b** which without purification was treated with excess  $NaBH_4$  in methanol for reductive amination. This reaction in an overall two steps produced the desired dibenzoxazepine **3b** in 67% yield (entry 3). Conducting the reductive amination step on the crude aldehyde in presence of additives (entries 4-5) and other reductants (entries 6-7) could not improve the yield of dibenzoxazepine formation considerably. Interestingly, addition of three equivalents of  $NaBH(OAc)_3$  in the same pot after complete consumption of tertiary amine afforded dibenzoxazepine **3b** with an enhanced yield of 77% (entry 8), and presence of an additive could not further improve the yield (entry 9). Changing the reductant to an oxidant in the second step should produce dibenzoxazepinone **4**. An initial attempt with tertiary amine **1a** with an addition of one equivalent of PCC in dichloromethane in the same pot led to a sluggish outcome. However, treatment of one equivalent of PCC on the isolated intermediate **2c** in an overnight reaction afforded dibenzoxazepinone **4c** in 70% yield (entry 10) and an increase of PCC to two equivalents led to reaction completion within one hour with 73% yield (entry 11). The choice of tertiary amine **1c** is pertinent in the context of optimization of this methodology due to the high relevance of nitro-substitution in dibenzoxazepinone based anti-depressant drug Sintamil. Even though other oxidants (entries 12-17) failed to afford the desired product, sodium hypochlorite in acetic acid

produced dibenzoxazepinone **4c** in 57% yield (entry 18) but failed while using acetonitrile (entry 19).

**Table 1.** Optimization of reaction conditions<sup>a</sup>



Entry	Additive	Reductant/ Oxidant	Yield <sup>h</sup>		
			<b>2a</b>	<b>3b</b> (2 steps)	<b>4c</b> (2 steps)
1	-	-	34	-	-
2	K <sub>2</sub> CO <sub>3</sub>	-	46	-	-
3 <sup>b</sup>	-	NaBH <sub>4</sub>	-	67	-
4 <sup>b</sup>	K <sub>2</sub> CO <sub>3</sub>	NaBH <sub>4</sub>	-	50	-
5 <sup>b</sup>	BF <sub>3</sub> .Et <sub>2</sub> O	NaBH <sub>4</sub>	-	70	-
6 <sup>b</sup>	-	NaBH(OAc) <sub>3</sub>	-	71	-
7 <sup>b</sup>	-	NaCNBH <sub>3</sub>	-	65	-
8 <sup>c</sup>	-	NaBH(OAc) <sub>3</sub>	-	77	-
9 <sup>c</sup>	BF <sub>3</sub> .Et <sub>2</sub> O	NaBH(OAc) <sub>3</sub>	-	69	-
10 <sup>d</sup>	-	PCC	-	-	70
11 <sup>e</sup>	-	PCC	-	-	73
12 <sup>d</sup>	-	DMP	-	-	n.d.
13 <sup>d</sup>	NaHCO <sub>3</sub>	DMP	-	-	n.d.
14 <sup>d</sup>	-	NBS	-	-	n.d.
15 <sup>d</sup>	-	NIS	-	-	n.d.
16 <sup>d</sup>	-	<i>m</i> -CPBA	-	-	n.d.
17 <sup>d</sup>	-	DDQ	-	-	n.d.



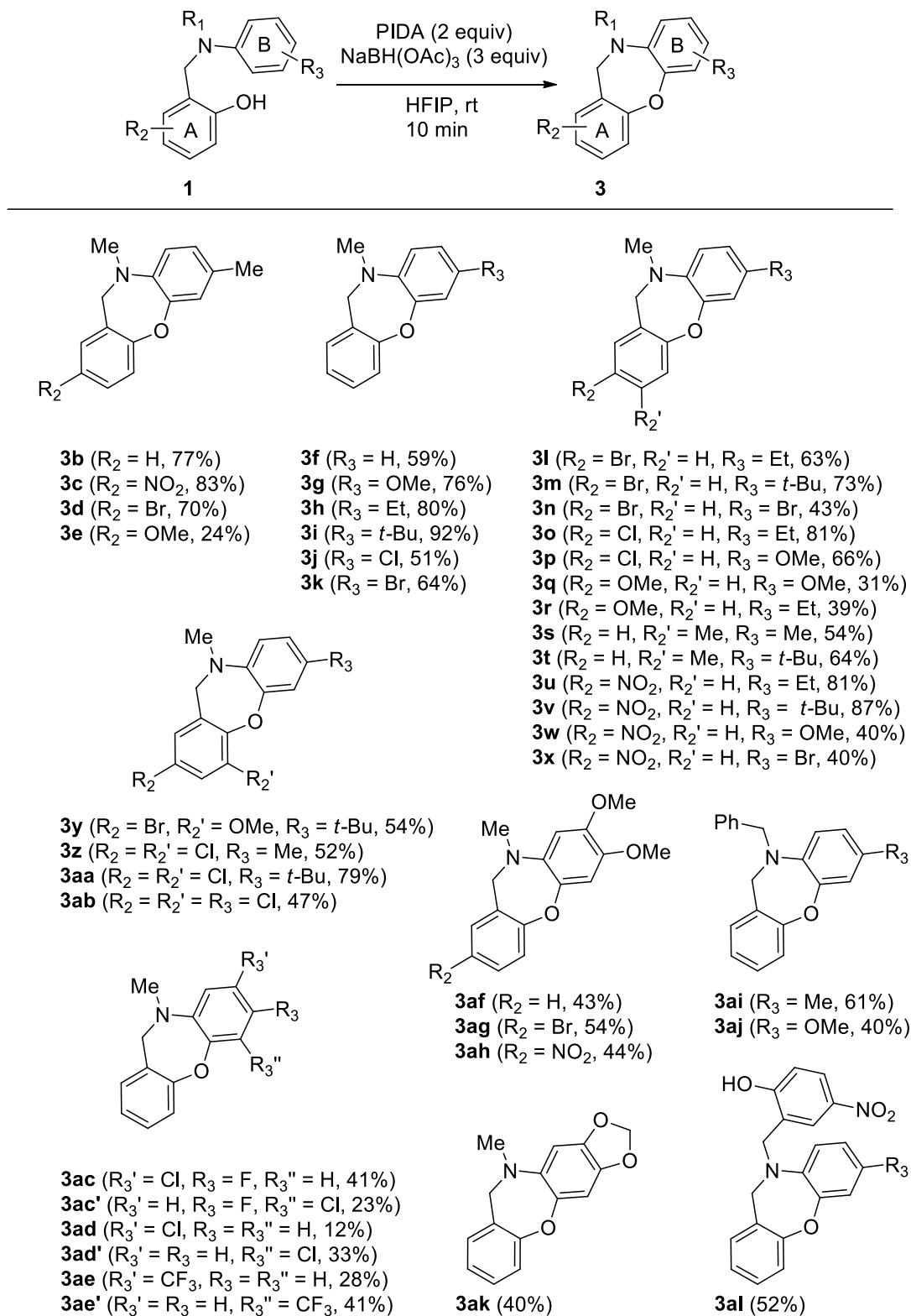
18 <sup>f</sup>	-	NaClO	-	-	57
19 <sup>g</sup>	-	NaClO	-	-	n.d.

---

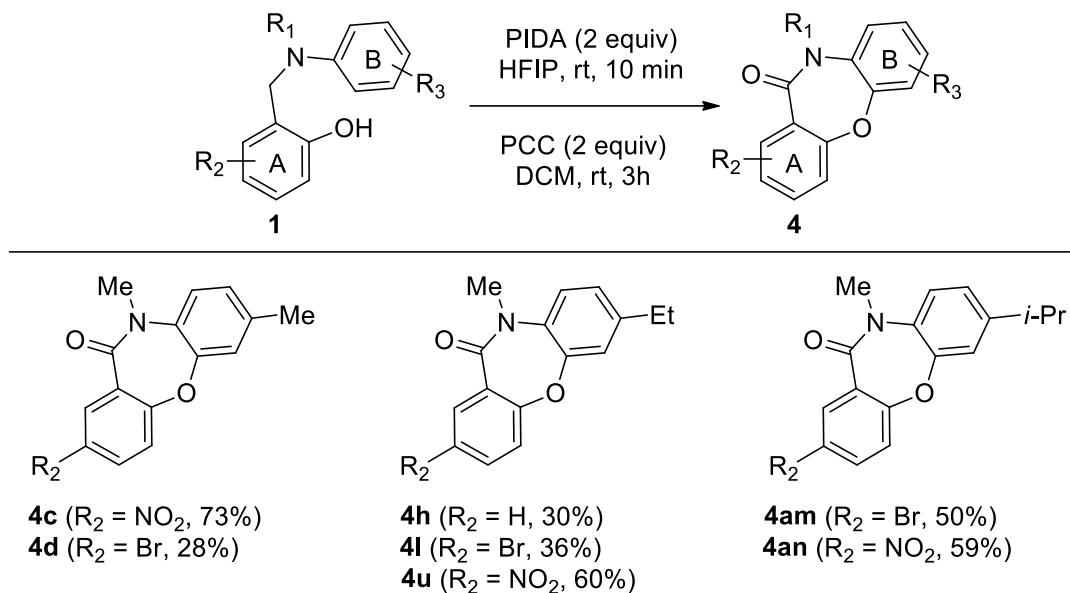
<sup>a</sup>Reaction conditions: All reactions were conducted at room temperature without using distilled solvents. Compound **1a/1b/1c** (0.18 mmol) in HFIP (1 mL) was the scale of the reactions for the first step. <sup>b</sup>To the crude mixture of compound **2**, after quenching, reductant (3 equiv) in MeOH (1 mL) was added. <sup>c</sup>NaBH(OAc)<sub>3</sub> (3 equiv) was added to the same pot. <sup>d</sup>To the isolated compound **2c** by column chromatography, oxidant (1 equiv) in DCM (1 mL) was added. <sup>e</sup>PCC (2 equiv) was used. <sup>f</sup>Solvent used in second step was AcOH. <sup>g</sup>Solvent used in second step was CH<sub>3</sub>CN. <sup>h</sup>Isolated yields. n.d. = not detected. The optimization studies revealed the broad scope of this methodology involving varied substitutions in benzyl (A ring), phenyl (B ring) and N-alkyl groups of the tertiary amines as shown in Scheme 1. Under the optimized conditions (entry 8, Table 1), tertiary amines bearing activating as well as deactivating groups in either of the mono- or di-substituted A ring and para-substituted B ring conveniently converted to dibenzoxazepines **3b–3ab** in moderate to good yields. In general, tertiary amines with deactivating groups (halo, nitro) in A ring and ones with activating groups (alkyl, methoxy) in B ring afforded dibenzoxazepines in good yields. For instance, substrate **1c** with nitro substitution in A ring and **1i** with tert-butyl substitution in B ring afforded dibenzoxazepines **3c** and **3i** in 83 and 92% yields, respectively. Accordingly, substrate **1v** with both nitro and tert-butyl substitutions in A and B rings, respectively, afforded dibenzoxazepine **3v** in 87% yield. Meta-substituted B rings afforded a mixture of separable regioisomers **3ac, 3ac'–3ae, 3ae'** since the nucleophilic attack by OH group is feasible in either of the ortho-positions of the B ring. Dimethoxy substituted B ring offered a single regioisomer **3af–3ah**, arising due to electronic reasons. Substrates with N-benzyl substitution afforded dibenzoxazepines **3ai** and **3aj** which serves as a third variable group in the tertiary amine for diversification. However, when the substrate bears an ortho-substitution in the B ring the cyclization did not occur. Presence of a 3,4-(methylenedioxy) group in the B ring produced the desired dibenzoxazepine **3ak** in 40% yield similar to substrates, *vide supra*, with dimethoxy substituted B ring. Compound **3ak** with a tetracyclic framework could be a novel entry in

the class of tetracyclic antidepressants. Tertiary amine with two benzylic alcohols where one of them containing nitro-substitution did not undergo ring formation and the other with no substitution participated in dibenzoxazepine **3al** formation in 52% yield, confirmed by HMBC analysis of its methylated analog (see Supporting Information). An attempt involving further cyclization using dibenzoxazepine **3al** under the optimized conditions led to seven-membered ring opening to afford the corresponding aldehyde **2al** which upon subsequent reduction reformed dibenzoxazepine **3al**. A successful dibenzoxazepinone **4c** formation by successive PIDA and PCC oxidations from the optimization studies prompted us to further demonstrate the substrate scope of this reaction (Scheme 2). Accordingly, tertiary amines with different substitutions in the A and B rings afforded dibenzoxazepinones **4** in moderate yields.

**Scheme 1.** Substrate scope of dibenzoxazepines



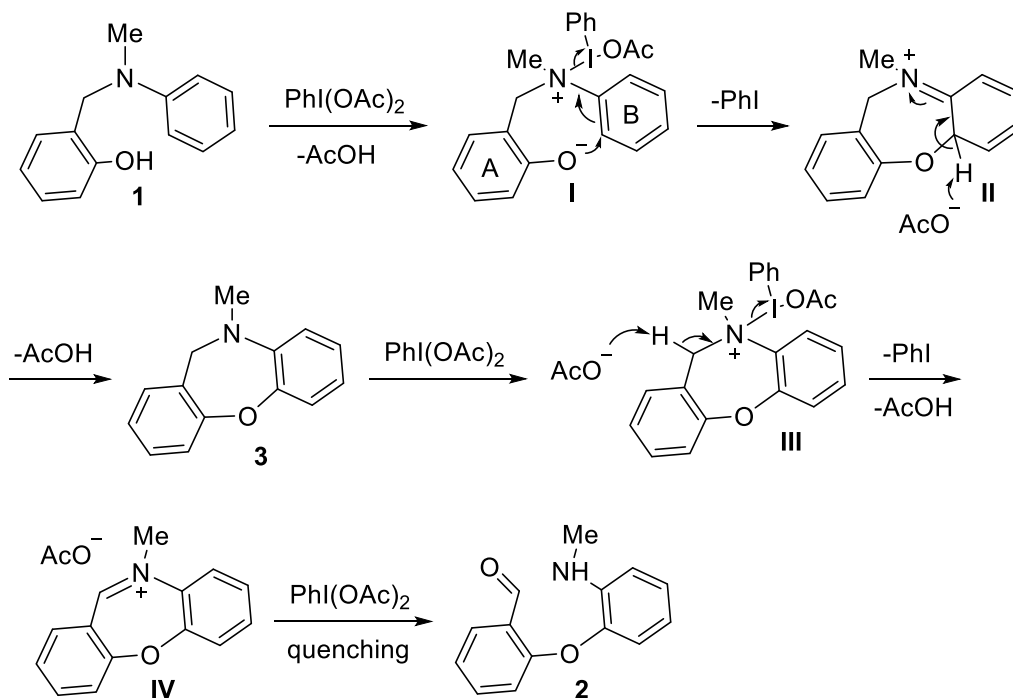
**Scheme 2.** Substrate scope of dibenzoxazepinones



A plausible mechanism has been proposed similar to activation of tertiary amines in presence of PIDA.<sup>[12]</sup> Oxidative dearomatization of phenols in presence of PIDA are well documented,<sup>[16]</sup> however, tertiary amine will be more reactive for the initial ligand exchange with PIDA. Accordingly, reaction of tertiary amine **1** with PIDA affords intermediate **I** (Scheme 3). Nucleophilic attack of the phenoxide on the electro-deficient ortho-carbon of the aniline ring in intermediate **I** is proposed analogous to a nucleophilic attack of the aniline ring on the electron-deficient aromatic carbon atom of the anthranilic ring after PIDA activation.<sup>[9]</sup> This key seven-membered ring formation accompanied by elimination of phenyl iodide affords intermediate **II** that rearomatizes to provide dibenzoxazepine **3**. It is worth mentioning that stabilization of intermediate **I** by the presence of deactivating groups in A ring and activating groups in B ring promotes formation of dibenzoxazepines in good yields, observed in substrate scope. Usage of one equivalent of PIDA produced a mixture of dibenzoxazepine **3** and diaryl ether **2** along with unreacted tertiary amine **1** as observed over TLC (see Supporting Information). Dibenzoxazepine **3** is further reactive with PIDA due to the presence of tertiary amine. Therefore, a second equivalent of PIDA affords intermediate iminium ion **IV** which is

formed by abstraction of benzylic proton from the activated tertiary amine **III**. The reaction mixture was quenched upon complete consumption of the dibenzoxazepine **3** which ensuring ring opening of iminium intermediate **IV** to afford diaryl ether **2**. This was again confirmed by the reaction of the dibenzoxazepine **3g** with 1 equiv of PIDA which led to the formation of diaryl ether **2g** in 87% yield (see Supporting Information). In absence of nucleophilic hydroxyl group, the competing benzylic proton abstraction to facilitate iminium ion formation takes place which upon hydrolysis produces benzaldehyde. Indeed formation of 2-methoxy-5-nitrobenzaldehyde was observed from tertiary amine **1c** with methyl protected hydroxyl group (see Supporting Information).

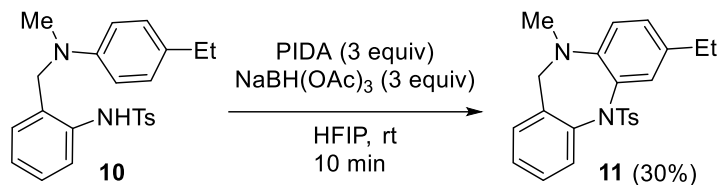
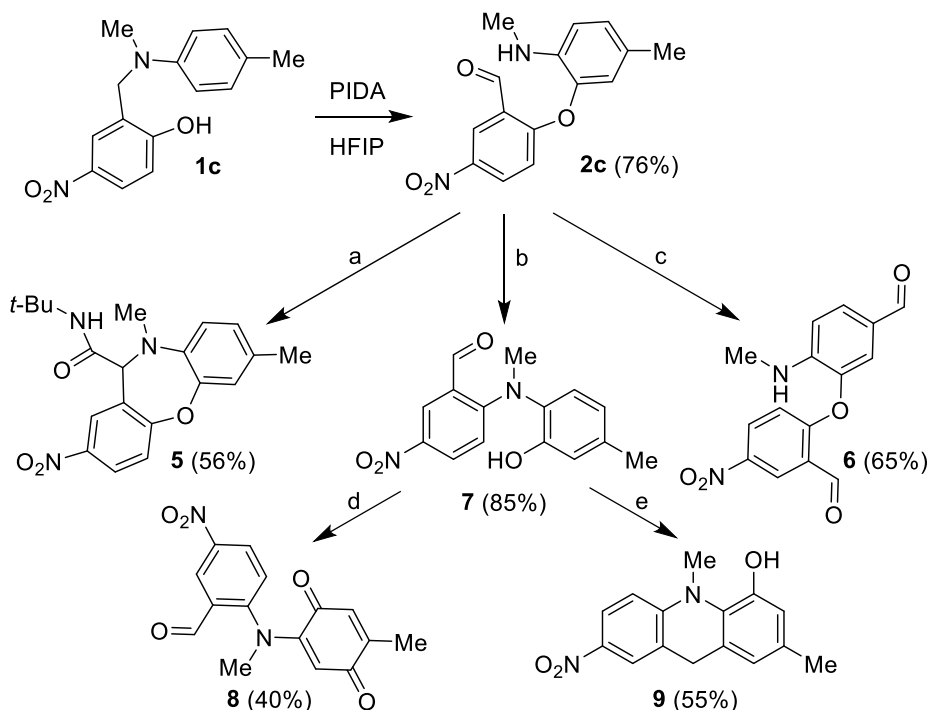
**Scheme 3.** Plausible mechanistic pathway



In order to further demonstrate the broad applicability of this methodology, an array of synthetic transformations were carried out on diaryl ether **2c** (Scheme 4). Treatment of compound **2c** with *tert*-butylisocyanide afforded a pharmaceutically relevant dibenzoxazepine-11-carboxamide **5**. A facile DDQ mediated oxidation of benzylic carbon afforded diaryl ether **6** flanked by three reactive functionalities. Presence of para-nitro substitution in ether facilitates an intramolecular *ipso*-substitution with secondary amine by

Smiles rearrangement, interestingly, undertaken in presence of bleach to afford tertiary amine **7** in 85% yield. During this rearrangement, events that take place such as hopping of the hydroxyl group of tertiary amine **1c** from A ring to B ring and benzylic amine transformation to diphenyl amine are otherwise conceived by multi-step synthesis. Furthermore, tertiary amine **7** in presence of Dess-Martin periodinane and *p*-TsOH afforded *para*-benzoquinone **8** and dihydroacridine **9** in 40 and 55% yields, respectively. Structural confirmation of all the products was carried out by extensive 2D NMR analysis (see Supporting Information). A further extension of this methodology to afford dibenzodiazepine **11**, categorized as privileged structure by Evans et al.,<sup>[17]</sup> was obtained from tertiary amine **10** with an appropriate NHTs substitution.

**Scheme 4.** Demonstration of applicability of methodology



Reaction conditions: (a) **2c** (1 equiv), *t*-BuNC (1 equiv),  $\text{InCl}_3$  (cat.), MeOH, 60 °C; (b) **2c** (1 equiv), NaClO (2 equiv), 1M NaOH (cat),  $\text{Bu}_4\text{NI}$  (1.5 equiv), DCM, rt; (c) **2c** (1 equiv), AcOH (cat.), DDQ (3 equiv), DCM, rt; (d) **7** (1 equiv), DMP (1.5 equiv), DCM, rt; (e) **7** (1 equiv), *p*-TsOH (cat.), EtOH, 60 °C.

In conclusion, tertiary amines with suitably substituted *ortho*-hydroxybenzyl, phenyl units with varied substituents underwent diaryl ether formation endowed with *ortho*-CHO and secondary amine functionalities in presence of PIDA by *ortho*-C( $\text{sp}^2$ )-H functionalization under mild conditions. An intramolecular seven-membered ring formation facilitated by  $\text{NaBH}(\text{OAc})_3$  and PCC provided dibenzoxazepines and dibenzoxazepinones, respectively. A broad substrate scope for dibenzoxazepine has been demonstrated, in particular,

substrates with deactivating groups in A ring and activating groups in B ring offered good yields in a one-pot reaction. Furthermore, an array of synthetic transformations to further demonstrate the broad applicability of this methodology was carried out which afforded diverse molecular motifs.

### Acknowledgements

Financial support from The Kerala State Council for Science, Technology & Environment (KSCSTE), India received by R.S.L. for Kerala State Young Scientist Award is gratefully acknowledged. R.S.L. is thankful to Dr. Sunil Varughese, CSIR-NIIST, for single crystal XRD analysis.

**Keywords:** Diaryl etherification • Hypervalent iodine reagent • Dibenzoxazepine • Dibenzoxazepinone • Metal-free • C(sp<sup>2</sup>)-H activation/functionalization

### References:

- [1] a) J. M. Klunder, J. K. D. Hargrave, M. West, E. Cullen, P. Mark, S. R. Kapadia, D. W. Mcneil, J. C. Wu, G. C. Chow, J. Adamst, *J. Med. Chem.* **1992**, *35*, 1887–1897; b) M. Binaschi, A. Boldetti, M. Gianni, C. A. Maggi, M. Gensini, M. Bigioni, M. Parlani, A. Giolitti, M. Fratelli, C. Valli, et al., *ACS Med. Chem. Lett.* **2010**, *1*, 411–415; c) A. Fiorentino, B. D'Abrosca, S. Pacifico, G. Cefarelli, P. Uzzo, P. Monaco, *Bioorganic Med. Chem. Lett.* **2007**, *17*, 636–639; d) P. P. M. A. Dols, B. J. B. Folmer, H. Hamersma, C. W. Kuil, H. Lucas, L. Ollero, J. B. M. Rewinkel, P. H. H. Hermkens, *Bioorganic Med. Chem. Lett.* **2008**, *18*, 1461–1467; e) H. J. M. Gijssen, D. Berthelot, M. Zaja, B. Brone, I. Geuens, M. Mercken, *J. Med. Chem.* **2010**, *53*, 7011–7020; f) S. M. Lynch, L. Tafesse, K. Carlin, P. Ghatak, D. J. Kyle, *Bioorg. Med. Chem. Lett.* **2015**, *25*, 43–47; g) K. Nagarajan, J. David, Y. S. Kulkarni, S. B. Hendi, S. J. Shenoy, P. Upadhyaya, *Eur. J. Med. Chem.* **1986**, *21*, 21–26; h) R. A. Smits, H. D. Lim, B. Stegink, R. A. Bakker, I. J. de Esch, R. Leurs, *J Med Chem* **2006**, *49*, 4512–4516; i) E. A. Hallinan, T. J. Hagen, S. Tsymbalov, R. K. Husa, A. C. Lee, A. Stapelfeld, M. A. Savage, *J. Med. Chem.* **1996**, *39*, 609–613.
- [2] a) A. Sapegin, E. Reutskaya, A. Smirnov, M. Korsakov, M. Krasavin, *Tetrahedron*



- Lett.* **2016**, *57*, 5877–5880; b) T. E. Hurst, M. O. Kitching, L. C. R. M. da Frotaa, K. G. Guimarães, M. E. Dalziela, V. Snieckus, *Synlett* **2015**, *26*, 1455–1460; c) S. Liu, Y. Hu, P. Qian, Y. Hu, G. Ao, S. Chen, S. Zhang, Y. Zhang, *Tetrahedron Lett.* **2015**, *56*, 2211–2213; d) Y. Liu, C. Chu, A. Huang, C. Zhan, Y. Ma, C. Ma, *ACS Comb. Sci.* **2011**, *13*, 547–553.
- [3] J. Feng, X. Wu, *Green Chem.* **2015**, *17*, 4522–4526.
- [4] J. Shi, J. Wu, C. Cui, W.-M. Dai, *J. Org. Chem.* **2016**, *81*, 10392–10403.
- [5] a) R. A. Bunce, J. E. Schammerhorn, *J. Heterocycl. Chem.* **2006**, *43*, 1031–1035; b) D. Tselikhovsky, S. L. Buchwald, *J. Am. Chem. Soc.* **2011**, *133*, 14228–14231; c) Q. Yang, H. Cao, A. Robertson, H. Alper, *J. Org. Chem.* **2010**, *75*, 6297–6299; d) Y. Zhou, J. Zhu, B. Li, Y. Zhang, J. Feng, A. Hall, J. Shi, W. Zhu, *Org. Lett.* **2016**, *18*, 380–383; e) M. O. Kitching, T. E. Hurst, V. Snieckus, *Angew. Chem. Int. Ed.* **2012**, *51*, 2925–2929.
- [6] a) K. Prabakaran, M. Zeller, K. Jayarampillai, R. Prasad, *Synlett* **2011**, 1835–1840; b) P. Mestichelli, M. J. Scott, W. R. J. D. Galloway, J. Selwyn, J. S. Parker, D. R. Spring, *Org. Lett.* **2013**, *15*, 5448–5451; c) C. Shen, H. Neumann, X.-F. Wu, *Green Chem.* **2015**, *17*, 2994–2999.
- [7] a) J.-Q. Zhang, Z.-H. Qi, S.-J. Yin, H.-Y. Li, Y. Wang, X.-W. Wang, *ChemCatChem* **2016**, *8*, 2797–2807; b) Y.-Y. Ren, Y.-Q. Wang, S. Liu, *J. Org. Chem.* **2014**, *79*, 11759–11767; c) A. F. Khlebnikov, M. S. Novikov, P. P. Petrovskii, A. S. Konev, D. S. Yufit, S. I. Selivanov, H. Frauendorf, *J. Org. Chem.* **2010**, *75*, 5211–5215; d) A. F. Khlebnikov, M. S. Novikov, P. P. Petrovskii, J. Magull, A. Ringe, *Org. Lett.* **2009**, *11*, 979–982.
- [8] X. Guo, D. Zhang-Negrerie, Y. Du, *RSC Adv.* **2015**, *5*, 94732–94736.
- [9] S. Shang, D. Zhang-Negrerie, Y. Du, K. Zhao, *Angew. Chem., Int. Ed.* **2014**, *53*, 6216–6219.
- [10] A. Yoshimura, V. V. Zhdankin, *Chem. Rev.* **2016**, *116*, 3328–3435.

- [11] a) L. Companys, Simon Pouysegu, P. A. Peixoto, S. Chassaing, S. Quideau, *J. Org. Chem.* **2017**, *82*, 3990–3995; b) S. P. Roche, J. Porco, John A., *Angew. Chem. Int. Ed.* **2011**, *50*, 4068–4093.
- [12] a) N. Zhang, R. Cheng, D. Zhang-Negrerie, Y. Du, K. Zhao, *J. Org. Chem.* **2014**, *79*, 10581–10587; b) H. Shen, X. Zhang, Q. Liu, J. Pan, W. Hu, Y. Xiong, X. Zhu, *Tetrahedron Lett.* **2015**, *56*, 5628–5631; c) L. Yang, D. Zhang-Negrerie, K. Zhao, Y. Du, *J. Org. Chem.* **2016**, *81*, 3372–3379; d) H. J. Rong, J. J. Yao, J. K. Li, J. Qu, *J. Org. Chem.* **2017**, *82*, 5557–5565; e) M. L. Deb, C. D. Pegu, P. J. Borpatra, P. K. Baruah, *Tetrahedron Lett.* **2016**, *57*, 5479–5483; f) N. A. Waghmode, A. H. Kalbandhe, P. B. Thorat, N. N. Karade, *Tetrahedron Lett.* **2016**, *57*, 680–683; g) X.-Z. Shu, X.-F. Xia, Y.-F. Yang, K.-F. Ji, X.-Y. Liu, Y.-M. Liang, *J. Org. Chem.* **2009**, *74*, 7464–7469.
- [13] As a recent example, see: R. Takise, R. Isshiki, K. Muto, K. Itami, J. Yamaguchi, *J. Am. Chem. Soc.* **2017**, *139*, 3340–3343, and references cited therein.
- [14] N. Jalalian, T. B. Petersen, B. Olofsson, *Chem. - A Eur. J.* **2012**, *18*, 14140–14149.
- [15] F. Liu, H. Yang, X. Hu, G. Jiang, *Org. Lett.* **2014**, *16*, 6408–6411.
- [16] a) S.-M. Lu, H. Alper, *J. Am. Chem. Soc.* **2005**, *127*, 14776–14784; b) D. Quideau, Stephane; Pouysegu, Laurent; Deffieux, *Synlett* **2008**, 467–495; c) L. Pouysegu, D. Deffieux, S. Quideau, *Tetrahedron* **2010**, *66*, 2235–2261; d) C. R. Reddy, R. Prajapati, Santosh Kumar Warudikar, Kamalkishor Ranjan, B. B. Rao, *Org. Biomol. Chem.* **2017**, *15*, 3130–3151; e) A. Pelter, R. S. Ward, *Tetrahedron* **2001**, *57*, 273–282.
- [17] B. E. Evans, K. E. Rittle, M. G. Bock, R. M. DiPardo, R. M. Freidinger, W. L. Whitter, G. F. Lundell, D. F. Veber, P. S. Anderson, R. S. L. Chang, et al., *J. Med. Chem.* **1988**, *31*, 2235–2246.

PP2.

## **Plant fibre cellulose polymer composites as a green alternative to conventional materials**

**Ramlath K T**<sup>1</sup> and Rajesh C<sup>2</sup>

*Department of Chemistry, MES Keveeyam College, Valanchery, Malappuram,  
Kerala, 676552, India*

With considerable awareness of preserving the environment, sincere efforts across the globe can be cited in looking for bio-degradable and bio-based sources.

Over the past decade, the concept of utilizing green materials has become more mainstream. Applications of bio-based materials from renewable and bio-degradable sources for preparation of higher valued green chemicals and bio-based products have forced many scientists to investigate the potential use of natural fibers and fiber cellulose as reinforcement materials for green bio-composites. Cellulosic fibers are becoming very interesting for bio-based material development as they possess advantages with their mechanical properties, low density, environmental benefits, renewability, and economic feasibility. Recently, natural- fiber polymer composites have received much attention for different industrial applications because of their low density and renewability. The bio-composites with natural fiber components are derivatives of depleting resources and can be considered to have substantial environmental and economic benefits. The composite materials are finding applications in diverse fields ranging from household, office appliances, power tools, and business equipment to space crafts.

The research and development of new biobased and biodegradable polymers and polymer composites from renewable resources as alternatives to conventional plastics has become an enticing area for both academic and industrial research due to the global concerns over plastic waste and pollution issues. These pro-environmental materials could be a promising solution for the global plastic waste problem. Traditional petroleum-based polymer composites have extensive use in a large number of diverse applications, ranging from small household devices to structural aircraft parts due to their high strength-to-weight ratios as compared to

conventional materials. The intensive reliance of plastics has led to an increasing amount of plastic waste in the environment. With the depletion of petroleum resources and growing global environmental concerns over climate change and environmental pollution, the development of sustainable biobased materials has been growing at a fast pace. Countries including China, France, United Kingdom, Germany, the United States, Japan, and Canada have developed strategies to adapt the circular economy model through sustainable and efficient resource management to help reduce the environmental strain from waste. These countries reinforce these strategies by emphasizing rules and regulations placed on industry manufacturers to develop more sustainable and environmentally friendly products from biobased and biodegradable materials.

This chapter addresses the potential utilization of natural fiber cellulose for the development of green polymer composite materials, with the objective to elucidate the possibility of using these bio composites for various industrial applications.

### **Composite**

A composite material is composed of at least two materials, which combine to give properties superior to those of the individual constituents. The many component materials and different processes that can be used make composites extremely versatile and efficient. They typically result in lighter, stronger, more durable solutions compared to traditional materials. The primary reason composite materials are chosen for components is because of weight saving for its relative stiffness and strength. For example, carbon-fiber reinforced composite can be five times stronger than 1020 grade steel while having only one fifth of the weight.

The two main components within a composite are the matrix and fiber. The matrix is the base material while the fiber is what reinforces the material. On top of the fiber reinforcements and matrix, composites can also include core materials, fillers, additives and surface finishes to provide unique performance attributes.

### **Properties of composite materials:**

- The tensile strength of composite materials is higher than conventional materials They have better torsion and stiffness properties.

- It has a high fatigue endurance limit (ultimate tensile strength of up to 60%).
- They are 30–45% lighter than aluminum structures designed for the same functional requirements.
- Also has low embedded energy.
- Composites make less noise during operation and provide less vibration.
- Composite materials are additional versatile.

Composite materials are commonly classified at following two distinct levels. Classification of composite materials. (a) Based on matrix materials and (b) based on reinforcement materials. The major composite classes based on matrix materials include organic matrix composites (OMCs), metal matrix composites (MMCs)

and ceramic matrix composites (CMCs). The term organic matrix composite includes two classes of composites, namely polymer matrix composites (PMCs) and carbon matrix composites commonly referred as carbon carbon matrices. Based on reinforcement materials -fiber reinforced composites, laminar composites and particulate composites. Fiber reinforced composites (FRP) can be further divided into those containing discontinuous or continuous fibers. Fiber reinforced composites are composed of fibers embedded in matrix material. Laminar composites are composed of layers of materials held together by matrix. Sandwich structures fall under this category. Particulate composites are composed of particles distributed or embedded in a matrix body. The particles may be flakes or in powder form.

### **Polymer composites**

Polymer matrix composites are materials made up of fibers that are embedded in an organic polymer matrix. Polymer matrix composites are classified based on their level of strength and stiffness into two distinct types: Reinforced plastics - confers additional strength by adding embedded fibrous matter into plastics

Advanced Composites - consists of fiber and matrix combinations that facilitate strength and superior stiffness. They mostly contain high-performance continuous fibers such as high-stiffness glass (S-glass), graphite, aramid, or other organic fibers.

The main advantages of polymer matrix composite materials are their strength and stiffness. Other qualities that come with the reinforcement of polymers are as follows:

Improved processing, Density control, Thermal Conductivity, Thermal Expansion Control, Flame retardancy, Cost reduction, Greater toughness

Abrasion resistance, Corrosion resistance, High specific strength to weight ratio

Improved fatigue strength, High creep resistance.

**Polymer composites have the following advantages:**

- Lightweight (potentially very high strength-to-weight ratio)
- High modulus and glass transition temperatures
- Ability to tailor properties for a wide range of applications
- Good fatigue resistance
- Easy to mould and bond to a variety of substrates or other composites
- Low thermal expansion
- Tailorable electrical properties o Insulating composites with non-conductive fillers

**Bio composites**

A biocomposite is a composite material formed by a matrix and a reinforcement of natural fibers. Environmental concern and cost of synthetic fibers have led the foundation of using natural fiber as reinforcement in polymeric composites. The matrix phase is formed by polymers derived from renewable and non-renewable resources. The matrix is important to protect the fibres from environmental degradation and mechanical damage, to hold the fibers together and to transfer the loads on it. In addition, bio fibre are the principal components of bio composites, which are derived from biological origins, for example fibres from crops (cotton, flax or hemp), recycled wood, waste paper, crop processing by-products or regenerated cellulose fibre (viscose/rayon). The interest in bio composites is rapidly growing in terms of industrial applications (automobiles, railway coach, aerospace, military applications, construction, and packaging) and fundamental research, due to its great benefits.

**Advantages of bio composites**

- Electrical resistance
- Easy process ability
- Less energy requirement in tooling and assembly

- Higher stiffness and strength
- Cheap
- Renewable source
- Completely recyclable
- Corrosion resistance

### Natural fibers

Natural fibres are fibres that are produced by geological processes, or from the bodies of plants or animals. Natural fibres can have different advantages over synthetic reinforcing fibres. Most notably they are biodegradable and renewable. Additionally, they often have low densities and lower processing costs than synthetic materials. The plants which produce cellulose fibers can be classified into bast fibers (flax, hemp, jute, kenaf, and ramie), leaf fibers (abaca, banana, pineapple, and sisal), seed fibers (coir, cotton, and kapok), as well as all other kinds (roots and wood). Many of the plant fibers such as banana, coir, flax, hemp, jute, pineapple, and sisal find applications as resource for industrial materials.

The main chemical components of natural plant fibers are cellulose, lignin, hemicelluloses, pectin, and wax. The components and their percentages vary depending on the type of natural plant fibers as shown in table below,

Fiber	Cellulose (wt%)	Lignin (wt%)	Hemicellulose (wt%)	Pectin (wt%)	Wax (wt%)	Moisture content (wt%)
Jute	61–71.5	12–13	13.6–20.4	0.4	0.5	12.6
Hemp	70.2–74.4	3.7–5.7	17.9–22.4	0.9	0.8	10
Kenaf	31–39	15–19	21.5	–	–	–
Flax	71	2.2	18.6–20.6	2.3	1.7	10
Ramie	68.6–76.2	0.6–0.7	13.1–16.7	1.9	0.3	8
Sunn	67.8	3.5	16.6	0.3	0.4	10
Sisal	67–78	8–11	10.0–14.2	10	2.0	11
Henquen	77.6	13.1	4–8	–	–	–
Cotton	82.7	–	5.7	–	0.6	–
Kapok	64	13	23	23	–	–
Coir	36–43	41–45	10–20	3–4	–	8
Banana	63–67.6	5	19	–	–	8.7
PALF	70–82	5–12	–	–	–	11.8

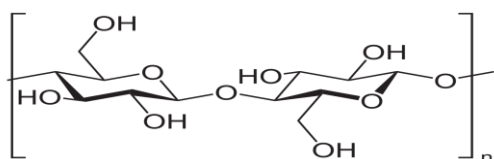
Natural fibres contain low cost, density and weight, less pollution during production resulting in minimal health hazards and eco-friendly nature. Composites reinforced

with natural fibres also have a short lifetime when it comes to degradation with limited environmental damage.

## Cellulose

Cellulose is an organic compound with formula  $(C_6H_{10}O_5)_n$ . It is polysaccharide made up of several hundreds or thousands of beta glucose unit. Cellulose is present in primary cell walls of green plants, present in algae, and in oomycetes. Some species of bacteria secrete it to form bio films. On earth, one of the abundant polymers is cellulose. In cotton the cellulose content is about 90%, in wood it is about 40-50% and in dried hemp it is about 57%.

Recently, cellulose has attracted considerable attention as one of the most well-known renewable and sustainable raw materials for obtaining environmentally friendly and biocompatible technological products. Due to its high tensile strength, chemical inertness, biodegradability and renewable nature cellulose is being extensively explored for applications in composite reinforcement, medicine, soft-tissue replacement, artificial bones, dental prostheses, food packaging, building materials etc. It is an odorless and tasteless compound. The appearance is a white powder. It is insoluble in water and most organic solvents. It is chiral and biodegradable. It has a hydrophilic nature and with contact angle of 20-30 degrees. The melting point is found to be 467 degrees in pulse test made by Dauenhauer. Cellulose can be broken down chemically into glucose units by concentrating with mineral acids at high temperature.



Beta glucose units condense through beta-(1, 4) - glycosidic bonds to form cellulose. A contrast with starch is that in starch, alpha-(1, 4)-glycosidic linkage is present. Cellulose is a straight chain polymer. In starch there is coiling and branches but in cellulose, such a coiling is absent. Cellulose molecule adopts an extended and a rather stiff rod like conformation, aided by equatorial conformation of glucose units. The multiple hydrogen bonds on one glucose form hydrogen bonds with oxygen atoms on the same or on a neighbor chain, holding the chains firmly together side by side and



forming micro fibrils with high tensile strength. This confers tensile strength in cell walls where cellulose micro fibrils are meshed into a polysaccharide matrix. The high tensile strength of plant stems and that of tree wood also arises from the arrangement of cellulose fibers intimately distributed into the lignin matrix.

Many properties of cellulose depend upon the chain length and degree of polymerization. The chain length of cellulose in wood pulp is between 300 and 1700 units. The bacterial cellulose, cotton and other plant fibers have chain length from 800 to 10,000 units. Cellodextrins have small length of chain resulting from break down of cellulose. Cellodextrins are soluble in water and organic solvents. Cellulose contains 44.4% carbon, 6.17% hydrogen and 43.39% oxygen. Plant derived cellulose is usually found in a mixture with hemicelluloses, lignin, pectin, and other substances, while bacterial cellulose is quite pure has much higher water content and higher tensile strength due to higher chain lengths.

### **Natural fibre reinforced biocomposite**

Natural plant fiber composites as environmentally attractive materials have been proven and emerged as an alternative to the glass reinforced composites used in many applications since the 1990s. It is a composite material that consists of three components: the natural fibres as the discontinuous or dispersed phase, the matrix as the continuous phase, and the interface. This is a type of advanced composite group, which makes use of rice husk, rice hull, rice shell, and plastic as ingredients. This technology involves a method of refining, blending, and compounding natural fibres from cellulosic waste streams to form a high-strength fibre composite material in a polymer matrix. It is high-performance fibre composite achieved and made possible by cross-linking cellulosic fibre molecules with resins in the composite material matrix through a proprietary molecular re-engineering process, yielding a product of exceptional structural properties.

### **Some important areas of applications include:**

- Aerospace industry
- Automotive industry
- Construction field
- Consumer goods

- Power industry
- Protective equipment
- Marine infrastructure.

Composite materials are revealing numerous enhancements in distinct material properties since their invention in the last century. Copious amounts of research efforts have been made to discover optimized material to perform in a more effective way for desired applications. Over the past few decades, reinforcements of fibers or particles in the matrix structure of composite materials have revealed outstanding remarks, making them a popular choice for topmost applications. Classifications of composite materials, along with the properties of their constituent elements, have been studied to understand the potentiality of different composite materials in various fields. Fiber-reinforced composite material was found to be one of the most promising and effective types of composites, as it claims dominance over the majority of applications from topmost fields. Composite materials are fabricated with a number of different techniques, among which every technique is applicable for certain material. Effectiveness of manufacturing technique is dependent on the combination of type and volume of matrix or fiber material used, as each material possesses different physical properties, such as melting point, stiffness, tensile strength, etc. Therefore, manufacturing techniques are defined as per the choice of material. For distinct applications in a variety of fields, certain solitary materials might be replaced with composite materials, depending on the enhancement in its required property. Composite structures have shown improvement in strength and stiffness of material, while the reduction in weight is magnificent. Composites have also revealed some remarkable features such as resistance to impact, wear, corrosion, and chemicals, but these properties are dependent upon the composition of the material, type of fiber, and type of manufacturing technique employed to create it. In accordance with the properties required, composite materials find their applications in many desired fields.

More future research is intended to discover new composite structures with a combination of different variants and adopting new manufacturing techniques.

## References

1. Alan J.L, Polymer Composites, *Polym. Compos*, **71**:1529-1622 (2018).
2. Brostow W, Dutta M and Rusek P, J.Modified epoxy coatings on Mild Steel: Tribology and Surface Energy, *Chem. Eur. J*, **46**:2181-2189(2010).
3. Cantwell WJ, Morton J. The impact resistance of composite materials—A review. *Composites*. 1991;**22**(5):347-362. DOI: 10.1016/0010-4361(91)90549-
4. Chanda M, Introduction to Polymer Science and Chemistry, CRC Press, Taylor and Francis Group, FL, USA, *J.Polym. Sci*, 12-14(2006).
5. Elias H.G, An Introduction to Polymer Science, Weinheim: VCH, *J.Polym. Sci. Technol*,1:19-59(1997).
6. Gowariker V.R, Viswanathan N.V and Sreedher J, *Polymer Science*, New Age International, New Delhi, 12-14(2005).
7. Gupta N, Singh Brar B and Worldeesenbet E, Effect of filler addition on the compressive and impact properties of glass fiber reinforced epoxy, *Bull. Mater. Sci*, **24**:219-223(2001).
8. Harsha A.P, An investigation on low stress abrasive wear characteristics of high performance engineering thermoplastic polymers, wears *Polym. Compos*, **46**:983-991(2011).
9. Ho MP, Wang H, Lee JH, Ho CK, Lau KT, Leng JS, Hui D. Critical factors on manufacturing processes of natural fibre composites. *Composites Part B Engineering*. 2012;**43**:3549-3562. DOI: 10.1016/j.compositesb.2011.10.001
10. Jand B.Z, Advanced polymer Composites: Principle and Applications, Material Park: ASM International, *J. Polym. Sci*, **4**:1-12(1994).
11. Jiang L, Zhang J, Wolcott M.P, Mechanical Performance of Polyhydroxyalkanoate (PHA) based Bio-composites, *J. Inorg. Biochem*, **3**:39-52(2015).
12. Joshia SV, Drzal LT, Mohanty AK, Arora S. Are natural fiber composites environmentally superior to glass fiber reinforced composites? *Composites Part A: Applied Science and Manufacturing*. 2004;**35**:371-376. DOI: 0.1016/j.compositesa.2003.09.016

13. Kalpakjian S, Schmid SR. Manufacturing Engineering and Technology. International Edition. 4th ed. Prentice Hall, Inc; New Jersey, USA; 2001. ISBN: 0-13-017440-8
14. Malcon P.S, Polymer chemistry: An introduction, *Oxford University Press*, **1**, 3-4 (1998).
15. Sanjay MR, Arpitha GR, Naik LL, Gopalakrishna K, Yogesha B. Applications of natural fibers and its composites: An overview. *Natural Resources*. 2016;**7**:108-114. DOI: 10.4236/nr.2016.730
16. Vinod kumar T, Chandrashekar M and Padmanabhan S, Characteristic and Mechanical properties of Reinforced Polymer Composites, Department of Mechanical Engineering, VELS University, *J. Polym. Sci.* **12**:567-601(2006-2007).
17. Yuanjian T, Isaac DH. Impact and fatigue behaviour of hemp fibre composites. *Composites Science and Technology*. 2007;**67**:3300-3307. DOI: 10.1016/j.compscitech.2007.03.039

**PP3.**

**Salinity Stress Alters the Secondary Metabolites Production in *Abrus precatorius* L.**

K.P. Lafna Farshana<sup>1</sup>, P. Deepa<sup>2\*</sup>, Shibla Banu<sup>3</sup>

<sup>1</sup>PG Department of Botany, MES Kalladi College, Palakkad, Kerala, India, 678583.

<sup>2,3</sup>PG Department of Botany, Korambayil Ahammed Haji Memorial Unity Women's College,  
Malappuram, Kerala, India, 676122.

\*deepapsaj@gmail.com

**ABSTRACT**

The white seeded *Abrus precatorius* L. is an important herbaceous medicinal plant with broad range of therapeutic effects. In the present study, the internode selected as explants for *in vitro* salt tolerance analysis. For callus induction, MS media with different concentrations and compositions of BAP, Kinetin and IBA were used. Better callus fresh weight and dry weight observed on MS medium supplemented with BAP 0.5 mg/L and Kinetin 1 mg/L. To detect the *in vitro* salt tolerance potential of callus, NaCl at different concentrations (0, 20, 40, 60, 80 and 100 mM) were supplemented on MS + BAP 0.5 mg/L + Kinetin 1 mg/L of which 40 mM NaCl induced better callus proliferation. The callus grown without NaCl stress showed the presence of eight phytochemical compounds in GC-MS analysis. While the NaCl stress tolerant callus exhibited the presence of seventeen phytochemical compounds. All these analyzed compounds are with antimicrobial / anti-oxidant properties. The present work will be very much helpful to ameliorate the production of medicinally significant compounds in pharmaceutical industry.

**KEY WORDS:** Callus, plant growth regulators, salt tolerance, secondary metabolites, GC-MS analysis, retention time.

## INTRODUCTION

The genus *Abrus* includes about 18 species which belongs to the family Leguminosae and native to Africa, Madagascar, India and Indo-China (Swanepoel & Kolberg, 2011). The generic name, *Abrus* is derived from the Greek word *habro* which means delicate, elegant, pretty or soft in reference to the leaflets (Lewis *et al.*, 2015). Among the species, white seeded *Abrus precatorius* L. is a garden ornamental plant characterized by climbing, twining or trailing vine with slender branches. It is commonly known as 'white kunki' in Malayalam and 'kunch' in Bengali. The plant is best known for its white seeds which are used as beads and in percussion instruments. The species contain various kinds of alkaloids such as glycerrhizin, precol, abrol, abrasion, abrin A and abrin B (Joshi & Joshi, 2000). Moreover, the presence of abrin indicates the toxicity of white seeds. In addition to the toxic effect, the plant parts have many medicinal properties due to the presence of different secondary metabolites that including antimicrobial, anti-inflammatory, immunomodulatory and antitumor activities (Roy *et al.*, 2012).

Plants need balanced abiotic factors for optimum biomass productivity. Occasionally, the proper plant development is arrested by different abiotic stresses. Salinity is one of the abiotic stresses that negatively influence the plant growth and development. Nowadays, soil salinity is a major issue in much crop plant cultivation, especially in case of rice cultivation. It can be negatively influenced on growth, development and yield of rice plants. In medicinal plants, salt stress induces the production of a number of secondary metabolites which are medicinally important (Jaleel *et al.*, 2008). Currently, this method of production of medicinal compounds has a significant role in the pharmaceutical industry. The tissue culture technique is a better opportunity to implement salt stress in *in vitro* cultured plants. This *in vitro* approach can be produced a lot of progenies from a single explant by direct or indirect organogenesis. The explant may be any tissue of the mother plant with desired characters including leaf, node, internode, seed, rhizome, apical meristem etc. Application of plant growth regulators like auxins and cytokinins in an optimum ratio causes the regeneration of *in vitro* plantlets directly from explants (Loberant & Altman, 2009). In contrast, somatic embryogenesis on callus tissue in turn results micropropagation of plantlets by the regeneration of embryos from somatic cells of the callus. The potential of

a single plant cell to regenerate an entire plant is the totipotency which is the basic reason behind the micropropagation (Marton & Czako, 2011).

*In vitro* salt stress has been researched in many medicinal plants like *Centella asiatica* (L.) Urb., *Catharanthus roseus* (L.) G. Don, *Trigonella foenum-graecum* L., *Carthamus tinctorius* L. etc. (Jaleel *et al.*, 2008; Gengmao *et al.*, 2015; Sahari *et al.*, 2016; Ibrahim *et al.*, 2018). To adapt unfavorable stress conditions, the salt tolerant plants produce different secondary metabolites to serve cellular functions essential for physiological processes. Secondary metabolites have no role in the growth and development of the plants, but they required to survive in the environment (Yang *et al.*, 2018). The *in vitro* produced metabolites can be separated using GC-MS (Gas Chromatography-Mass Spectrometry) analysis, a technology for secondary metabolite profiling in extracts of plant and non-plant species. Gas chromatography separates the components of the mixture and mass spectroscopy analyzes each of the components separately (Sermakkani & Thangapandian, 2012). These stress induced metabolites frequently show medicinal properties to suppress different microbial diseases (Patra & Mohanta, 2014). Due to the present relevance, the study was focused on *in vitro* salt tolerance and related metabolite production in white seeded *A. precatorius*.

## **MATERIALS AND METHODS**

### **Plant material and sterilization**

The shoots of *A. precatorius* collected from Botanical Garden of Korambayil Ahammed Haji Memorial Unity Women's College, Manjeri, Kerala, India and immediately transferred to sterile polythene bag and tightly tied. Using a sterile blade, the internodes of the plants were separated and used as explants for *in vitro* studies. The explants incubated in 0.1 % Bavistine for 3 hours followed by 1% Teepol treatment for 1 hour. Then, the explants washed thoroughly with double distilled water to remove the sterilizing agents. For further sterilization process, the explants treated with 0.1% mercuric chloride (HgCl<sub>2</sub>) for 3-5 minutes that followed by washing with sterile double distilled water and 70 % ethanol.

### **Callogenesis**

The sterile explants inoculated in selected culture media supplemented with proper concentrations of plant growth regulators. The MS media supplemented with different plant growth regulators including MS + BAP 0.5 mg/L+ IBA 0.5 mg/L, MS + BAP 1 mg/L+ IBA 1 mg/L, MS + BAP 0.5 mg/L + IBA 1 mg/L, MS + BAP 1 mg/L+ IBA 0.5 mg/L, MS + BAP 0.5 mg/L+ Kinetin 0.5 mg/L, MS + BAP 1 mg/L+ Kinetin 1 mg/L, MS + BAP 0.5 mg/L+ Kinetin 1 mg/L and MS + BAP 1 mg/L+ Kinetin 0.5 mg/L, were used to induce callus from the internodes. The prepared media sterilized at 121 °C for 30 minutes in an autoclave at the pressure of 15 psi. The pH of the medium maintained to 5.8 for optimum growth. The cultures kept under controlled conditions of light intensity, temperature and photoperiod which maintained in the incubation room.

### ***In vitro* salinity stress**

The different concentrations of NaCl (0, 20, 40, 60, 80 and 100 mM) used to provide salt stress in *in vitro* culture. The best callus inducing and proliferating medium, MS + BAP 0.5 mg/L+ Kinetin 1 mg/L, with pH of 5.8 selected to supply the salinity stress. The cultures were maintained at  $24 \pm 2$  °C with light intensity of  $1500 \mu\text{Em}^{-2}\text{S}^{-1}$  and photoperiod of 8 hours. The growth changes were observed and photographed weekly. The data analyzed statistically using single factor ANOVA.

### **Secondary metabolite analysis**

The secondary metabolites in the hexane extract of the calli which were grown with and without NaCl stress analyzed using GC-MS method. The analysis carried out using the instrument method - C:/Xcaliber/RCE KKD/DRUGS//METHOD/NAT.PRODUCTS. Meth - from Department of Applied Chemistry, KFRI (Kerala Forest Research Institute), Peechi, Trissur, Kerala, India.



## RESULTS AND DISCUSSION

### Callus induction

The valuable medicinal plant, *A. precatorius*, is using to treat different types of human diseases due to the presence of different secondary metabolites. While the hard seed coat and difficulty in vegetative propagation is the major problem to produce the healthy seedlings in bulk. To overcome the issue, the tissue culture technique is highly useful nowadays. The present study reveals the callus regeneration from inter nodal explant within 14 days when cultured on MS medium fortified with BAP 0.5 mg/L + Kinetin 1 mg/L and BAP 1 mg/L + IBA 0.5 mg/L. The remaining media induced callus regeneration on explants within 21 days (Table 1). The specific concentration and combination of BAP, IBA and Kinetin is the basic reason for callogenesis. Each plant needs an optimum concentration of cytokinine and / or auxin for callogenesis from the explants. In the investigation of Biswas *et al.* (2007), the callus developed from the cut surface of nodal explants that cultured on MS medium fortified with 5.0 mg/L BAP and 0.5 mg/L NAA. While the callus induction from nodal, intermodal and tendrill explants of *A. precatorius* was successfully done by Ramar *et al.* (2018).

In the study, the callus was white in colour, compact and non-embryogenic initially; but gradually it turned to green (Figure 1). In contrast, the formation of yellowish and compact callus from the nodal segments of *A. precatorius* on MS + 2,4-D 1 mg/L + NAA 1 mg/L reported by Hassan *et al.* (2009) in which the different concentration of auxins induced the callus formation. The callus is the mass of undifferentiated tissue that in turn regenerates the *in vitro* plantlets. The nature of the callus, compact or friable / embryogenic or non-embryogenic, depends to the plant species. Within 63 days, the callus grown on MS medium supplemented with BAP 0.5 mg/L + Kinetin 1 mg/L and BAP 1 mg/L + IBA 0.5 mg/L showed maximum rate of fresh weight (FW) and dry weight (DW). It proves the higher callus induction and proliferation potential in presence of specific media composition. As the age of calli increased, the colour changed gradually from green to yellowish-brown. The browning of calli may be due to nutrient depletion or accumulation

of phenolic compounds in cells. Sometimes, these cells get ruptured by higher plasmolysis that causes releasing of phenolics into the media (Jones & Saxena, 2013).

Table 1: Fresh weight (gm), dry weight (gm) and biomass (gm) of calli that grown on different media. The values are mean  $\pm$  SE, N = 5, significant at 5 % level using single factor ANOVA.

Compositions of media	Fresh weight (gm) + SE	Dry weight (gm) + SE	Callus biomass (gm) + SE
MS+BAP0.5mg/L+IBA0.5mg/L	1.84 $\pm$ 0.01	0.75 $\pm$ 0.02	1.43 $\pm$ 0.02
MS+BAP1mg/L+IBA1mg/L	1.72 $\pm$ 0.03	0.78 $\pm$ 0.01	1.15 $\pm$ 0.01
MS+BAP0.5mg/L+IBA1mg/L	1.88 $\pm$ 0.01	0.73 $\pm$ 0.01	1.57 $\pm$ 0.03
MS+BAP1mg/L+IBA0.5mg/L	2.05 $\pm$ 0.02	0.80 $\pm$ 0.03	1.56 $\pm$ 0.01
MS+BAP0.5mg/L+Kinetin0.5mg/L	1.76 $\pm$ 0.03	0.80 $\pm$ 0.006	1.20 $\pm$ 0.02
MS+BAP1mg/L+Kinetin1mg/L	1.80 $\pm$ 0.04	0.79 $\pm$ 0.01	1.28 $\pm$ 0.01
MS+BAP0.5mg/L+Kinetin1mg/L	2.08 $\pm$ 0.01	0.72 $\pm$ 0.02	1.89 $\pm$ 0.04
MS+BAP1mg/L+Kinetin0.5mg/L	1.96 $\pm$ 0.02	0.72 $\pm$ 0.01	1.72 $\pm$ 0.01
MS+BAP0.5mg/L+Kinetin1mg/L+NaCl20mM	1.24 $\pm$ 0.02	0.59 $\pm$ 0.02	1.10 $\pm$ 0.03
MS+BAP0.5mg/L+Kinetin1mg/L+NaCl40mM	1.68 $\pm$ 0.04	0.65 $\pm$ 0.01	1.58 $\pm$ 0.02
MS+BAP0.5mg/L+Kinetin1mg/L+NaCl60mM	1.06 $\pm$ 0.05	0.46 $\pm$ 0.002	1.30 $\pm$ 0.01
MS+BAP0.5mg/L+Kinetin1mg/L+NaCl80mM	0.81 $\pm$ 0.01	0.45 $\pm$ 0.003	0.80 $\pm$ 0.005
MS+BAP0.5mg/L+Kinetin1mg/L+NaCl100mM	0.47 $\pm$ 0.04	0.29 $\pm$ 0.001	0.62 $\pm$ 0.01

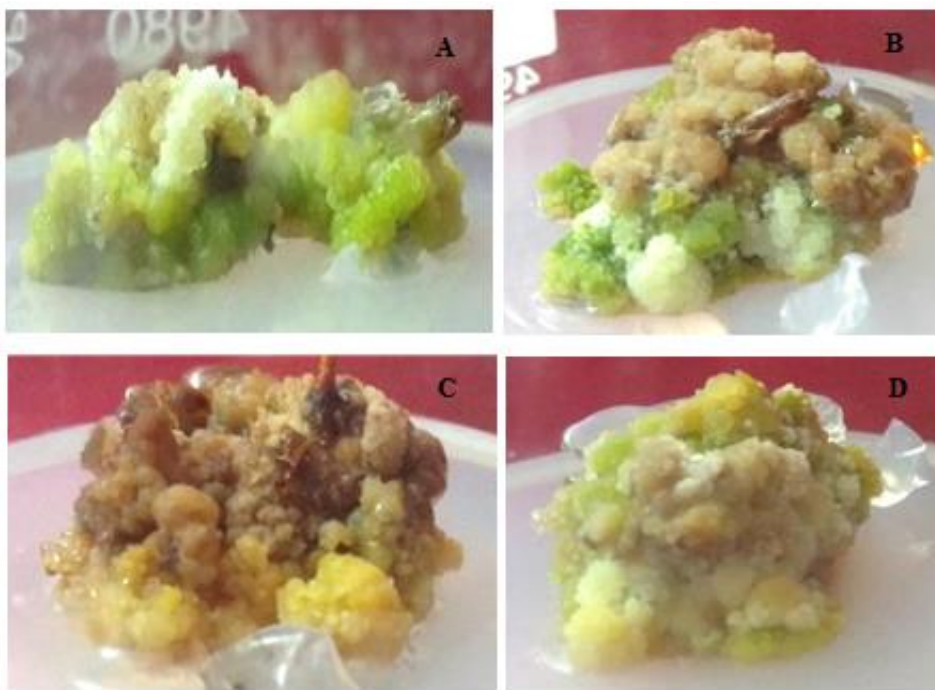


Figure 1: Callus induction from the internodes of *A. precatorius* on different culture media; **A.** MS + BAP 0.5 mg/L + Kinetin 1 mg/L, **B.** MS + BAP 1 mg/L + IBA 0.5 mg/L, **C.** MS + BAP 1 mg/L + Kinetin 0.5 mg/L and **D.** MS + BAP 0.5 mg/L + IBA 1 mg/L.

### ***In vitro* salt stress**

*In vitro* production of salt tolerant lines has a significant role in agriculture and pharmacognosy. The regenerated plants can overcome the salinity stress by the presence of an internal genetic mechanism that controls the salt tolerant plant metabolism (Tuteja, 2007). Typically, the salt stress declines the callus induction and regeneration frequency in salt sensitive plants. But, some plants can resist the negative influence of *in vitro* salinity and regenerate the salt tolerant lines (Basu *et al.*, 2002).

In the study, the salinity brings about the morphological and biochemical changes in calli that were sub-cultured on MS medium supplemented with BAP 0.5 mg/L, Kinetin 1 mg/L and different concentrations of NaCl (20, 40, 60, 80 and 100 mM). The proliferation, fresh weight, dry weight and biomass of calli were enhanced when the calli cultured on MS medium fortified with NaCl concentration up to 40 mM (Table 1). Then the calli

proliferation gradually decreased when the concentration of NaCl increased from 40 mM to 100 mM. Now, many of the recent studies have focused on the regeneration of salt tolerant rice varieties viz., Navara, IR-64, SR-26B, Chini Kanai, BRRI Dhan 38 etc. through the tissue culture techniques in which the plantlets urged the genetic potential to survive under salt stress condition (Basu *et al.*, 2002; Priya *et al.*, 2011; Zinnah *et al.*, 2013). Furthermore, the reduction of proliferation frequency and fresh weight of *in vitro* calli under salinity stress observed in different medicinal plants (Patade *et al.*, 2008). The influence of salinity leads to the colour variations in calli. The calli of *A. precatorius* grown on medium supplemented with NaCl upto 40 mM concentration showed yellow colour with compact and non-embryogenic consistency. While the yellowish callus changed to brown colour when the concentration of NaCl increased from 60 mM to 100 mM (Figure 2).

Most of the studies related to salinity stress encompass the darkening of calli. It may due to the unavailability of water for proper metabolic activities. Meanwhile, the higher concentration of NaCl has an influence on the secondary metabolism that results in the amelioration of medicinally important metabolite production compared to the calli cultured without salt stress (Hasegawa *et al.*, 2000; Zhu, 2011). The presence of these metabolites also causes the browning of calli. To avoid the negative impact of soil salinity on agriculture, the regeneration of salt tolerant plantlets is significant which can be done by the application of appropriate ratio of auxins and cytokinins in the culture medium of salt tolerant calli.

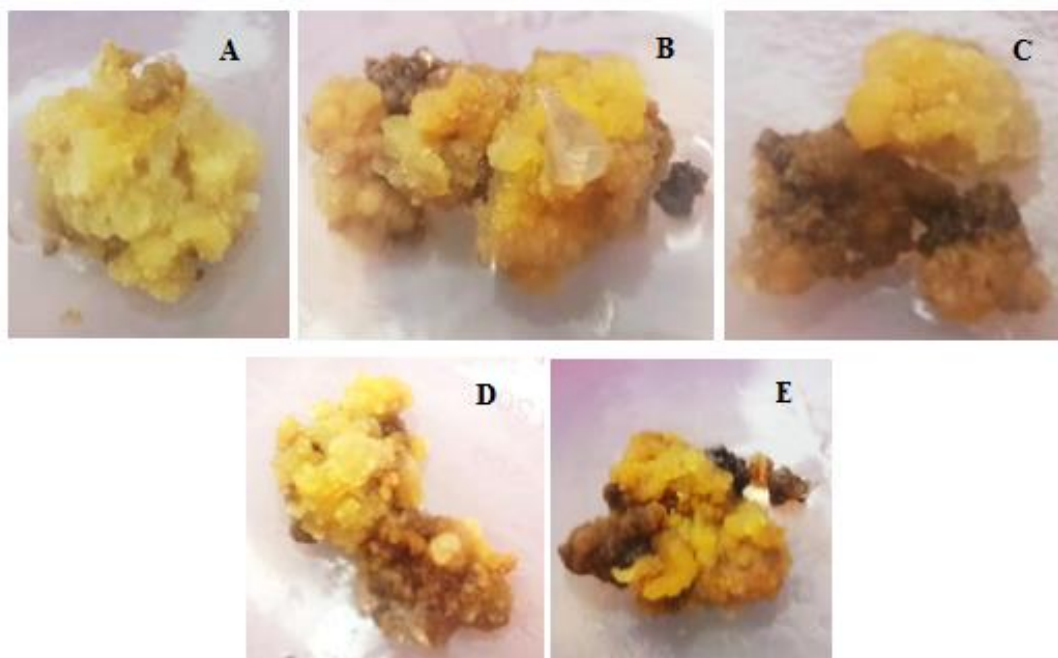


Figure 2: Callus proliferation of *A. precatorius* on MS + BAP 0.5 mg/L + Kinetin 1 mg/L supplemented with different concentrations of NaCl (20 (A), 40 (B), 60 (C), 80 (D) and 100 (E) mM).

### Secondary metabolite production

Application of salt stress in *in vitro* culture is a better method to produce valuable secondary metabolites with medicinal value. In the pharmaceutical industry, there are different methods to isolate and detect secondary metabolites from plant extracts. GC-MS analysis is one of the advanced techniques to identify different organic metabolites from the extracts of medicinal plants (Safaei-Ghomi *et al.*, 2009). In the study, the secondary compounds of calli which cultured on medium with and without NaCl stress were detected using the GC-MS method. The number of detected compounds was higher in callus grown under NaCl stress compared to the calli cultured without NaCl. The enhancement of secondary metabolite production under salt stress is detected in many of the *in vitro* plant cultures (Jaleel *et al.*, 2008; Rishla *et al.*, 2017). In *Carthamus tinctorius* L., the supplementation of NaCl below 100 mM concentration in Hoagland solution improved the production of medicinal flavonoids (Gengmao *et al.*, 2015). Presently, seventeen compounds were analyzed from the salt tolerant callus of *A. precatorius*; of

which the compound, 5-ethyl-1-nonene showed the lowest retention time (RT), 4.24. While, the highest RT exhibited by 1,1,1-trifluoroheptadecen-2-one, 33.19. Retention time indicates the time taken by the organic compounds / solutes to pass through the chromatography column that influenced by many factors including column length, column degradation, gas flow rate etc. (Ezhilan & Neelamegam, 2012). Among the compounds, stigmasterol showed the highest area percentage (33.94%) and the lowest area percentage by ethyl palmitate (0.43%) (Table 2, Figure 3 & Figure 4). Interestingly, thirteen new compounds were detected from the salt tolerant callus that was not observed in the callus grown without NaCl stress. The type and concentration of secondary metabolites produced by an *in vitro* plant is determined by its genotype, physiology, developmental stage and environmental factors during growth (Isah, 2019). Moreover, the different environmental factors viz. temperature, light intensity, the supply of water and minerals, has a considerable role in secondary metabolite production (Akula & Ravishankar, 2011). Though, eight different secondary metabolites were analyzed in calli cultured on medium without NaCl to which dodecanoic acid showed the lesser RT, 13.45 and sitostenone exhibited higher value. In the analysis, stigmasterol and dodecanoic acid were with higher and lower area percentage respectively (Table 2). As reported by many researchers, the detected metabolites in calli of *A. precatorius* show antimicrobial, antioxidant and anti-inflammatory activities (Agboke, 2015; Parasuraman *et al.*, 2016; Patel *et al.*, 2016). Remarkably, the present study will be very much helpful in pharmacology to produce medicinally significant compounds in future.

Table 2: Compounds analyzed from callus grown with and without NaCl stress using GC-MS.

Sl. No.	Retention Time	Area %	Compounds	Nature of callus
1	13.45	0.89	Dodecanoic acid	
2	18.82	0.98	Pentadecanoic acid	
3	22.69	5.79	Campesterol	

PROCEEDINGS OF THE SEMINAR ON  
'EMERGING AREAS OF CHEMICAL SCIENCES'

4	25.24	49.18	Stigmasterol	Callus grown without NaCl
5	28.17	34.85	beta-Sitosterol	
6	28.95	4.93	beta-Amyrin	
7	30.60	2.39	Spinasterone	
8	32.75	0.99	Sitostenone	
1	4.24	2.72	5-Ethyl-1-nonene	Callus grown with NaCl
2	13.36	0.79	Dodecanoic acid	
3	18.77	3.90	Pentadecanoic acid	
4	18.91	1.14	Dibutyl phthalate	
5	19.16	0.43	Ethyl palmitate	
6	22.46	1.92	trans-Pinosylvin dimethyl ether	
7	23.18	3.83	Stigmasterol methyl ether	
8	23.98	33.94	Stigmasterol	
9	24.50	0.46	Pinostrobin chalcone	
10	27.05	24.81	Gamma-Sitosterol	
11	28.49	1.76	Beta-Amyrin	
12	28.70	10.00	5 Alpha-Stigmastane-3,6-dione	
13	28.82	1.77	Illudol	
14	29.27	0.69	Squalene	
15	29.92	6.82	Citrost-7-en-3-ol	
16	30.90	2.52	Beta-Saccharostenone	
17	33.19	2.49	1,1,1-Trifluoroheptadecen-2-one	

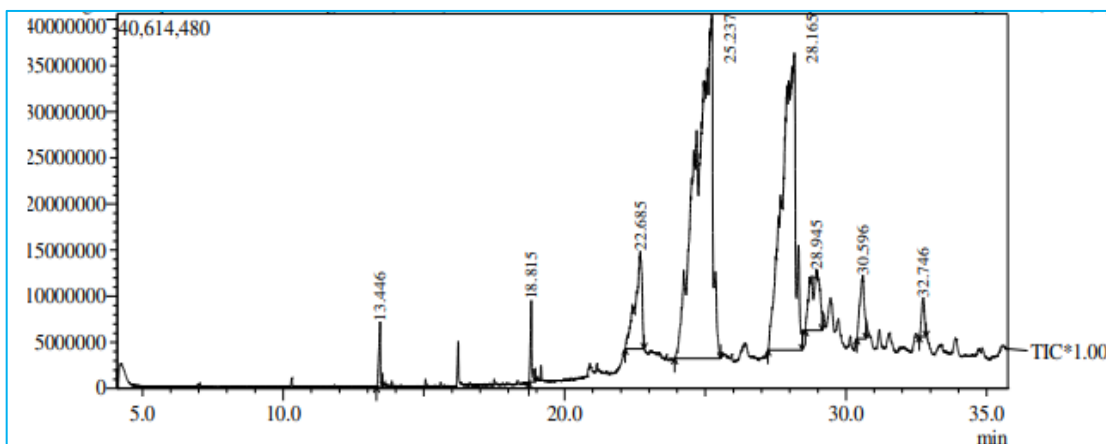


Figure 3. GC-MS chromatogram of compounds observed in callus grown without NaCl stress

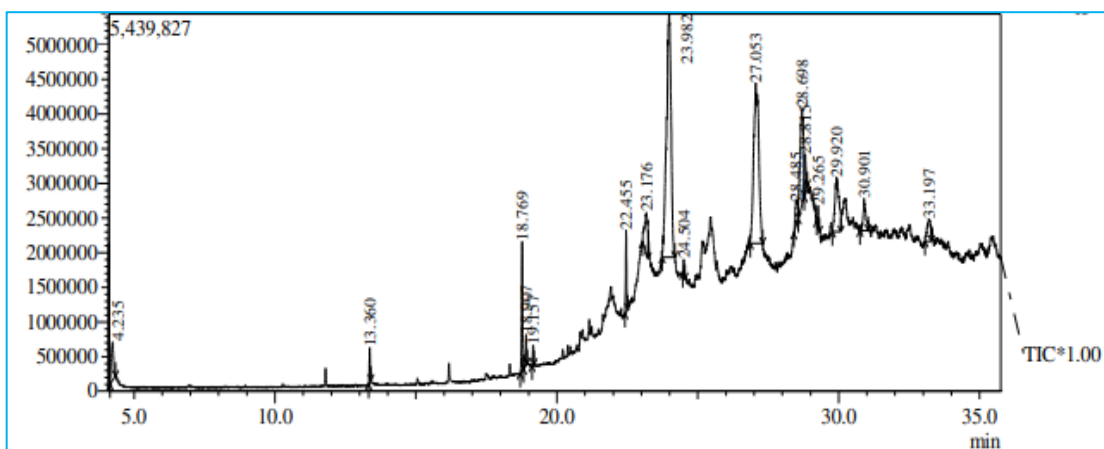


Figure 4. GC-MS chromatogram of compounds observed in callus grown with NaCl stress

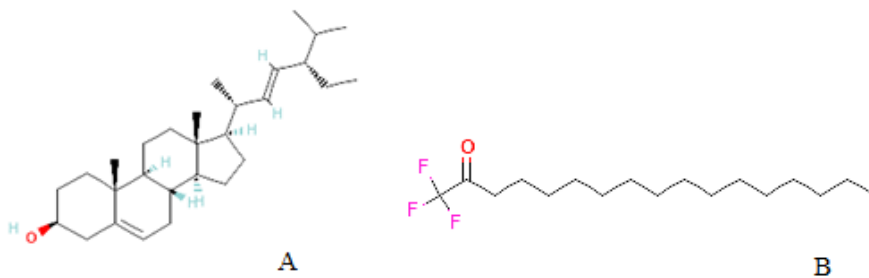


Figure 5. Structure of (A) stigmasterol and (B) 1,1,1-Trifluoroheptadecen-2-one



## CONCLUSION

The white seeded *A. precatorius* is an important source of organic compounds with therapeutic effects. *In vitro* culture plays as the best method to multiply the species. The MS medium supplemented with BAP 0.5 mg/L + Kinetin 1 mg/L and BAP 1 mg/L + IBA 0.5 mg/L showed better callus induction within a short period. These green compact non-embryogenic calli were with highest fresh weight, dry weight and biomass. The presence of NaCl negatively influenced callus proliferation of which calli cultured with 40 mM NaCl exhibited a greater degree of callus biomass. This salt tolerant calli is the source of 17 different medicinally important metabolic compounds that may be a new breakthrough in the field of drug discovery.

## ACKNOWLEDGEMENT

The authors are very much thankful to the Principal, Korambayil Ahammed Haji Memorial Unity Women's College, Manjeri, Kerala, India for providing the laboratory facilities to complete the work.

## REFERENCES

- Agboke, A. A. (2015). Antimicrobial activity of ethanol extract and fractions of *Moringa oleifera* Lam. root bark on clinical isolates of methicillin resistant *Staphylococcus aureus*. *Methods*, 8, 17-19.
- Akula, R., & Ravishankar, G. A. (2011). Influence of abiotic stress signals on secondary metabolites in plants. *Plant Signaling and Behavior*, 6(11), 1720-1731.
- Basu, S., Gangopadhyay, G., & Mukherjee, B. B. (2002). Salt tolerance in rice *in vitro*: Implication of accumulation of Na<sup>+</sup>, K<sup>+</sup> and proline. *Plant Cell, Tissue and Organ Culture*, 69(1), 55-64.
- Biswas, A., Roy, M., Miah, M. B., & Bhadra, S. K. (2007). *In vitro* propagation of *Abrus precatorius* L. - a rare medicinal plant of Chittagong hill tracts. *Plant Tissue Culture and Biotechnology*, 17(1), 59-64.

- Ezhilan, B. P., & Neelamegam, R. (2012). GC-MS analysis of phytochemicals in the ethanol extract of *Polygonum chinense* L. *Pharmacognosy Research*, 4(1), 11-14.
- Gengmao, Z., Yu, H., Xing, S., Shihui, L., Quanmei, S., & Changhai, W. (2015). Salinity stress increases secondary metabolites and enzyme activity in safflower. *Industrial Crops and Products*, 64, 175-181.
- Hasegawa, P. M., Bressan, R. A., Zhu, J. K., & Bohnert, H. J. (2000). Plant cellular and molecular responses to high salinity. *Annual Review of Plant Biology*, 51(1), 463-499.
- Hassan, M. M., Azam, F. S., Chowdhury, M. H., & Rahmatullah, M. (2009). Callus induction of *Abrus precatorius*: screening of phytohormones. *American-Eurasian Journal of Sustainable Agriculture*, 512-519.
- Ibrahim, M. H., Shibli, N. I., Izad, A. A., & Zain, N. A. M. (2018). Growth, chlorophyll fluorescence, leaf gas exchange and phytochemicals of *Centella asiatica* exposed to salinity stress. *Annual Research & Review in Biology*, 27(2), 1-13.
- Isah, T. (2019). Stress and defense responses in plant secondary metabolites production. *Biological Research*, 52(1), 1-25.
- Jaleel, C. A., Sankar, B., Sridharan, R., & Panneerselvam, R. (2008). Soil salinity alters growth, chlorophyll content, and secondary metabolite accumulation in *Catharanthus roseus*. *Turkish Journal of Biology*, 32(2), 79-83.
- Jones, A. M. P., & Saxena, P. K. (2013). Inhibition of phenylpropanoid biosynthesis in *Artemisia annua* L.: a novel approach to reduce oxidative browning in plant tissue culture. *PLoS One*, 8(10), e76802.
- Joshi, S. G., & Joshi, S. G. (2000). Medicinal plants. Oxford and IBH publishing.
- Lewis, G., Schrire, B., Mackinder, B., & Lock, M. (2005). Tribe Abreae. Legumes of the world: Royal Botanic Gardens, Kew, 389-392.

- Loberant, B., & Altman, A. (2009). Micropropagation of plants. *Encyclopedia of industrial biotechnology: bioprocess, bioseparation, and cell technology*, 1-17.
- Marton, L., & Czako, M. U. S. (2011). Washington, DC: U.S. Patent and Trademark Office. Patent No. 7,863,046.
- Parasuraman, S., Ren, L. Y., Chuon, B. L. C., Yee, S. W. K., Qi, T. S., Ching, J. Y. S., & Raj, P. V. (2016). Phytochemical, antimicrobial and mast cell stabilizing activity of ethanolic extract of *Solanum trilobatum* Linn. leaves. *Malaysian Journal of Microbiology*, 12(5), 359-364.
- Patade, V. Y., Suprasanna, P., & Bapat, V. A. (2008). Effects of salt stress in relation to osmotic adjustment on sugarcane (*Saccharum officinarum* L.) callus cultures. *Plant Growth Regulation*, 55(3), 169.
- Patel, N. K., Jaiswal, G., & Bhutani, K. K. (2016). A review on biological sources, chemistry and pharmacological activities of pinostrobin. *Natural Product Research*, 30(18), 2017-2027.
- Patra, J. K., & Mohanta, Y. K. (2014). Antimicrobial compounds from mangrove plants: A pharmaceutical prospective. *Chinese Journal of Integrative Medicine*, 20(4), 311-320.
- Priya, A. M., Pandian, S. K., & Ramesh, M. (2011). Effect of NaCl on *in vitro* plant regeneration from embryogenic callus cultures of cv IR 64 indica rice (*Oryza sativa* L.). *African Journal of Biotechnology*, 10(36), 6947-6953.
- Ramar, K., Dhinesh, V., Kannanur, T., & Kanimozhi, A. (2018). *In vitro* callus induction studies on *Abrus precatorius* L., A medicinal plant. *International Journal of Advance Research, Ideas and Innovations in Technology*, 4(2), 1496-1500.
- Rishla, K., Sithara, A., & Deepa, P. (2017). Effect of NaCl stress on callus induction in *Centella asiatica* (L.) Urban. *European Journal of Biomedical and Pharmaceutical Sciences*, 1, 1-50.

- Roy, S., Acharya, R., Mandal, N. C., Barman, S., Ghosh, R., & Roy, R. (2012). A comparative antibacterial evaluation of raw and processed Gunja (*Abrus precatorius* Linn.) seeds. *Ancient Science of Life*, 32(1), 20-23.
- Safaei-Ghomi, J., Ebrahimabadi, A. H., Djafari-Bidgoli, Z., & Batooli, H. (2009). GC/MS analysis and *in vitro* antioxidant activity of essential oil and methanol extracts of *Thymus caramanicus* Jalas and its main constituent carvacrol. *Food Chemistry*, 115(4), 1524-1528.
- Sahari, M. A., Mehrafarin, A., & Naghdi, B. H. (2016). Changes of trigonelline, nicotinic acid and proline content in early growth stages of *Trigonella foenum-graecum* L. under Saline condition. *Journal of Medicinal Plants*, 15(57), 47-55.
- Sermakkani, M., & Thangapandian, V. (2012). GC-MS analysis of *Cassia italica* leaf methanol extract. *Asian Journal of Pharmaceutical and Clinical Research*, 5(2), 90-94.
- Swanepoel, W., & Kolberg, H. (2011). *Abrus kaokoensis* (Leguminosae-Papilionoideae-Abreae), a new species from Namibia. *South African Journal of Botany*, 77(3), 613-617.
- Tuteja, N. (2007). Mechanisms of high salinity tolerance in plants. In *Methods in enzymology*, Academic Press, 428, 419-438.
- Yang, L., Wen, K. S., Ruan, X., Zhao, Y. X., Wei, F., & Wang, Q. (2018). Response of plant secondary metabolites to environmental factors. *Molecules*, 23(4), 762.
- Zhu, J. K. (2011). Cell signaling under salt, water and cold stresses. *Current Opinion in Plant Biology*, 4(5), 401-406.
- Zinnah, K. M. A., Zobayer, N. S., Sikdar, S. U., Liza, L. N., Chowdhury, M. A. N., & Ashrafuzzaman, M. (2013). *In vitro* regeneration and screening for salt tolerance in rice (*Oryza sativa* L.). *International Research Journal of Biological Sciences*, 2(11), 29-36.

**PP4.**

**Studies on Structure and DNA interaction of Nickel(II) complexes of  
NO donor Schiff base**

**Dr. Deepa K**

**Korambayil Ahamed Haji Memorial Unity Women's College, Manjeri,  
Malappuram, Kerala**

**(Authors email: deepakarat08@gmail.com Mobile: +919447477514)**

**Abstract**

A series of Nickel(II) complexes ligated by 2,3-Dimethyl-4-formyl-[2'-(aminomethyl)pyridine]-1-phenyl-3-pyrazolin-5-one (DFAPP),  $[\text{Ni}(\text{DFAPP})_2\text{X}_2]$  (where X =  $\text{Cl}^-$  or  $\text{Br}^-$ ) (**1**) (**2**),  $[\text{Ni}(\text{DFAPP})_2(\text{NO}_3)]\text{NO}_3$  (**3**), and  $[\text{Ni}(\text{DFAPP})_2(\text{ClO}_4)]\text{ClO}_4$  (**4**) has been synthesized and characterized with the help of elemental analysis, molar conductance magnetic moments and IR and UV spectroscopic data. The Schiff base is found to act as bidentate ligand using NO donor set of atoms leading to an octahedral geometry around central metal ion in all the complexes. The interaction of the complexes with calf thymus DNA (CT-DNA) has been investigated by UV absorption method and viscometry method. The mode of binding of the complexes with DNA was evaluated and is found to be groove binding.

**Keywords**

Nickel(II) complexes, Schiff base, Spectra, Magnetic Susceptibility, DNA binding behavior, intercalation, hyperchromism, Viscosity.

**Introduction**

Transition metal complexes with Schiff base as ligands have been amongst the widely studied coordination compounds in the past few years, since they are found to be widely applicable in biochemical, analytical and antimicrobial fields [1, 2, 3]. The metal ions present in complexes can accelerate the drug action and efficacy of the organic

therapeutic agents [4]. Transition metal complexes are currently being used to bind and react at specific sequences of DNA in a search for novel chemotherapeutic agents and better anticancer drugs [5]. Herein, we have synthesized and characterized a series of novel Nickel(II) complexes of Schiff base ligand 2,3-Dimethyl-4-formyl-[2'-(aminomethyl)pyridine]-1-phenyl-3-pyrazolin-5-one and investigated their DNA binding activity.

### Materials and Methods

High purity 4-antipyrine carboxaldehyde, 2-amino methylpyridine, Calf thymus DNA (CT DNA) (Aldrich,USA), Nickel(II) chloride hexahydrate, Nickel(II) nitrate hexahydrate, *Tris*-HCl (E.Merck,India) was purchased from respective concerns and used as such. Bromide and perchlorate of Nickel(II) were prepared by dissolving Analar Nickel carbonate in the respective 50% acids and crystallizing the salts after concentrating the resulting solutions on a steam bath. All other chemicals and solvents were of AR grade.

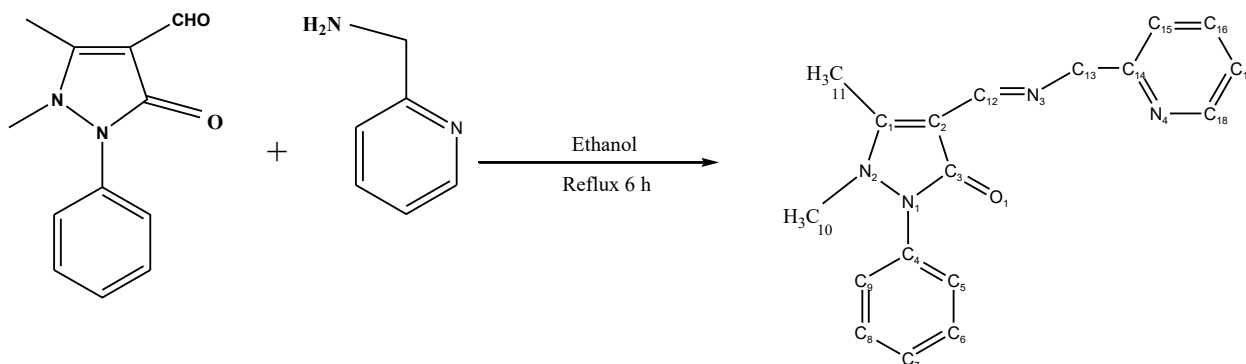
The C, H and N contents in the complexes were determined on a perkin –Elmer 240 CHN analyser. All the complexes were analyzed for their metal, halide and perchlorate contents by standard methods [6, 7]. Molar conductivities were measured using freshly prepared  $10^{-3}$  M solutions dimethyl formamide, acetonitrile, nitrobenzene and methanol at room temperature using a Thoshniwal conductivity bridge with dip type conductance cell (cell constant 0.9741) which was calibrated with 0.01M KCl solution [8]. The infrared spectra were recorded in the range  $4000-100\text{ cm}^{-1}$  on a Shimadzu IR 470 spectrometer.  $^1\text{H}$  and  $^{13}\text{C}$  NMR spectra were recorded on a Bruker AV-400 spectrophotometer using acetone- $\text{d}_6$  as solvent. Magnetic susceptibility measurements were performed on pulverized samples at room temperature on a Sherwood Magwy MSB MK1 balance. The diamagnetic corrections were calculated using pascal's constants.

All experiments involving the interaction of the complex with DNA were carried out in twice distilled buffer (5 mM *Tris*-HCl, 50 mM NaCl, pH 7.2) at room temperature. Stock solutions were stored at  $4\text{ }^\circ\text{C}$  and used after no more than 4 days. A solution of calf thymus DNA in the buffer gave a ratio of UV absorbance at 260 and 280 nm of 1.8-1.9

indicating that the DNA was sufficiently free of protein. The DNA concentration per nucleotide was determined by absorption spectroscopy using molar absorption coefficient ( $6600 \text{ cm}^{-1}$ ) at 260 nm. Viscometry measurements were carried out on semimicro dilution capillary viscometer with a thermostatic bath at room temperature.

### Synthesis of 2,3-Dimethyl-4-formyl-[2'-(aminomethyl)pyridine]-1-phenyl-3-pyrazolin-5-one

The ligand, DFAPP, was prepared by the condensation of antipyrine-4-carboxaldehyde and 2-(aminomethyl)pyridine in ethanolic medium. To a boiling solution of 10 mmol (1.0815 g) 2-(aminomethyl)pyridine in ethanol (20 ml), 10 mmol (2.1624 g) antipyrine-4-carboxaldehyde in ethanol (30 ml) was added and refluxed on a steam bath for about 6 h. The light brown crystals that obtained after cooling the resulting solution were filtered out and washed with cold ethanol to remove the unreacted reactants if any. It was then recrystallised from ethyl acetate and dried over phosphorus(V)oxide under vacuum. DFAPP is light yellow in colour, its molecular formula is  $\text{C}_{18}\text{H}_{18}\text{N}_4\text{O}$ , molecular mass is 306.37.



### Scheme1. 2,3-dimethyl-4-formyl-[2'-(aminomethyl)pyridine]-1-phenyl-3-pyrazoline-5-one (DFAPP)

The yield: 85%. m.p.148°C. Anal. Cal. for  $\text{C}_{18}\text{H}_{18}\text{N}_4\text{O}$  (306.37) C, 70.57; H, 5.92; N, 18.29. Found: C, 70.47; H, 5.87; N, 18.26%. IR( $\text{cm}^{-1}$ ): 1660 ( $-\text{C}=\text{O}$ ), 1562 ( $-\text{CH}=\text{N}-$ ), 1460, 698 (Pyridyl N).  $^1\text{H}$  NMR( $\delta$ ): 8.42 (s,1H,  $-\text{CH}=\text{N}-$ ), 7.23-7.67 (m, -Ph), 7.14-8.67 (m, py. ring), 3.71 (s,2H,  $-\text{N}-\text{CH}_2-$ ), 3.34(s,3H,  $-\text{N}-\text{CH}_3$ ), 2.55 (s,3H,  $=\text{C}-\text{CH}_3$ ).  $^{13}\text{C}$  NMR ( $\delta$ ):166.71 (C12). UV-VIS ( $\lambda_{\text{Max/nm}}$ ): 335 ( $\text{n} - \pi^*$ ), 247 ( $\pi - \pi^*$ ).

### Synthesis of complexes

A solution of NiCl<sub>2</sub>.6H<sub>2</sub>O, NiBr<sub>2</sub>.6H<sub>2</sub>O, Ni(ClO<sub>4</sub>)<sub>2</sub>.6H<sub>2</sub>O or Ni(NO<sub>3</sub>)<sub>2</sub>.6H<sub>2</sub>O in methanol (1 mmol, 10 mL) was added drop wise to a hot solution of DFAPP (2 mmol, 20 mL) in ethyl acetate and refluxed for about 3h on a water bath. The precipitated complexes were filtered and washed repeatedly with hot benzene. The complexes were recrystallized from methanol and dried under vacuum over phosphorous(V) oxide. Yield: **1** = 85%, **2** = 75%, **3** = 77%, **4** = 78%.

### Results and discussion

#### Physical characterization

The metal, chloride, bromide (6), perchlorate (7), carbon, hydrogen and nitrogen content in the complexes were determined. The elemental analysis data of the Ni(II) complexes are presented in the Table 1. The data suggest that the complexes **1- 4** may be formulated as [Ni(DFAPP)<sub>2</sub>X<sub>2</sub>] (where X = Cl<sup>-</sup> or Br<sup>-</sup>) (**1**) (**2**), [Ni(DFAPP)<sub>2</sub>(NO<sub>3</sub>)]NO<sub>3</sub> (**3**), and [Ni(DFAPP)<sub>2</sub>(ClO<sub>4</sub>)]ClO<sub>4</sub>(**4**). The molar conductance data reveal that the complexes [Ni(DFAPP)<sub>2</sub>Cl<sub>2</sub>](**1**) and [Ni(DFAPP)<sub>2</sub>Br<sub>2</sub>](**2**) behave as non- electrolytes, [Ni(DFAPP)<sub>2</sub>(NO<sub>3</sub>)]NO<sub>3</sub>(**3**) and [Ni(DFAPP)<sub>2</sub>(ClO<sub>4</sub>)]ClO<sub>4</sub>(**4**) behave as 1:1 electrolytes (8). All the complexes are soluble in acetonitrile, dimethylformamide, methanol and ethanol. All of them are insoluble in acetone, toluene, benzene, carbon tetrachloride, ethyl acetate, and chloroform.

#### Infrared spectral studies

The important infrared spectral bands of DFAPP and its Ni(II) complexes together with the tentative assignments are given in Table 2.

The infrared spectrum of the ligand exhibits a strong absorption at 1660 cm<sup>-1</sup> corresponding to stretching vibrations of the pyrazolone ring carbonyl oxygen. The band observed at 1562 cm<sup>-1</sup> is attributable to -C=N stretching vibrations. The absorptions at 1460 and 698 cm<sup>-1</sup> in the ligand are assigned respectively to ring stretching and out of plane deformation modes of pyridine moiety of DFAPP [9].



In the complexes, the band at  $1660\text{ cm}^{-1}$  is shifted to  $1650\text{ cm}^{-1}$  indicating coordination of carbonyl oxygen. At the same time strong band at  $1562\text{ cm}^{-1}$  is shifted to the region  $1573\text{-}1581\text{ cm}^{-1}$  suggesting coordination of imine nitrogen. The bands at  $1460$  and  $698\text{ cm}^{-1}$  remain unaltered indicating non participation of pyridyl nitrogen in coordination [10]. Thus DFAPP acts as a neutral bidentate ligand coordinating through carbonyl oxygen and imine nitrogen.

The nitrate complex exhibits the vibrational frequencies characteristic of uncoordinated nitrate ions. A very strong band at  $1384\text{ cm}^{-1}$  and a medium band at  $829\text{ cm}^{-1}$  are attributable to  $\nu_3$  and  $\nu_2$  vibrations of uncoordinated nitrate ion of  $D_{3h}$  symmetry [11]. The two medium bands at  $1492$  and  $1315\text{ cm}^{-1}$  are attributable to  $\nu_4$  and  $\nu_1$  vibrations respectively of coordinated nitrate ion of  $C_{2v}$  symmetry. Since  $(\nu_4 - \nu_1) = 177\text{ cm}^{-1}$ , the nitrate ion is coordinated in a bidentate fashion [12].

In perchlorate complex, the triply split band maxima at  $1148$ ,  $1115$  and  $1022\text{ cm}^{-1}$  are due to  $\nu_8$ ,  $\nu_6$  and  $\nu_1$  vibrations, respectively of perchlorate ion of  $C_{2v}$  symmetry, indicating coordination of perchlorate ion in a bidentate fashion [13]. The very strong band at  $1087\text{ cm}^{-1}$  is attributable to the  $\nu_3$  vibration of uncoordinated perchlorate ion of  $T_d$  symmetry. The bands observed at  $944$  and  $630\text{ cm}^{-1}$  due to  $\nu_2$  and  $\nu_3$  vibrations respectively of the coordinated perchlorate ( $C_{2v}$ ) ion and band at  $624\text{ cm}^{-1}$  due to  $\nu_4$  vibration of uncoordinated perchlorate ( $T_d$ ) ion [14] also support the co-existence of both coordinated and uncoordinated perchlorate ions in the complex.

There are two low frequency skeletal vibrations in the range  $554\text{-}562\text{ cm}^{-1}$  and  $440\text{-}461\text{ cm}^{-1}$  are due to M-O and M-N stretching respectively provide direct evidence for complexation.

In the infrared spectra of the halide complexes **1** and **2** the bands at  $287\text{ cm}^{-1}$  and  $302\text{ cm}^{-1}$  were due to the  $\nu(\text{Ni-Cl})$  and  $\nu(\text{Ni-Br})$  vibrations which are absent in the spectrum of the ligand.

### **Electronic spectra and Magnetis2**

The electronic spectral data with tentative assignments and magnetic moments of Ni(II) complexes of DFAPP are presented in the Table 3.

The electronic spectrum of DFAPP exhibits two main peaks at about 335 and 247 nm which are assignable to the  $n-\pi^*$  and  $\pi-\pi^*$  transitions respectively. In the complexes **1-4**, the  $n-\pi^*$  band is red shifted to 339-342 nm region and  $\pi-\pi^*$  band is blue shifted to 234-240 nm compared to DFAPP.

In complexes **1, 2, 3** and **4** the three main bands in the regions  $\nu_1 = 1037-1068$  nm,  $\nu_2 = 618-686$  nm and  $\nu_3 = 474-500$  nm corresponds to  ${}^3A_{2g}(F) \rightarrow {}^3T_{2g}(F)$ ,  ${}^3A_{2g}(F) \rightarrow {}^3T_{1g}(F)$  and  ${}^3A_{2g}(F) \rightarrow {}^3T_{1g}(P)$  transitions and are indicative of an octahedral geometry around nickel(II) ion. Besides the room temperature magnetic moments of the complexes **1, 2, 3** and **4** are 2.91, 2.96, 2.94 and 2.80 BM respectively indicating an octahedral geometry around nickel(II) ion [15, 16].

Furthermore, the complexes **1-4** show an intense absorption band in the 390-410 nm region which may be due to charge transfer transition [17].

**Table 1** Analytical data of Ni(II) complexes of DFAPP

Complex Molecular Formula/Weight	Analytical data. Obs.(Cal.)					M.P. (°C)	Yield (%)
	Carbon (%)	Hydrogen (%)	Nitrogen (%)	Metal (%)	Anion (%)		
[Ni(DFAPP) <sub>2</sub> Cl <sub>2</sub> ]( <b>1</b> ) C <sub>36</sub> H <sub>36</sub> N <sub>8</sub> O <sub>2</sub> Cl <sub>2</sub> Ni (742.31)	58.18 (58.25)	4.82 (4.88)	15.01 (15.09)	7.82 (7.90)	9.47 (9.55)	212	76
[Ni(DFAPP) <sub>2</sub> Br <sub>2</sub> ]( <b>2</b> ) C <sub>36</sub> H <sub>36</sub> N <sub>8</sub> O <sub>2</sub> Br <sub>2</sub> Ni (831.22)	51.92 (52.01)	4.30 (4.36)	13.39 (13.47)	6.97 (7.06)	19.16 (19.22)	211	82
Ni(DFAPP) <sub>2</sub> (NO <sub>3</sub> )]NO <sub>3</sub> ( <b>3</b> ) C <sub>36</sub> H <sub>36</sub> N <sub>10</sub> O <sub>8</sub> Ni (795.42)	54.23 (54.35)	4.41 (4.56)	17.49 (17.60)	7.28 (7.37)	27.32 (27.43)	221	77
[Ni(DFAPP) <sub>2</sub> (ClO <sub>4</sub> )]ClO <sub>4</sub> ( <b>4</b> ) C <sub>36</sub> H <sub>36</sub> N <sub>8</sub> O <sub>10</sub> Cl <sub>2</sub> Ni (870.31)	49.59 (49.68)	4.08 (4.16)	12.80 (12.87)	6.66 (6.74)	22.67 (22.85)	280	79

**Table 2** Important Infrared Spectral bands of Ni(II) complexes of DFAPP

DFAPP	(1)	(2)	(3)	(14)	Assignment
1660	1650	1650	1650	1650	$\nu(-C=O)$
1562	1581	1577	1577	1577	$\nu(-CH=N-)$
1460	1462	1459	1460	1461	$\nu_{py}$ ring str.
698	698	698	698	698	$\nu_{py}$ out plane str.
				1384	$\nu_3$ - uncoordinated $NO_3$
				829	$\nu_2$ - uncoordinated $NO_3$
				1492	$\nu_4$ - coordinated $NO_3$
				1315	$\nu_1$ - coordinated $NO_3$
			1148		$\nu_8$ - coordinated $ClO_4$
			1115		$\nu_6$ - coordinated $ClO_4$
			1022		$\nu_1$ - coordinated $ClO_4$
			944		$\nu_2$ - coordinated $ClO_4$
			630		$\nu_3$ - coordinated $ClO_4$
			1087		$\nu_3$ - uncoordinated $ClO_4$
			624		$\nu_4$ - uncoordinated $ClO_4$
	562	557	554	562	$\nu(Ni-O)$
	440	448	455	460	$\nu(Ni-N)$
	287				$\nu(Ni-Cl)$
		302			$\nu(Ni-Br)$

**Table 3** Electronic Spectral data and Magnetic Moments of Ni(II) complexes of DFAPP

Complex	Abs. Max (nm)	Tentative Assignments	$\mu_{eff}$ (BM)
DFAPP	335 247	$n-\pi^*$ $\pi-\pi^*$	
$[Ni(DFAPP)_2Cl_2](1)$	342 240	$n-\pi^*$ $\pi-\pi^*$	

	390 500 620 1054	Charge Transfer ${}^3A_{2g}(F) \rightarrow {}^3T_{1g}(P)$ ${}^3A_{2g}(F) \rightarrow {}^3T_{1g}(F)$ ${}^3A_{2g}(F) \rightarrow {}^3T_{2g}(F)$	2.91
[Ni(DFAPP) <sub>2</sub> Br <sub>2</sub> ](2)	341 236 392 476 685 1038	n- $\pi^*$ $\pi$ - $\pi^*$ Charge Transfer ${}^3A_{2g}(F) \rightarrow {}^3T_{1g}(P)$ ${}^3A_{2g}(F) \rightarrow {}^3T_{1g}(F)$ ${}^3A_{2g}(F) \rightarrow {}^3T_{2g}(F)$	2.96
[Ni(DFAPP) <sub>2</sub> (NO <sub>3</sub> )] NO <sub>3</sub> (3)	339 234 400 500 618 1068	n- $\pi^*$ $\pi$ - $\pi^*$ Charge Transfer ${}^3A_{2g}(F) \rightarrow {}^3T_{1g}(P)$ ${}^3A_{2g}(F) \rightarrow {}^3T_{1g}(F)$ ${}^3A_{2g}(F) \rightarrow {}^3T_{2g}(F)$	2.80
[Ni(DFAPP) <sub>2</sub> (ClO <sub>4</sub> )]ClO <sub>4</sub> (4)	342 238 410 474 686 1037	n- $\pi^*$ $\pi$ - $\pi^*$ Charge Transfer ${}^3A_{2g}(F) \rightarrow {}^3T_{1g}(P)$ ${}^3A_{2g}(F) \rightarrow {}^3T_{1g}(F)$ ${}^3A_{2g}(F) \rightarrow {}^3T_{2g}(F)$	2.94

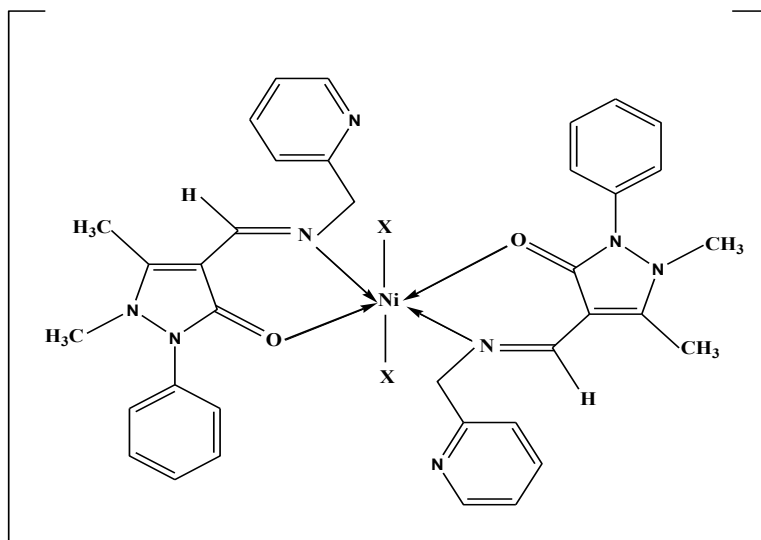
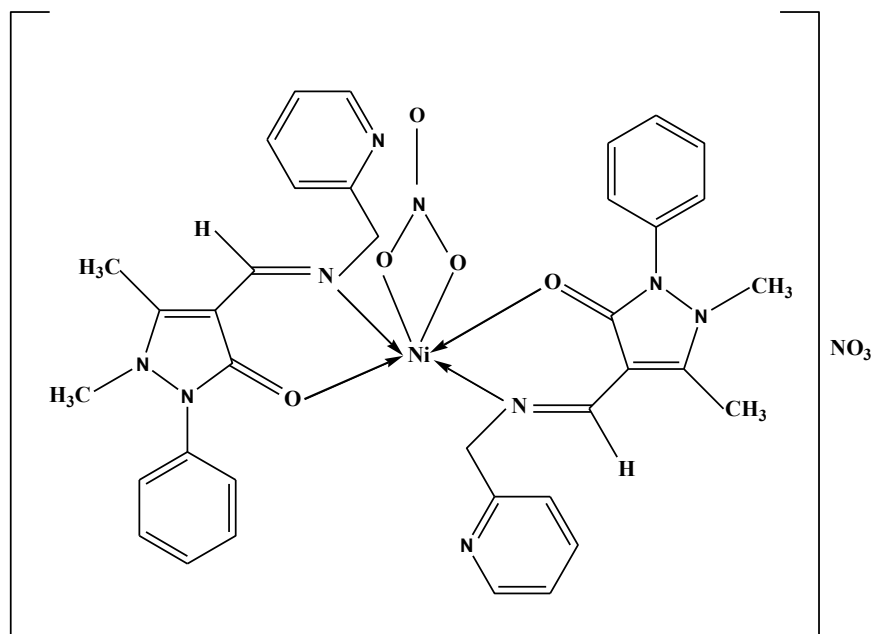
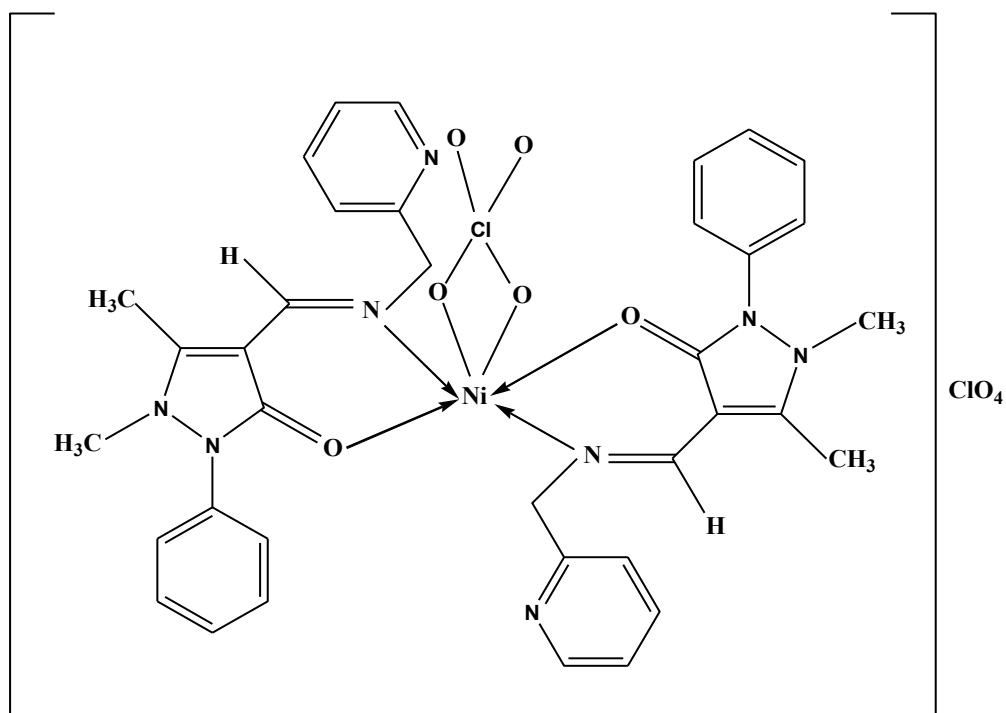


Fig 1 [Ni(DFAPP)<sub>2</sub>X<sub>2</sub>] (where X = Br<sup>-</sup> or Cl<sup>-</sup>) (1 and 2)



**Fig. 2** [Ni(DFAPP)<sub>2</sub>(NO<sub>3</sub>)]NO<sub>3</sub>(3)



**Fig. 3** [Ni(DFAPP)<sub>2</sub>(ClO<sub>4</sub>)]ClO<sub>4</sub>(4)

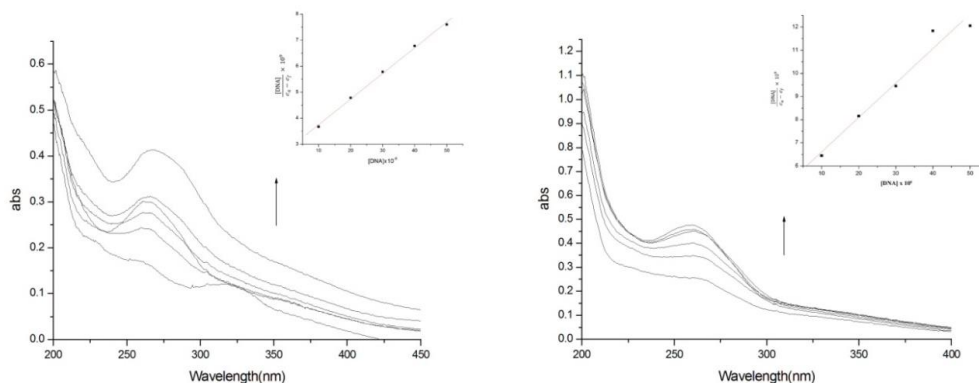
## DNA binding experiments

### Electronic spectral studies

The binding of complexes **1** - **4** were investigated by the technique of UV-Visible absorption titrations upon addition of increasing amount of DNA solution from 0 to 50  $\mu\text{M}$  to a constant concentration of complex (25  $\mu\text{M}$ ) the intense ligand based  $\pi\text{-}\pi^*$  absorption band of the complexes were used to monitor the interaction of present Nickel(II) complexes with CT DNA. The complexes exhibited hyperchromism in  $\pi\text{-}\pi^*$  absorption band which indicates that the complexes underwent a non-intercalative binding with DNA [18]. The absorption spectra of the complexes in the absence and in presence of CT-DNA (with constant concentration of complex) is given in Fig 4. The absorption data were analyzed to evaluate the intrinsic binding constant  $K_b$  which can be determined by the eqn.

$$[\text{DNA}]/(\epsilon_a - \epsilon_f) = [\text{DNA}]/(\epsilon_0 - \epsilon_f) + K_b/(\epsilon_0 - \epsilon_f)$$

Where  $[\text{DNA}]$  is the concentration of DNA in base pairs, the apparent absorption coefficients  $\epsilon_a$ ,  $\epsilon_0$  and  $\epsilon_f$  correspond to  $A_{\text{obsd}}/[\text{M}]$ . The extinction coefficient for the free copper complex and the extinction coefficient for the complex in fully bound form. The ratio of slope to intercept in plots of  $[\text{DNA}]/(\epsilon_a - \epsilon_f)$  versus  $[\text{DNA}]$  (Fig 4) gives the value of intrinsic binding constant  $K_b$ . The value of  $K_b$  for **1**, **2**, **3** and **4** are  $2.905 \times 10^5$ ,  $3 \times 10^4 \text{ M}^{-1}$ ,  $7.03 \times 10^6$  and  $1.44 \times 10^4$  respectively.



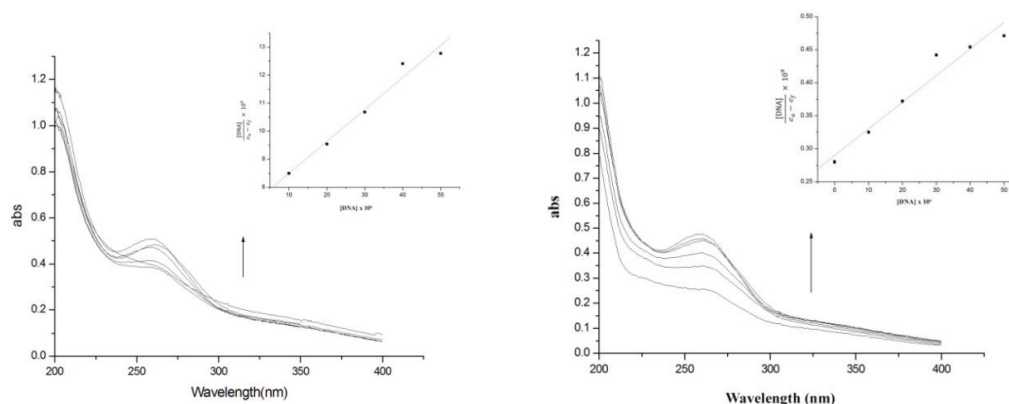


Fig. 4 The absorption spectra of the complexes in the absence and in presence of CT-DNA  
Viscosity measurements

The viscosity measurements of CT-DNA are regarded as the least ambiguous and most essential analysis of DNA binding mode in solution. In the absence of crystallographic structural data, viscosity measurements are regarded as most critical test of a binding model in solution. To clarify further the mode of interaction between the complexes and DNA, viscosity measurements were performed. The values of relative viscosities of complexes  $(\eta/\eta_0)^{1/3}$  (where  $\eta$  is the viscosity of DNA in presence of complex and  $\eta_0$  is the viscosity of DNA alone) is plotted against  $[\text{complex}]/[\text{DNA}]$  with increase in the amount of complex, the DNA viscosity shows only a small increase with increase of concentration of complex but the increase is less when compared to a classical intercalator. This observation is consistent with DNA groove binding [19]. The plots of  $(\eta/\eta_0)^{1/3}$  vs  $[\text{complex}]/[\text{DNA}]$  of the complexes is shown in Fig 5.

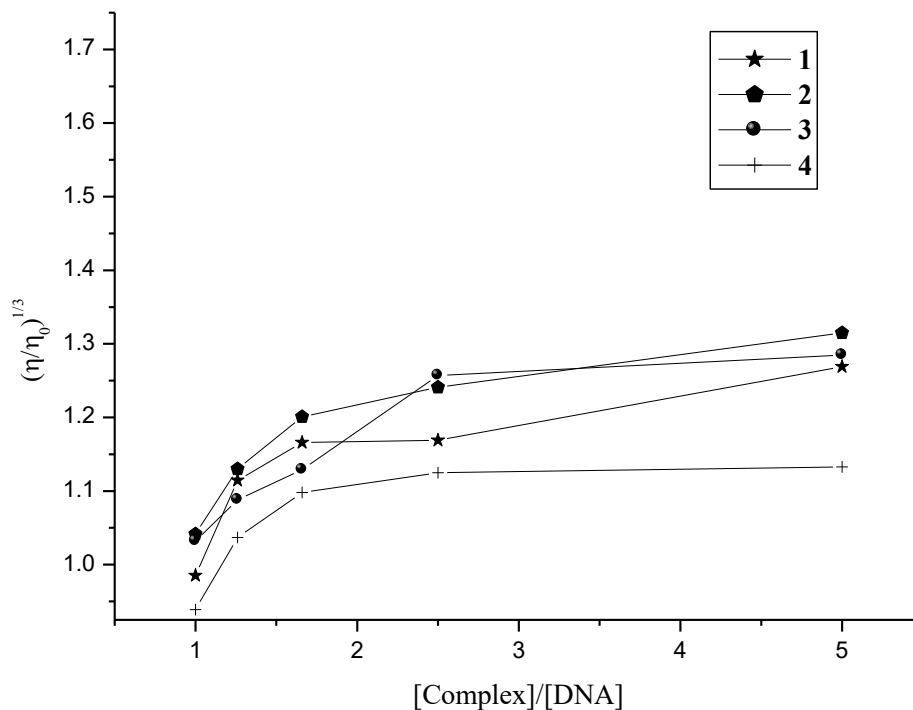


Fig 5 Effect of increasing amounts of complexes on viscosity of CT DNA ( $5 \times 10^{-5}M$ ).  
[Complex]/[DNA] = 1, 1.25, 1.66, 2.50, 5.

### Conclusions

Elemental studies and magnetic moment and spectral data reveal that DFAPP acts as a neutral bidentate ligand coordinating through pyrazolone carbonyl oxygen and imine nitrogen in all the complexes and both the anions are coordinated in chloride and bromide complexes, while only one of the anions is coordinated to the metal ion in nitrate and perchlorate complexes suggesting an octahedral geometry around central metal ion in all complexes. The interaction studies of the complexes with calf thymus DNA (CT-DNA) by UV absorption method and viscometry method suggest that the mode of binding is groove binding.

### Acknowledgements



I express my sincere gratitude to UGC=CSIR for financial support and School of Chemical Sciences, M G University, Kottayam for providing laboratory and instrumental facilities.

### References

1. Joseyphus RS, Sivasankaran Nair M (2008) Antibacterial and antifungal studies on some Schiff base complexes of Zinc(II), *Mycobiology* 36: 93-98.
2. Singh K, Kumar Y, Puri P, Sharma C, Anju KR (2012) Synthesis, spectroscopic, thermal and antimicrobial studies of Co(II), Ni(II), Cu(II) and Zn(II) complexes with Schiff bases derived from 4-amino-3-mercapto-6-methyl-5-oxo-1,2,4 triazine, *Med Chem Res* 21:1708-1716.
3. Kurdekar GS, Sathisha MP, Budagumbi S, Kulkarni NV, Revankar VK, Suresh DK (2012) 4-aminoantipyrine-based Schiff base transition metal complexes as potent anticonvulsant agents, *Med Chem Res* 21:2273-2279.
4. Siddiqi ZA, Khalid M, Kumar S, Shahid M, Noor S (2010) Antimicrobial and SOD activities of novel transition metal complexes of pyridine-2,6-dicarboxylic acid containing 4-picoline as auxiliary agent, *Euro J Med Chem* 45:264-269.
5. Arjmand F, Muddassir M (2010) Design and synthesis of heterometallic topoisomerase I and II inhibitor complexes: In vitro DNA binding interaction with 5'-GMP and 5'-TMP and cleavage studies, *Journal of Photochemistry and Photobiology ; Biology* 101: 37-46.
6. Vogel AI (1999) A text book of quantitative chemical analysis, 5<sup>th</sup> edn, Edn Addison Wesley Longman.
7. Kurz E, Kober G, Berl M (1958) Determination of Perchlorates by Fusion with Nitrite, *Anal Chem* 30: 1983-1986.
8. Geary WJ (1971) The use of conductivity measurements in organic solvents for characterization of coordination compounds, *Coordination Chemistry Reviews* 7: 81-114.
9. Ajithkumar G, P.K. Radhakrishnan (2011) Yttrium and lanthanide nitrate complexes of 2,3-dimethyl-4-formyl-[2'-aminomethyl]pyridine]-1-phenyl-3-pyrazoline-5-one, *Journal of Indian Chemical Society* 88:635-639.

10. Marykutty TM, Madhu NT, Radhakrishnan PK (2001) Manganese(II) complexes of 1,2-di(imino-4'-antipyrynyl)ethane, *Synth React Inorg Met -Org Chem* 31: 1239-1247.
11. Khandar AA, Yazdi SAH, Khatamian M, Mc Ardle P, Zarei SA (2007) Synthesis, characterization and structure of nickel(II) complexes of a 16-membered mixed-donor macrocyclic Schiff base ligand, potentially hexadentate, bearing two pendant alcohol functions, *Polyhedron* 26: 33-38.
12. Raju KC, Radhakrishnan PK (2002) Complexes of Cobalt(II) with N,N'-Bis(4-antipyrylmethylenedene)ethylenediamine, *Synth React Inorg Met -Org Chem* 32: 1719-1728.
13. N.T. Madhu, P.K. Radhakrishnan, (2000) Cobalt(II) complexes of 1,2-(diimino-4'-antipyrynyl)ethane and 4-N-(4'-antipyrylmethylidene)aminoantipyrine, *Trans. Met. Chem.*, 25, 287-292.
14. N. Shahabadi, S. Kashanian, F. Darabi, (2010). DNA binding and DNA cleavage studies of a water soluble cobalt(II) complex containing dinitrogen Schiff base ligand: The effect of metal on the mode of binding, *European. J. Med. Chem.*, 45 4329.
15. N. Raman, S. Ravichandran, C. Thankaraja, (2004) Copper(II), cobalt(II), nickel(II) and zinc(II) complexes of Schiff base derived from benzil-2,4-dinitrophenylhydrazone with aniline, *J. Chem. Sci.*, 116(4), 215-219.
16. E. Canpolat, M. Kaya, (2004) Studies on mononuclear chelates derived from substituted Schiff-base ligands (part 2): synthesis and characterization of a new 5-bromosalicyliden- *p* -aminoacetophenoneoxime and its complexes with Co(II), Ni(II), Cu(II) and Zn(II) *J. Coord. Chem.*, 57(14) 1217-1223.
17. C. Spinu, A. Kriza, Co(II), Ni(II) and Cu(II) Complexes of Bidentate Schiff bases (2000) *Acta Chim. Solv.*, 47 179-185.
18. Shahabadi N, Kashanian S, Darabi F (2010) DNA binding and DNA cleavage studies of a water soluble cobalt(III) complex containing dinitrogen Schiff base ligand : The effect of metal on the mode of binding, *Euro J Med Chem* 45: 4239-4245.
19. Selvi PT, Palaniandavar M (2002) Spectral, Viscometric and electrochemical studies on mixed ligand cobalt(III) complexes of certain diimine ligands bound to Calf thymus DNA, *Inorganica Chimica Acta* 337 : 420-428.

**PP5.**

**ASSESSMENT OF WATER QUALITY PARAMETERS OF  
WATERBODIES IN AND NEAR THE PADDY FIELD**

Dr. Jyothi P

Associate Professor and Head, Department of Chemistry,  
KAHM Unity Women's College, Manjeri, Kerala, India, 676122

Email: jyothipuramana@gmail.com

**Introduction**

Today the easy availability of fresh water is a major problem as 80% of our rivers are polluted due to industrial and domestic discharge with increase pollution availability of fresh water is decreasing at greater rate. Industrial discharge increases the water pollutants such as high biochemical oxygen discharge (BOD), acidity, alkalinity, hardness, heavy metals etc., presence of high values of these parameters makes the water unfit for human consumption. Domestic sewage also creates a major problem, as organic wastes from domestic water causes problems of eutrophication, so makes water unsuitable for consumption.

**Water Quality Parameters**

Quality of water can be assessed by evaluating certain parameters, called water quality parameters. The following are the important parameters usually determined.

**1. pH of the water**

The pH of pure water refers to the measure of hydrogen ions concentrations in water. It ranges from 0 to 14. In general water with a pH of 7 is considered neutral while lower of it referred acidic and pH greater than 7 known basic. Normally, water pH ranges from 6 to 8.5. It is noticed that water with low pH is tend to be toxic and with high degree of pH is turned into a bitter taste. According to WHO standards of pH of water should be

6.5 to 8.5.

## **2. Electrical conductivity ( ec )**

Electrical conductivity is a measure of water's capacity to convey electric current . Pure water is not a good conductor of electric current rather a good insulator . According to WHO standards EC value should not exceeded  $400 \mu\text{S} / \text{cm}$  . Conductivity of water varies directly with temperature and it is proportional to its dissolved minerals and matter content.

## **3. Hardness**

Water hardness is the measures of the amount of calcium and magnesium salts dissolved in water . According to World Health Organization ( WHO ) hardness of water should be  $500 \text{ mg} / \text{l}$  . Hard water requires more soap and synthetic detergents for home laundry and washing , to contribute to scaling in boilers and industrial equipment.

## **4. Degree of hardness of drinking water**

- Soft  $0\text{-}60 \text{ mg} / \text{L}$
- Medium  $60\text{-}120 \text{ mg} / \text{L}$
- Hard  $120\text{-}180 \text{ mg} / \text{L}$
- Very hard  $> 180 \text{ mg} / \text{L}$

## **5. Turbidity**

Turbidity is a measure of cloudiness or haziness in water caused by suspended solids ( eg sediment , algae ) . Turbidity is expressed in Nephelometric turbidity units ( NTU ) and is measured using a relationship of light reflected from a given sample . Turbidity is a variable in the lower lakes and influenced primarily by wind events .

## **6. Total acidity**

The acidity in water sample is its capacity to neutralise hydroxide ions . Acidity may be caused by mineral acids such as sulphuric or hydrochloric acid or by dissolves carbon dioxide . Most commonly in drinking water , carbon dioxide is the principal cause of acidity .

## **7. Alkalinity**

Alkalinity is a measure of water's ability to neutralize acids or resist changes that cause acidity, maintaining a stable pH. Titration is used to measure the alkalinity of a water sample, and water with a pH of 8 or higher is considered alkaline. Soils and geology have the biggest influence on water pH and alkalinity.

## **8. Ammonia content**

Ammonia gas is extremely soluble in water. It is the natural product of decay of organic nitrogen compounds. Natural levels in ground waters are usually below 0.2 mg of ammonia per litre. If drinking water containing more than 0.2 mg of ammonia per litre is chlorinated, as up to 68 % of chlorine may react with ammonia and become unavailable for disinfection.

## **9. Sulphate content**

Sulphate is second to bicarbonate as major anion in hard water reservoirs. Sulphates can be naturally occurring or as a result of municipal or industrial discharges. It can be naturally occurring as a result of breakdown of leaves that falls into a stream of water passing through rock or soil containing gypsum and other common minerals or atmospheric deposition. Runoff from fertilized agricultural lands also contributes sulphate to water bodies.

## **10. Chloride content**

Chloride is a naturally occurring element that is common in most natural waters and is most often found as a component of salt ( sodium chloride ) or in some cases in combination with potassium or calcium. Chlorides are leached from different rocks into soil and water due to weathering. Chloride levels in unpolluted water are generally below 10mg/L and sometimes even below 1mg/L.

## **Review of literature**

Analysis of water quality parameters of water bodies in and near the paddy field by Brantas' upper stream along paddy fields, Karangploso Subdistrict, Malang District. The river water samples were collected along the paddy field. The samples were collected when ahead of the harvest season. During the harvest season, pesticides were not sprayed but the concentration of pesticides in the river is quite high.[7]

Gala lake is an international important lake due to its location on one of the world's most important bird migration routes. For this reason water quality of this lake is very important because the lake is surrounded by paddy Fields, it may contain eutrophication and toxic metals due to the excess use fertilizers. So the impacts of paddy fields on water quality of the gala lake was investigated. The concentrations of metals and physico-chemical parameters in surface water samples taken and compared with standard guidelines. NO<sub>2</sub>, BOD content in the lake was exceed the permissible level. High BOD indicates contaminated water quality.[8]

Water Quality analysis of River Tawi near Sitlee pumping station by Meenakshi Khajuria and S.P.S Dutta consists of the assessment of physico-chemical characteristics of the raw water of the Tawi river near Sitlee water treatment complex and at Sitlee water treatment complex, for two years (2000-2001 and 2001-2002). The results showed that the WQI value of the water samples during both the years is less than 50 and is indicative of water quality that is optimum for drinking.[9]

The water quality analysis of River Yamuna using water quality index in the national capital territory, India (2000-2009) by Deepshikha Sharma and Arun Kansal identifies the critical pollutants affecting the river water quality during its course through the city. BOD, DetO, total and faecal coliforms and free ammonia were found to be critical parameters for the stretch.[10]

Sarala C. et al. studied the groundwater quality parameters in the surrounding wells of Jawaharnagar, in upper Musi catchment area of Ranga Reddy district in Andhra Pradesh. The bore wells data was collected from the study area for two seasons i.e., post

monsoon in December 2007 and pre monsoon in June 2008. The groundwater is acidic in nature and very hard. It is done by using Arc GIS software. The study reveals that the concentrations of major constituents are well within the permissible limits of IS-10500-1994, except in few cases where total hardness and fluoride concentrations are high. The fluoride conc. exceeded the permissible limit. From the analysis it was observed that the groundwater is polluted in the entire study area. During last few years, the utilization of surface and groundwater for drinking, industrial and agricultural purposes has increased manifolds but consequently it is observed that the water is polluted and affecting the human health, soil nutrients, livestock, biomass and environment in certain areas.[13]

Shimaa M. Ghoraba et.al collected 120 ground water samples from 29 Districts of Balochistan, Pakistan. The various parameters are selected for the testing of samples.

All samples were analyzed for pH, Calcium, Carbonate, Magnesium, Sodium, Potassium, Chlorides, Sulphate and Nitrate, TDS and bicarbonate. The results revealed highly variable hydrochemistry. The chloride is found to be most predominating. The groundwater in Balochistan has high concentrations of fluoride, iron and nitrate in many districts. The pH part of the Durov diagram reveals that groundwater in study area is alkaline and electrical conductivity of most of samples lies in the range of drinking water standards adapted in Pakistan. From the SAR and conductivity plot it was found that most of groundwater cannot be used on soil without restricted drainage and special requirement of Management for salinity control. Comparison of data with WHO(2011) standards for drinking water indicate that the groundwater in the most of study area are suitable for drinking purpose except some few places. The groundwater recorded a wide range in TDS.[14]

### **Results and discussion**

We analyzed ten samples from different sources. They are:

Sample 1 – Pond near paddy  
field

Sample 2 – Pond near paddy field

Sample 3 – Pond near paddy field

Sample 4 – Well in the field

Sample 5 – Well near the field

Sample 6 – Well near the field

Sample 7 – Well near the field

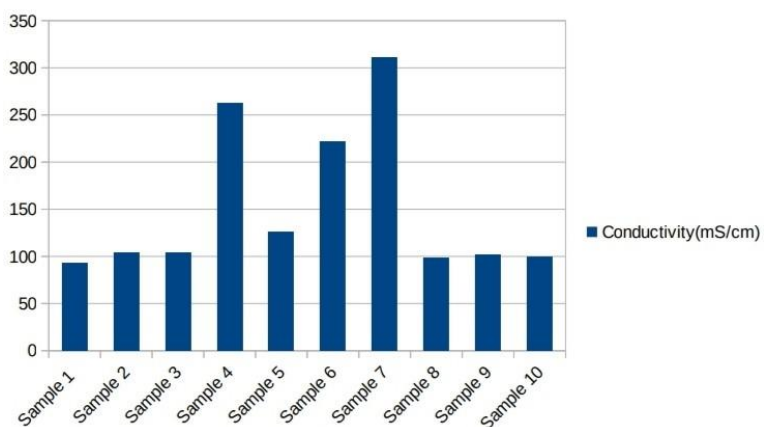
Sample 8 – Canal near the field

Sample 9- Canal near the field

Sample 10 – Canal near the field

The results obtained for various parameters are as follows

### 1. CONDUCTIVITY



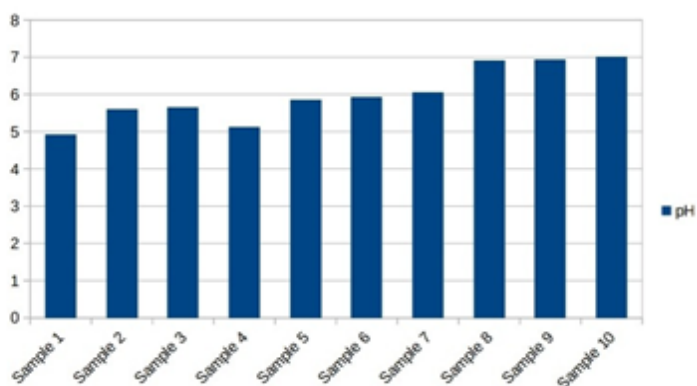
Samples	Conductivity(mS/cm)
Sample 1	93
Sample 2	104
Sample 3	104
Sample 4	263
Sample 5	126
Sample 6	222
Sample 7	311
Sample 8	99
Sample 9	102
Sample 10	100



Since conductivity is a measure of dissolved solvents, sample 7 conducts most and it may contain high amount. Conductivity of sample 1 is very less. So it contains less amount of dissolved solvents and comparatively pure than other samples.

## 2. pH

Samples	pH
Sample 1	4.92
Sample 2	5.61
Sample 3	5.66
Sample 4	5.13
Sample 5	5.86
Sample 6	5.93
Sample 7	6.05
Sample 8	6.92
Sample 9	6.94
Sample 10	7.0

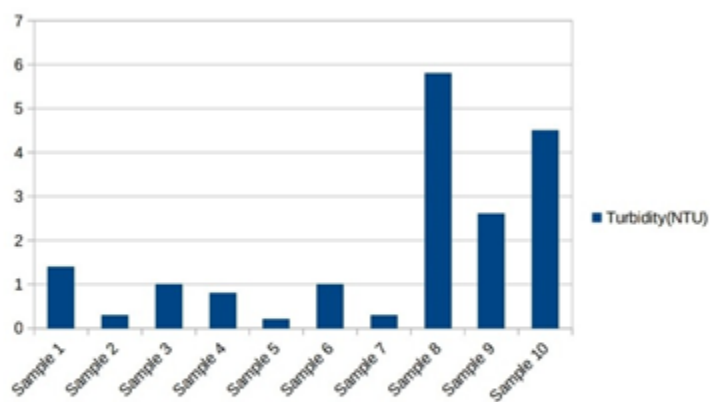


Most of the samples are acidic and only sample 10 is comparatively basic. Sample 1 is more acidic. As per Indian standard, for drinking water, pH value between 6.5 and 8.5 is desirable range. So samples 1,2,3,4,5,6,7 are not suitable for drinking purpose. pH can be raised by adding quantity of lime(Calcium hydroxide).

### 3. TURBIDITY

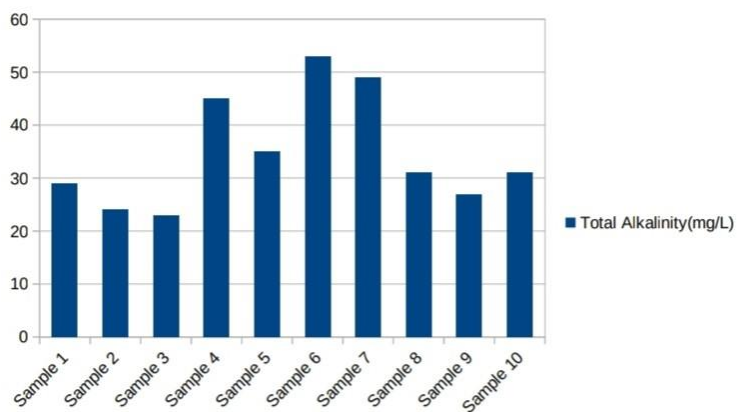
The maximum available limit of turbidity is 1 NTU. Here samples 1,3,6,8,9 and 10 have turbidity equal to greater than 1 NTU. Sample 8 has the highest turbidity.

Samples	Turbidity(NTU)
Sample 1	1.4
Sample 2	0.3
Sample 3	1.0
Sample 4	0.8
Sample 5	0.2
Sample 6	1.0
Sample 7	0.3
Sample 8	5.8
Sample 9	2.6
Sample 10	4.5



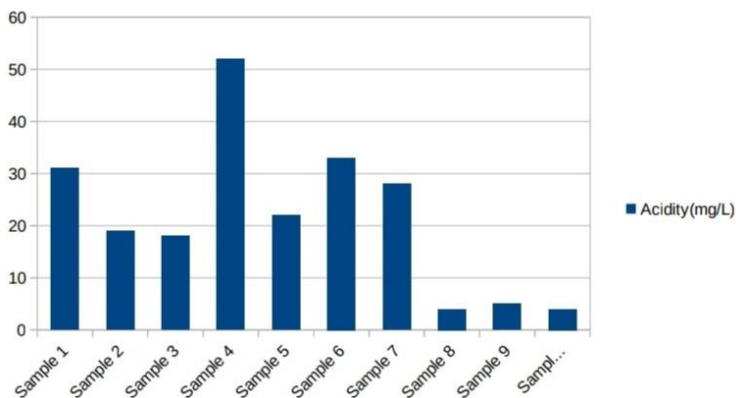
#### 4. ALKALINITY

Samples	Total Alkalinity(mg/L)
Sample 1	29
Sample 2	24
Sample 3	23
Sample 4	45
Sample 5	35
Sample 6	53
Sample 7	49
Sample 8	31
Sample 9	27
Sample 10	31



The maximum available limit of total alkalinity is 200 mg/L. Here for all samples, the total alkalinity is less than 200 mg/L.

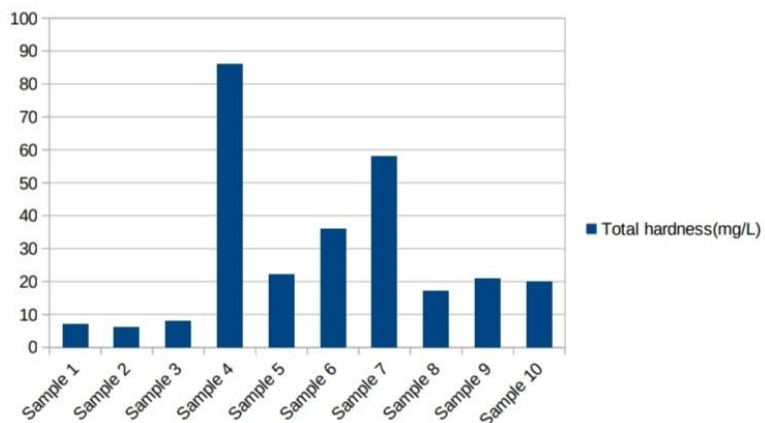
#### 5. ACIDITY



Samples	Acidity(mg/L)
Sample 1	31
Sample 2	19
Sample 3	18
Sample 4	52
Sample 5	22
Sample 6	33
Sample 7	28
Sample 8	4
Sample 9	5
Sample 10	4

## 6.HARDNESS

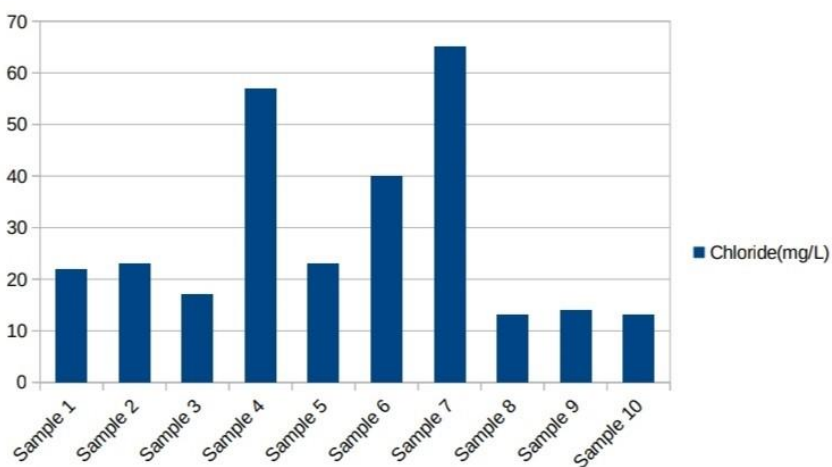
Samples	Total hardness(mg/L)
Sample 1	7
Sample 2	6
Sample 3	8
Sample 4	86
Sample 5	22
Sample 6	36
Sample 7	58
Sample 8	17
Sample 9	21
Sample 10	20



The maximum limit of total hardness is 200 mg/L. Here for samples, hardness is less than 200 mg/L.

## 7.CHLORIDE

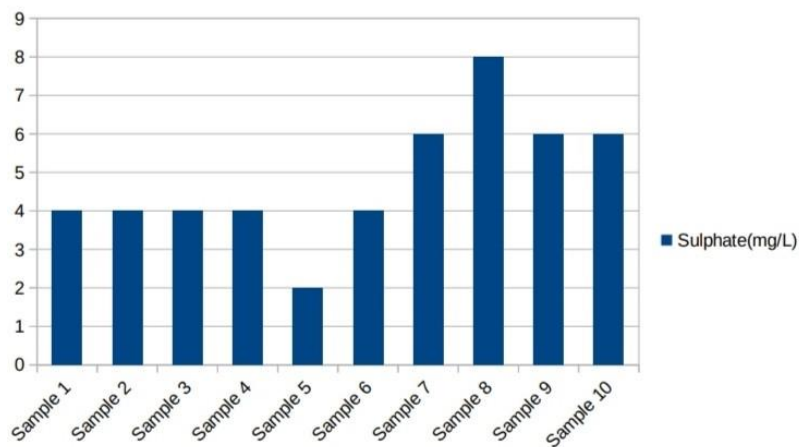
Samples	Chloride(mg/L)
Sample 1	22
Sample 2	23
Sample 3	17
Sample 4	57
Sample 5	23
Sample 6	40
Sample 7	65
Sample 8	13
Sample 9	14
Sample 10	13



The maximum available limit of chloride in water is 250 mg/L. Here for all samples, chloride level is less than 250 mg/

## 8.SULPHATE

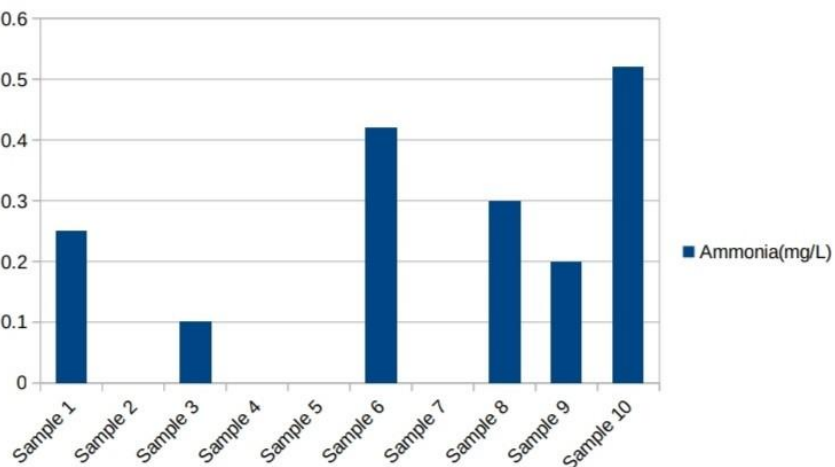
Samples	Sulphate(mg/L)
Sample 1	4
Sample 2	4
Sample 3	4
Sample 4	4
Sample 5	2
Sample 6	4
Sample 7	6
Sample 8	8
Sample 9	6
Sample 10	6



The maximum limit of sulphate is 200 mg/L. Here for all samples, sulphate level is very less than 200mg/L.

## 9.AMMONIA

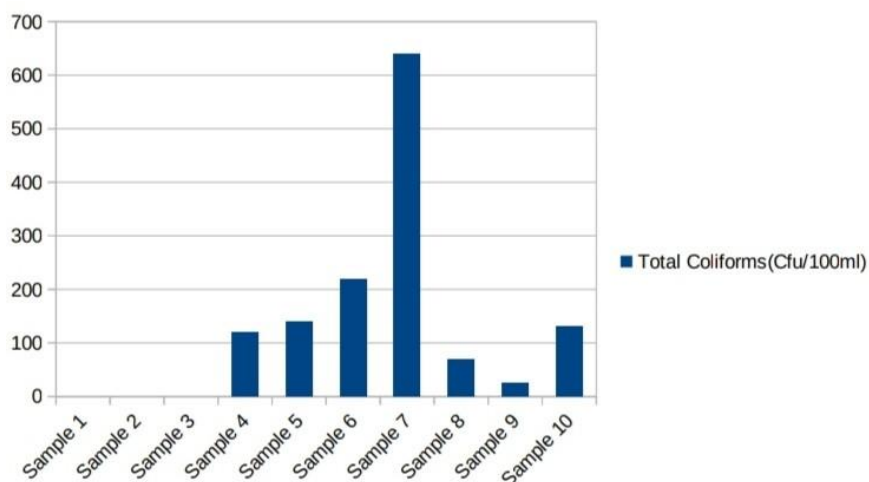
Samples	Ammonia(mg/L)
Sample 1	0.25
Sample 2	0
Sample 3	0.1
Sample 4	0
Sample 5	0
Sample 6	0.42
Sample 7	>5.0
Sample 8	0.3
Sample 9	0.2
Sample 10	0.52



The maximum limit is 0.50mg/L. Here samples 7 and 10 have exceeded the permissible limit and sample 7 has very high ammonia content.

### 10.TOTAL COLIFORMS

Samples	Total Coliforms(Cfu/100ml)
Sample 1	0
Sample 2	0
Sample 3	0
Sample 4	120
Sample 5	140
Sample 6	220
Sample 7	640
Sample 8	70
Sample 9	25
Sample 10	130



Total coliforms should be absent in a sample. Samples 1,2 and 3 are free of coliform bacteria. Other samples have bacteria content and sample 7 has very high coliform bacteria cont

## DISCUSSION

Total 10 samples collected from different water sources of the study area from water bodies in and near the paddy field and analysed for physico-chemical parameters such as pH, electrical conductivity, turbidity, ammonia content, total hardness, acidity, alkalinity and chloride. A qualitative study to know the presence or absence of sulphate ions was also conducted.

pH is an indicator of acidic or alkaline condition of water. The pH of most neutral water falls within 4-9. Low pH causes corrosion. In the present study area, the pH value ranges from 4.92-7. In water solution, variations in pH value from 7 are mainly due to hydrolysis of salts of strong bases and weak acids or vice versa. Water pH has generally major role in the determination of solubility and biological availability of chemical constituents such as nutrients and heavy metals. The pH values of the samples are given in Table and a graphical representation also.

Electrical conductivity is the capacity of water to carry an electrical current, and varies with the number and type of ions in solution. The maximum permissible limit of conductivity in drinking water is 300 mS/cm. In present day the conductance of well water samples varies between 33 and 194. The conductivity values of the samples were listed in Table and a graphical representation of the same also.

Turbidity is beyond the limit of 1 NTU for samples 1,3,6,8,9 and 10 and sample 8 has the most.

Natural and anthropogenic sources contribute to ammonia content in water. Presence of ammonia will accelerate algal growth in water bodies. Out of 10 samples collected, ammonia is present in majority of the samples. The samples 7 and 10 contain ammonia which exceeded the permissible limit. The ammonia content in different samples are listed in a table and a graphical representation also.

The total hardness in water samples ranges from 6mg/L to 86mg/L which shows that all samples are soft and safe for drinking purpose. The chief disadvantages of hard waters are that they neutralise the lathering power of soap and,

more important that they can cause blockage of pipes and severely reduced boiler efficiency because of scale formation. The hardness measurements of samples were given in Table and a graphical representation also.

Acidity of water will affect its corrosiveness and acidity in water can corrode copper pipes. Further acidity of water will interfere in water softening. The acidity value of present samples varies from 4mg/L to 52mg/L. The acidity values of samples are given in table and a graphical representation.

Naturally sulphates are found in various minerals such as epsomite ( $\text{MgSO}_4 \cdot 7\text{H}_2\text{O}$ ), gypsum ( $\text{CaSO}_4 \cdot 2\text{H}_2\text{O}$ ) and barite ( $\text{BaSO}_4$ ).such dissolved minerals constitute the mineral content in drinking water. Out of 10 samples sulphates contents are less than maximum limit. Water containing sulphates in excess may attack the fabric of concrete sewer pipes.

Alkalinity of water is an important parameter. The maximum limit is 200 mg/L. The samples's alkalinity ranges from 23 to 53 mg/L. That means all samples are not beyond the permissible limit. Like that chloride is less than permissible limit of 250mg/L for all samples.

Some of the samples are detected with coliform content. It leads to health issues and some diseases.

## CONCLUSION

The Present investigation gives an insight Into the probable impact of water pollution by excessive use of chemical fertilizers and pesticides used in Paddy fields.

The results of water investigation shows that most water samples of study area have all parameters within limits.This shows that water samples were least affected by urbanization. The presence of large amount of ionic substances and soluble salt may have resulted in increased value of electrical conductivity.Here sample 7 have high electrical conductivity and 1 have least. Sample 8 is more turbid and sample 10 is more basic. But the most harmful thing is the presence of coliform bacteria in almost



samples except 1,2,3, it shows that the water sources highly contaminated and chlorination or UVfiltration is essential for before it use

The parameters alkalinity, acidity, hardness, chloride, and sulphate were determined for the 10 samples and all these parameters were found within the permissible limit. The maximum ammonia limit of a sample is 0.50. Here the samples 7 and 10 exceed the permissible limit. Based on these parameters we can say that all water samples except 7 are suitable for drinking purpose.

As the value of total hardness come within the limits, the metal ion concentration is low. So the toxic effect of water is less. So the water samples collected from in and near paddy fields are not much polluted.

## REFERENCES

1. Laboratory manual of water and waste water analysis by Dr .R. Khanna,R.Bhutiani
2. Laboratory manual of water and waste water analysis by Dr .R. Khanna,R.Bhutiani
3. Water can exacerbate inequality-or it can help solve it-Betsy Otto ,Leah Schleifer, (WRI).March 10,2020
4. <https://ourworldindata.org>  
(Water use and stress-Hannah Ritchie and Max Roser,2015)
5. Assessment of water resources and water availability in the world-Shiklomanov,1997
- 6.Mahamat Seid A.M,Maoudombaye Theophile, Ahmat Altidjani, Mahamat Nour Sakine,Ndoutamia A. G.Study Of The Physico-Chemical Water Quality Of The Company's Pumping Stations Chadian Water And Suburbs Of Manual Drilling N'djamena,International Journal of Scientific Technology Research Volume 5,Issue 10,October 2016,ISSN 2277-8616,147-153
7. Water Bodies Quality along Paddy Field in Karang Ploso Sub District,Malang City,Indonesia Kiki Gustinasari,Joni Hermanaand Ellina S.Pandebesie Department of Environmental Engineering, Faculty of Civil, Environmental and Geo

Engineering, Sepuluh Nopember Institute of Technology, Surabaya-Indonesia

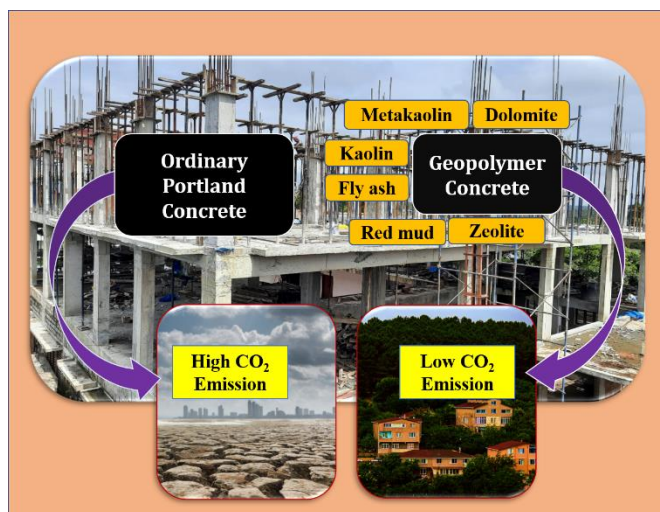
8. Impact of paddy fields on water quality of Gala Lake(Turkey):An important migratory bird stopover habitat. Memet Varol et.al. Environ Pollut.2021,Oct 15 ; 287 : 117640.Doi:10.1016/j.envpol.2021.117640.Epub 2021 June 22
9. Meenakshi Khajuria, S.P.S Dutta.Water Quality of River Tawi near Sitlee pumping station, Environment Conservation Journal 2012,ISSN 0972-3099,13(1 AND 2) 203-210.
10. Deepshikha Sharma, Arun Kansal. Water quality analysis of River Yamuna using water quality index in the national capital territory,India(2000-2009), Appl Water Sci(2011) 1:147-157
11. Vikas Tomar, Kamra S.K, Kumar S, Kumar Ajay and Vishal Khajuria, "Hydro-chemical analysis and evaluation of groundwater quality for irrigation in Karnal district of Haryana state, India", International Journal of Environmental Sciences, Volume 3, No 2, 2012, pp.756-766
12. Chidanand Patil, Shreekant Narayanakar and Arjun Virupakshi,'Assessment of Ground Water Quality Around Solid Waste Landfill Area-A Case Study,International Journal of Innovative Research in Science, Engineering and Technology, Vol. 2,Issue 7,July 2013,pp,3131-3136
13. Sarala C, Ravi Babu P, " Assessment of Groundwater Quality Parameters in and around Jawaharnagar, Hyderabad, International Journal of Scientific and Research Publications, Volume 2, Issue 10, 2012, pp.1-6.
14. Shimaa M. Ghoraba & A.D.Khan, " hydrochemistry and groundwater quality assessment in balochistan province, Pakistan", IJRRAS 17 (2) November 2013, 185-199.
15. Adetunde L.A, Glover R.L.K &Oguntola G.O, "assessment of the ground water quality in ogbomoso township of oyo state of nigeria", IJRRAS8 (1) july 2011, 115-122.

PP6.

## GEOPOLYMER MATERIALS: AN ECO-FRIENDLY NEXT-GENERATION ALTERNATIVE FOR CONSTRUCTION INDUSTRY

Thasleena Panakkal<sup>1</sup>, Resha Kasim Vellattu Chola<sup>1</sup> and Farsana Ozhukka Parambil<sup>1</sup>  
<sup>1</sup>Department of Chemistry, Pocker Sahib Memorial Orphanage College, Tirurangadi,  
Malappuram, Kerala, India

Email: [chempsmotgi@gmail.com](mailto:chempsmotgi@gmail.com)



Geopolymer materials have been increasingly embraced as a potential material for building restoration due to their remarkable properties and environmentally friendly nature. These next-generation materials, created with the assistance of geopolymerisation reactions of alumino-silicates with alkali

activators, have remarkable benefits such as high strength, fire resistance, and corrosion resistance. Geopolymerisation involves relatively low levels of CO<sub>2</sub> emissions and energy use, which significantly reduces global warming. As such, these materials are highly suitable for building restoration and have the potential to revolutionize the construction industry. This technology is already being used in some parts of the world and is expected to grow in popularity in the coming years. The cost of its implementation is relatively low, and its environmental benefits are significant. Due to its high strength, it can replace ordinary Portland cement in the construction industry. This work highlights the recent advances in geopolymeric materials, giving special emphasis to zeolite, fly ash, kaolin, dolomite, red mud and clay-based materials. These

materials are widely used in the construction industry due to their low cost, abundance, and ease of availability. They are also environmentally friendly and have good fire-resistance properties. Additionally, they can be used to produce lightweight and durable building materials.

PP7.

**Chitosan-Cu Catalyzed Novel Ferrocenated Spiropyrrolidines: Green Synthesis, Single Crystal X-ray Diffraction, Hirshfeld Surface and antibacterial Studies.**

Mohammad Asad<sup>1,2\*</sup>, Muhammad Nadeem Arshad<sup>1,2</sup>, Abdullah M. Asiri<sup>1,2</sup>, Snigdha. K<sup>3</sup>,  
Mohammed Musthafa T.N.<sup>3\*</sup>

<sup>1</sup> *Center of Excellence for Advanced Materials Research (CEAMR), King Abdulaziz University, P.O. Box 80203, Jeddah 21589, Saudi Arabia*

<sup>2</sup> *Chemistry Department, Faculty of Science, King Abdulaziz University, P.O. Box 80203, Jeddah 21589, Saudi Arabia*

<sup>3</sup> *Research & Postgraduate Department of Chemistry, MES Kalladi College, Mannarkkad (Affiliated to University of Calicut), Kerala, 678583, India;*

\* Correspondence: [magkhan@kau.edu.sa](mailto:magkhan@kau.edu.sa) (M.A),  
[drmusthafa@meskc.ac.in](mailto:drmusthafa@meskc.ac.in) (M.M. T.N.)

**Abstract:** Chitosan-bounded copper (chitosan–Cu) was introduced for green synthesis of novel ferrocenated spiropyrrolidine hybrids, namely 30 -(4-bromobenzoyl)-50 -(4-hydroxybenzyl)-40 -ferrocenylspiro [indoline-3,20 -pyrrolidin]-2-one and 30 -(4-bromobenzoyl)-40 -ferrocenylspiro[indoline-3,20 -pyrrolidin]- 2-one, in good yield. A one-pot three-component 1,3-dipolar cycloaddition reaction was employed for the formation of spiropyrrolidines from 1-(4-bromophenyl)-ferrocene-prop-2-en-1-one and azomethine ylides, which were developed in situ from tyrosine, glycine, and isatin, respectively. Various spectroscopic methods were used to establish the structures of spiropyrrolidines, and a single crystal X-ray diffraction study of a spiropyrrolidine provided additional confirmation. The crystallographic study revealed that compound 3a has one independent molecule in its unit cell, which is correlated with Hirshfeld surface analysis, and describes intramolecular contacts adversely. The highly yielded products in

green conditions were determined for their antibacterial significance and were found to have good activity against Gram-positive and Gram-negative bacterial strains.

**Keywords:** green synthesis; spiropyrrolidines; X-ray crystallography; Hirshfeld surface analysis; antibacterial activity

## References

1. Asad, M.; Arshad, M.N.; Oves, M.; Khalid, M.; Khan, S.A.; Asiri, A.M.; Rehan, M.; Dzudzevic-Cancar, H. N-Trifluoroacetylated pyrazolines: Synthesis, characterization and antimicrobial studies. *Bioorg. Chem.* 2020, 99, 103842.
2. Asad, M.; Siddiqui, Z.N.; Asiri, A.M.; Mahmood, A. Synthesis, DFT and biological studies of novel 3,6-dimethyl-1,8-diphenyldiazocino[3,4-c:7,8-c']bispyrazole. *J. Mol. Struct.* 2019, 1176, 66–72.
3. Pandey, G.; Banerjee, P.; Gadre, S.R. Construction of Enantiopure Pyrrolidine Ring System via Asymmetric [3+2]-Cycloaddition of Azomethine Ylides. *Chem. Rev.* 2006, 106, 4484–4517.
4. Kaur, N.; Ziegelmeyer, E.C.; Farinde, O.N.; Truong, J.T.; Huynh, M.M.; Li, W. Visible light bromide catalysis for oxazoline, pyrrolidine, and dihydrooxazine syntheses via C sp<sup>3</sup> –H functionalizations. *Chem. Commun.* 2021, 57, 10387–10390.
5. Kasturi, S.; Surarapu, S.; Uppalanchi, S.; Anireddy, J.S.; Dwivedi, S.; Anantaraju, H.S.; Perumal, Y.; Sigalapalli, D.K.; Babu, B.N.; Ethiraj, K.S. Synthesis and  $\alpha$ -glucosidase inhibition activity of dihydroxy pyrrolidines. *Bioorg. Med. Chem. Lett.* 2017, 27, 2818–2823.
6. Shen, C.; Xu, J.; Yu, W.; Zhang, P. A highly active and easily recoverable chitosan@copper catalyst for the C–S coupling and its application in the synthesis of zolimidine. *Green Chem.* 2014, 16, 3007–3012.

7. Sun, W.; Xia, C.G.; Wang, H.W. Efficient heterogeneous catalysts for the cyclopropanation of olefins. *New J. Chem.* 2002, 26, 755–758.
8. Baig, R.N.; Varma, R.S. Organic synthesis via magnetic attraction: Benign and sustainable protocols using magnetic nanoferrites. *Green Chem.* 2013, 15, 1834.
9. Ahmed, M.; Qadir, M.A.; Hameed, A.; Arshad, M.N.; Asiri, A.M.; Muddassar, M. Azomethines, isoxazole, N-substituted pyrazoles and pyrimidine containing curcumin derivatives: Urease inhibition and molecular modeling studies. *Biochem. Biophys. Res. Commun.* 2017, 490, 434–440.
10. Arshad, M.N.; Sahin, O.; Zia-ur-Rehman, M.; Shafiq, M.; Khan, I.U.; Asiri, A.M.; Khan, S.B.; Alamry, K.A. Crystallographic Studies of Dehydration Phenomenon in Methyl 3-hydroxy-2-methyl-1,1,4-trioxo-1,2,3,4-tetrahydro-1λ 6-benzo[e][1,2]thiazine-3- carboxylate. *J. Chem. Crystallogr.* 2013, 43, 671–676.

**PP8.**

## **Adsorption characteristics of multivalent cations onto microplastic polymers from aqueous solutions**

**Suhada Kottakuth Matavil**<sup>a,b</sup> and Yamuna Kunhi Mouvenchery<sup>a,c\*</sup>

<sup>(a)</sup>Malabar Christian college, Calicut, <sup>(b)</sup>KAHM Unity Women's College, Manjeri, <sup>(c)</sup> NSS College, Manjeri

\* Corresponding author: Dr. Yamuna K.M, Assistant Professor, Department of Chemistry, NSS College, Manjeri, E-mail: kmyamunanssmji@gmail.com

### **Abstract**

Microplastics (MP) that are plastic particles of less than 5mm diameter<sup>1</sup> are being increasingly attended by researchers across the world, owing to the pollution threat they pose, in all compartments of the environment including living organisms<sup>2</sup>. They find their way into soil and water usually through sludge, tear and wear, washing machine, cleansing agents etc<sup>3,4,5&6</sup>. Apart from the intrinsic potential to harm the environment, they may serve as carriers of organic<sup>7</sup> and inorganic pollutants<sup>8</sup>. Therefore, adsorption behaviour of MPs towards organic contaminants and inorganic ions (both contaminants and nutrients) needs to be explored.

This pilot study, therefore, addresses the adsorption of cations of different valences - Na<sup>+</sup>, Ca<sup>2+</sup> and Al<sup>3+</sup> - on to surfaces of engineered polyethylene (PE), polystyrene (PS) and polyvinylchloride (PVC) microparticles, in aqueous medium. The sorption mechanism as well as the effect of cation sorption on surface characteristics of MP were investigated.

Results revealed that sorptive properties for cations on different polymers differed, depending on characteristics of both the cations and the polymer type. Interestingly, sorption process induced alterations in surface characteristics of polymer particles. These results would imply that pollution threat of MP polymers have added intensity that they can (1) limit the nutrient availability (2) enhance spatial distribution of contaminants both in water and soil.

1. Arthur, C., Baker, J. & Bamford, H. Proceedings of the International Research Workshop on the Occurrence, Effects, and Fate of Microplastic Marine Debris. *Group 530* (2009)
2. Carbery, M., O'Connor, W. & Palanisami, T. Trophic transfer of microplastics and mixed contaminants in the marine food web and implications for human health. *Environ. Int.* **115**, 400–409 (2018).



PROCEEDINGS OF THE SEMINAR ON  
'EMERGING AREAS OF CHEMICAL SCIENCES'

3. 3. Conley, K., Clum, A., Deepe, J., Lane, H. & Beckingham, B. Wastewater treatment plants as a source of microplastics to an urban estuary: Removal efficiencies and loading per capita over one year. *Water Res. X* **3**, 100030 (2019).
4. 4. Corradini, F. *et al.* Evidence of microplastic accumulation in agricultural soils from sewage sludge disposal. *Sci. Total Environ.* **671**, 411–420 (2019).
5. 5. Piehl, S. *et al.* Identification and quantification of macro- and microplastics on an agricultural farmland. *Sci. Rep.* **8**, 1–9 (2018).
6. 6. Jan Kole, P., Löhr, A. J., Van Belleghem, F. G. A. J. & Ragas, A. M. J. Wear and tear of tyres: A stealthy source of microplastics in the environment. *Int. J. Environ. Res. Public Health* **14**, (2017).
7. Fu, L., Li, J., Wang, G., Luan, Y. & Dai, W. Adsorption behavior of organic pollutants on microplastics. *Ecotoxicol. Environ. Saf.* **217**, 112207 (2021).
8. Wang, F. *et al.* Adsorption characteristics of cadmium onto microplastics from aqueous solutions. *Chemosphere* **235**, 1073–1080 (2019)

PROCEEDINGS OF THE SEMINAR ON  
'EMERGING AREAS OF CHEMICAL SCIENCES'

**ISBN: 978-93-5913-421-5**